874

2138

R and D CENTER
LABORATORY
TECHNICAL REPORT

NO. 12896

COLD WORKING AND ANNEALING EFFECTS ON THE CREEP AND RUPTURE RESISTANCE OF THE OXIDE-DISPERSION-STRENGTHENED ALLOY MA754

DEPARTMENT OF THE ARMY PROJECT NO. DAAE07-82-C-4017
NOVEMBER 1983

BY:

Dr. L.J. Ebert
M.L. Telich
Case Western Reserve Univ.
Cleveland, Ohio

and

M. Holly
Dr. B. Roopchand
U.S. Army Tank Automotive Command
DRSTA-RCKM
Warren, Michigan

U.S. ARMY TANK-AUTOMOTIVE COMMAND
RESEARCH AND DEVELOPMENT CENTER
Warren, Michigan 48090

DISCLAIMER NOTICE

THIS DOCUMENT IS BEST QUALITY PRACTICABLE. THE COPY FURNISHED TO DTIC CONTAINED A SIGNIFICANT NUMBER OF PAGES WHICH DO NOT REPRODUCE LEGIBLY.

NOTICES

The findings in this report are not to be construed as an official Department of the Army position.

Mention of trade names or manufacturers in this report shall not be construed as advertising nor as an official endorsement or approval of such products or companies.

Destroy this report when it is no longer needed. Do not return to the originator.

TABLE OF CONTENTS

LIST OF ILLUSTRATIONS

LIST OF TABLES

PREFACE

The investigation reported upon herein was carried out in cooperation with the US Army Tank-Automotive research and Development command, Department of Defense, Warren Michigan, under the terms of Contract No. DAEE07-82-C-4017. The Case Western Reserve University Investigators, Professor L.J. Ebert and Mr. M.L. Telich, wish to acknowledge the support and assistance of Dr. James Chevalier, Chief, Armor and Components Function, and that of Mr. M.L. Holly of the Command.

REPORT DOCUMENTATION PAGE

READ INSTRUCTIONS BEFORE COMPLETING FORM

1. REPORT NUMBER

2. GOVT ACCESSION NO.

3. RECIPIENT'S CATALOG NUMBER

4. TITLE (and Subtitle)

Cold Working and Annealing Effects on the Creep and Rupture Resistance of Oxide-Dispersion-Strengthened Alloy MA754

5. TYPE OF REPORT & PERIOD COVERED

Final Report

6. PERFORMING ORG. REPORT NUMBER

7. AUTHOR(s)

L. J. Ebert, M. H. Telich, M. L. Holly

8. CONTRACT OR GRANT NUMBER(s)

DAAE07-82-C-4017

9. PERFORMING ORGANIZATION NAME AND ADDRESS

Case Institute of Technology
Case Western Reserve University
Cleveland, Ohio

10. PROGRAM ELEMENT, PROJECT, TASK AREA & WORK UNIT NUMBERS

RDT&E 1L162601AH91

11. CONTROLLING OFFICE NAME AND ADDRESS

US Army Tank-Automotive Command
ATTN: DRSTA-RCKM
Warren, MI 48090

12. REPORT DATE

Nov 83

13. NUMBER OF PAGES

119

14. MONITORING AGENCY NAME & ADDRESS(if different from Controlling Office)

15. SECURITY CLASS. (of this report)

Unclassified

15a. DECLASSIFICATION/DOWNGRADING SCHEDULE

16. DISTRIBUTION STATEMENT (of this Report)

Approved for public release, distribution unlimited.

17. DISTRIBUTION STATEMENT (of the abstract entered in Block 20, if different from Report)

18. SUPPLEMENTARY NOTES

19. KEY WORDS (Continue on reverse side if necessary and identify by block number)

Oxide dispersion strengthened alloy
Rupture resistance
Powder Metallurgy
High temperature
MA754
Cold working
Creep resistance
Cold Rolling
Annealing

20. ABSTRACT (Continue on reverse side if necessary and identify by block number)

The mechanisms of the deformation and annealing response of MA754 were examined through a study of the inter-relationships between cold work and thermal treatments as they affect various material performance parameters at elevated temperatures. Various cold rolling plus annealing experiments indicate that the recrystallization of MA754 is controlled by primary recrystallization principles. It has been found that, through the application of a

stepwise cold rolling plus annealing schedule, total reductions of at least 40% (reduction in thickness) at ambient temperature can be obtained while at the same time maintaining a grain morphology favorable for good high temperature properties.

High temperature ($0.94T_m$) annealing treatments given to stabilize the grain structure following cold work produce a change in both the size and distribution of the dispersoid phase. Measurements reveal that the average particle size increases as $(\text{time})^{1/3}$, typical of diffusion-controlled Ostwald ripening. The coarsening observed in the process material is restricted to the grain boundaries, and results in a significant loss in creep resistance.

COLD WORKING AND ANNEALING EFFECTS ON THE CREEP AND RUPTURE RESISTANCE OF THE OXIDE-DISPERSION-STRENGTHENED ALLOY MA754

1.0. INTRODUCTION

1.1. Background

Oxide Dispersion Strengthened (ODS) alloys were developed in order to produce maximum resistance to deformation in high temperature applications. These alloys consist of a fine dispersion of particles, thermodynamically incompatible, with the matrix, which itself has reasonably good high temperature properties. The presence of a stable dispersion of proper size and spacing acts to impede deformation at temperature at which thermodynamically compatible precipitated particles would agglomerate or dissolve.

The ODS alloys have evolved from the Sintered Aluminum Powder alloys (SAP)[1] which have a fine dispersion of alumina (Al_2O_3) in an aluminum alloy matrix. Although these alloys were shown to have better elevated temperature properties than the base aluminum alloys, the relatively low melting point of the matrix resulted in properties which were far from optimum. Consequently, research efforts were concentrated upon dispersion strengthening of higher melting temperature matrix materials.

Modern, high performance, commercial ODS alloys began with the introduction of Thoria Dispersed Nickel (TD-nickel).[2] The alloy contained a dispersion of thoria (ThO_2) in a commercially pure nickel matrix. The primary advantages of this alloy were its very high usable strength temperature (2000°F) and its excellent formability.

However, its use in most high temperature applications was limited by the poor oxidation resistance of the nickel matrix, and the unavailability of suitable coating materials.

In order to overcome the poor oxidation resistance of TD-Ni, a second generation alloy was developed. This alloy was Thoria Dispersed Nickel Chromium (TD-NiCr or TD Nichrome),[3] which contained 78% Ni, 20% Cr, and 2% thoria (wt %). This alloy had all of the excellent high temperature mechanical properties of TD-Ni, together with high temperature oxidation resistance afforded to it by the chromium.

Subsequent extensive testing proved that, although TD-NiCr had good corrosion resistance in static hot air, it had very poor resistance in high velocity flowing hot air. At the same time, concern developed around the use of ThO_2 as a dispersoid phase, because of its measurable (albeit slight) radioactivity. As a result, the nickel base was further alloyed with aluminum, and the thoria dispersed phase was replaced with yttria (Y_2O_3). This alloy was termed "NiCrAlY," and had the nominal composition of 16% Cr, 4% Al, 2-3% Y_2O_3, balance nickel. Despite showing promise as a viable high temperature material, the high basic cost of NiCrAlY, coupled with the very high material losses on machining the material to final finished shape, removed the alloy from the field of economically viable commercial high temperature alloys.

Within the last decade, an important development has taken place in the area of ODS superalloy manufacturing. It involved a process called mechanical alloying,[4] which has had a significant

impact on the design and operating costs of high temperature equipment. The main advantage of this process over previous methods is the high degree of dispersoid uniformity (both in distribution and size) within the final structure.

Two of the more popular mechanically alloyed materials commercially available are MA754 and MA6000. MA754 was developed as a gas turbine vane alloy and is basically a nichrome, strengthened with a dispersion of 0.6% yttrium oxide. Its high temperature properties are somewhat superior to those of Td-NiCr.[5]

MA6000 is an advanced high temperature gas turbine blade material. The nominal composition of the alloy is 15% Cr, 1.1% Y_2O_3, 4.5% Al, 2.5% Ti, 2% Ta, 2% Mo, 4% W, 0.1% Zr, 0.01% B, balance Ni. The unique feature of this alloy is its ability to combine oxide dispersion strengthening with γ'[1] precipitate hardening. This enables the alloy to exhibit maximum performance over a wide range of temperatures.

1.2. Elevated Temperature Deformation of Ni-Base ODS Alloys

Elevated temperature deformation of Ni base ODS alloys has been found to be sensitive to the following factors: 1) grain size, 2) grain shape (length-to-diameter, or L/D, ratio), and 3) nature of the particle dispersion. In this section, the relationship of these factors to the tensile and creep properties will be discussed. All investigations cited are concerned with the behavior of these alloys above one-half their absolute melting temperature, the temperature range in which maximum demand is placed on innate deformation and rupture resistance.

1.2.1. Tensile Properties

Tensile test results on various high temperature alloys reveal that both the tensile and yield strength increase with increasing grain size and increasing L/D ratio.[6,7,8,9,10] Fraser and Evans[11] noted that the ultimate tensile strength increased with an increase in dispersion volume fraction (up to 3% v/o) according to the relation:

$$\sigma_{UTS} \propto f^{\frac{1}{2}}$$ where f = dispersion volume fraction

Generally, ductility varies inversely as strength with respect to changes in grain size and shape. Fine grained, equiaxed material possesses maximum ductility, but minimum strength. Ductility and strength increase with increasing tensile strain rate, independent of grain size and shape.[9,12]

Anisotropy of the tensile properties exists in ODS alloys with elongated grain structures. Both strength and ductility levels decrease as the test direction varies from the direction of grain elongation. However, ductility appears to be affected to a greater degree.[13]

1.2.2. Creep Properties

ODS materials exhibit the classical three stage creep.[14,15] The first stage represents a region of continuously decreasing creep rate (with increasing strain), and is followed by a region of constant creep rate, or steady state creep. Generally, the final creep stage, tertiary creep, occurs only to a limited degree. However, high stress rupture ductilities have been reported for certain alloys.[16] The steady state creep rate increases with increasing

stress and temperature.

In order to explain the elevated temperature creep behavior of dispersion strengthened materials, three types of models have been proposed: 1) dislocation models, 2) grain boundary sliding models, and 3) concurrent process models.

The primary deformation mechanism contained within various dislocation models was suggested by Ansell and Weertman.[17] The rate controlling process was assumed to be the glide and climb of dislocations over second phase particles. This process was later shown to be heavily dependent upon interparticle spacing, particle size and volume fraction.[18,19] Further analysis[8,20] revealed that both glide and climb of dislocations are strongly influenced by matrix stresses at the particles. These matrix stresses are due to surface tension effects at the non-coherent particle-matrix interface. Under the action of the shear stresses generated on creep loading, the surface tension stresses interact with the mobile dislocations, producing pinning forces which interfere with dislocation motion. Although dislocation models can adequately describe the creep behavior of dispersion strengthened materials in certain situations, the models fail to consider other processes which may be concurrently active, and cannot describe the role of grain size and shape in influencing the elevated temperature properties of these materials.

In order to explain the effects of grain boundaries upon the elevated temperature deformation of dispersion strengthened materials, Fraser and Evans[11] developed the "fiber composite" model. The model suggested that each grain within a dispersion strengthened

material acts as a fiber within a composite material. The total strength of the "composite" depends upon the strength of each grain and the grain boundaries between the grains. At temperatures above the equi-cohesive point, grain boundary effects will determine the strength of the material. Consequently, in order to increase the resistance of the material to high temperature deformation (in this case, diffusion controlled grain boundary sliding), it is necessary to increase the load-carrying capability of the grain boundaries by decreasing grain boundary surface area. In other words, it is possible to increase high temperature deformation resistance by increasing the grain size of L/D ratio.

The presence of the dispersed phase has been shown to have an influence upon grain boundary sliding processes.[21,22] Their effect was attributed to the fact that particles prevent grain boundaries from acting as perfect sources or sinks for vacancies. This leads to the introduction of a high threshold stress for diffusion controlled grain boundary sliding.

The concurrent process model developed by Petrovic and Ebert[8,20] proposes that elevated temperature deformation of polycrystalline dispersion strengthened materials is controlled by the relative contribution of both dislocation motion and diffusion controlled grain boundary sliding. As a result, the steady state creep rate will have the form:

$$\dot{\epsilon}_S = \dot{\epsilon}_{DIS} + \dot{\epsilon}_{GBS}$$

where $\dot{\epsilon}_{DIS}$ = strain rate from dislocation motion and $\dot{\epsilon}_{GBS}$ = strain rate from diffusion controlled grain boundary sliding. This model

was shown to predict not only the high activation enthalpies and stress sensitivities observed in ODS alloys, but it also takes into account the grain size and shape dependencies, since the relative contribution of each mode is highly dependent upon grain size, applied stress, and temperature. The grain boundary sliding mode will predominate under conditions of low stress, high temperature, and small grain size.

1.3. Control of Grain Size and Shape of Dispersion Strengthened Materials

The control of grain size and shape of dispersion strengthened materials is critical in the development of any technique by which these materials can be made to have performance characteristics superior to those which they normally possess. Two techniques, thermomechanical processing (TMP) and directional recrystallization (DR), have shown some success in this area. They are discussed below.

1.3.1. Thermomechanical Processing (TMP)

Previous investigations[12,23-25] revealed that TMP by cold working and annealing gives control of both grain size and shape of TD nickel. Several generalizations have been proposed regarding the behavior of TD nickel which has been hot extruded, cold worked, and annealed: 1) The transformation to a large grained structure is sensitive to the direction of working. It was found that, on annealing, the transformation proceeds readily after transverse rolling, but is completely inhibited by longitudinal rolling or swaging

deformations, even for annealing temperatures as high as 2408°F (1320°C). Two possible explanations were proposed for this behavior. First, a strong texture would reduce the heterogeneity in the distribution of stored strain energy, thereby restricting the movement of grain boundaries. Second, a highly elongated worked grain structure represents a stable configuration which is resistant to initial boundary movement. Secondly, increasing the degree of cold reduction leads to an increase in recrystallized grain size. Such an observation was found to be compatible with abnormal grain growth concepts. Finally, it is suggested that, as the L/D ratio increases, there is an increasing tendency for grain boundaries to lie along bands of high particle density.[26]

As stated earlier, extensive use of TD-Ni in high temperature applications was limited by its inferior oxidation and corrosion resistance which subsequently led to the development of TD-NiCr.[8] However, it was found that the generalizations which characterized the behavior of TD-Ni following TMP did not apply to TD-NiCr. That is, as extruded TD-NiCr recrystallized to a fine grain size following cold working and annealing, and did so independent of the direction of working. The recrystallization behavior of TD-NiCr is believed to be the result of the lower stacking fault energy of this alloy (caused by the addition of Cr into the Ni matrix) and the presence of any short range order. It is suggested that these factors would create large gradients of stored energy leading to nucleation.[24]

It was later shown[8,24] that TD-NiCr could recrystallize to a

large grain size following a proper TMP treatment. Instead of cold rolling the as-extruded TD-NiCr, the material was hot rolled (in the range 2000°F-2100°F) and annealed at 2400°F. The recrystallized grain size was shown to increase by a factor of 200 as compared to the unrecrystallized material. Hot rolling is presently used in the commercial processing of ODS materials in order to achieve completeness of recrystallization and proper texture.

1.3.2. Directional Recrystallization

It has been demonstrated[27,28] that directional recrystallization can produce either columnar grains or monocrystals in several different alloys. Structures of very large, elongated grains have been produced by passing unrecrystallized TD-NiCr through a steep temperature gradient. The final grain size is dependent upon several factors, including steepness of the temperature gradient, maximum temperature, and rate of movement of the material through the gradient.

The mechanically alloyed materials appear to exhibit a mixed response to directional recrystallization. Directional heat treatment of MA754 produces the same grain elongation as conventional heat treatment. The cause of this response may be related in some way to the extrusion-hot working process. An exception to this behavior appears to be MA6000, in which columnar grains can be grown in both transverse and extrusion directions by appropriate application of thermal gradients.[29]

1.4. Purpose of the Present Investigation

In addition to its beneficial effects upon grain structure (and consequently the high temperature performance) of ODS materials, TMP is being sought as a means by which the alloys can be brought to near net-finish shape components without a loss of the optimal grain size and shape. Present practice involves machining the components from the extruded bar stock so that the favorable grain characteristics of this material can be retained. This leads to an enormous loss of material, in some cases as much as 90% of the purchased extruded bar. This added cost, together with the already high base material cost, has been a major deterrent to the use of ODS alloys in many applications when properties would otherwise dictate their use.

Commercially, the processes of interest in the generation of near net-shapes involve hot working, because it is well known that cold working of ODS alloys imparts sufficient stored energy that it promotes recrystallization to fine grain microstructures (with resultant loss of high temperature properties) at the high use temperatures. However, not all hot working modes (i.e., forging) have been shown to be successful in retaining the necessary coarse grained microstructure. It has been suggested[30] that the use of a relatively low temperature stress relaxation treatment after cold work might reduce the stored strain energy in the formed material to the point where it would not recrystallize even at temperatures within 100°F of the material's melting point. In addition, the material which had been cold worked and then given the stress relaxation treatment exhibited vastly superior high temperature mechanical properties

compared to the as-received material. The possibility of the use of such post-working treatments opens the door to a myriad of finishing operations which would more than compensate for the basic high material cost.

The purpose of the present investigation was one of pursuing the implications of the beneficial effects of stress relaxation treatments through a basic study of the mechanisms governing the deformation and annealing response of MA754. The main focus was placed upon the quantitative examination of the basic principles behind the interrelationships among the cold working and thermal treatments as they affect the grain morphology, dispersoid phase size and distribution, and, of course, the ultimate high temperature strength and creep resistance.

2.0. WORK EFFORT SUMMARY

2.1. Materials and Procedures

2.1.1. Material

The material used in this project was the oxide dispersion strengthened nickel-base alloy MA754 containing nominally 20% chromium, 0.3% aluminum, 0.4% titanium, and 0.6% yttria (Y_2O_3). The material is manufactured by Huntington Alloys, Inc., utilizing the mechanical alloying technique. The processing history is as follows: Constituent powders of the above proportions are milled simultaneously with the eventual result of complete homogenization. The homogenized mixture is then "canned" in an evacuated steel jacket, and hot extruded into rectangular bars. The material is subsequently hot rolled in the extrusion direction at temperatures in the range 1600°F-1900°F (871°C-1038°C), then annealed for 1 hour at 2400°F (1315°C).

Three bars from two different lots (both manufactured by the same procedure) totalling 75 inches in length were used in the investigation. The lots were coded as #B3512 and #B3527. Bars 1 and 2 were from lot #B3512 and were approximately 3.3 inches (83.8 mm) wide, and 1.4 inches (35.6 mm) thick. Bar 3 was from lot #B3527 and was 3.4 inches (86.4 mm) wide, 1.1 inches (27.9 mm) thick. Vendor's chemical analyses of the as-received material are given in Table 1.

Table 2-1.

Vendor's Chemical Analyses of the As-Received MA754 Used in the Investigation

Lot 3512

Element	% (By Weight)
C	0.06
Fe	0.93
S	0.002
Ni	77.20
Cr	20.15
Al	0.31
Ti	0.41
O	0.33
Y_2O_3	0.61

Lot 3527

Element	% (By Weight)
C	0.06
Fe	0.87
S	0.002
Ni	76.84
Cr	20.42
Al	0.33
Ti	0.42
O	0.35
Y_2O_3	0.58
N_2	0.13

2.1.2. Metallography

In order to describe the grain structure of MA754 accurately, it was necessary to utilize quantitative microscopy which requires adequate grain boundary delineation. No single grain boundary delineation technique was found to be suitable for use over the wide range of grain structures encountered in this investigation.

Effective polishing of the various samples was accomplished through either mechanical or electropolishing procedures. The mechanical polishing consisted of: 1) rough polishing with a series of SiC papers, 240 grit thru 600 grit; 2) final polishing involving the use of diamond paste impregnated texmet wheels followed by lapping on a 0.3 Al_2O_3 wheel. Electropolishing was accomplished by the use of a solution consisting of 12% H_2O, 70% ethanol (99%), 10% butyl cellosolve, 8% perchloric acid at 40°F (4.4°c) and 4-5 amps.

Grain boundary etching of MA754 proved to be difficult. However, three etching techniques were found to give satisfactory results. The first technique was a standard chemical etch, consisting of 56% HCl (conc), 22% HNO_3 (conc), and 22% methanol (95%). Acid staining of the surface was greatly reduced by swabbing the etch onto the surface instead of immersing the specimens. The second technique was electrochemical, employing a solution of 95% H_2O, 1% HF (conc), 1.5% HCl (conc) and 2.5% HNO_3 (conc), used at 6-7 amps and 40°F (4.4°c). The third technique involved thermal etching. Specimens whose surfaces had been polished were annealed for 1 hour at 1100°F (593°c) in air to produce the thermal etch.

2.1.3. Quantitative Grain Size Measurements

Quantitative grain dimension measurements were made by the line-intercept method, using at least 35 test lines for each of the three orthogonal directions. The basic quantity measured in the line intercept method is N, the number of grain boundary intersections per length of test line. The linear grain dimension L is defined as the inverse of N. By measurements of L in the three orthogonal directions, it was possible to estimate an average grain diameter by the following relations:

$$L_{AVE} = 0.844\ (L_1 L_2 L_3)^{1/3}$$

where L_{AVE} = average grain diameter

L_1 = grain diameter in the longitudinal (extrusion) direction

L_2 = grain diameter, long transverse (width) direction

L_3 = grain diameter, short transverse (thickness) direction.

Grain shape measurements were also made for the material. Grain shape is defined as the ratio of the length to width of the individual grains or L/D, and is computed from the linear grain dimension measurements described earlier:

$$L/D = 2L_1/(L_2 + L_3)$$

where L/D = length to width ratio

L_1, L_2, L_3 = grain diameters as defined above.

2.1.4. Elevated Temperature Tensile Tests

The various material conditions employed during the investigation were evaluated (in duplicate) in the temperature range 75°F (23.8°c) to 2000°F (1093°c). Size limitations of the different

specimen blanks required the use of two specimen geometries, namely sheet and cylindrical. Specifications of the cylindrical and sheet specimen geometries are shown in Figures 2-1. and 2-2.

The specimen grips used in testing were made of MAR M246 and were designed to undergo no deformation during use at the elevated test temperatures. A boron nitride powder was used to prevent diffusion bonding between the specimen heads and grips. The test apparatus used to perform the tensile tests was an Instron-Satec furnace combination. Temperature was controlled to ±2°F (±1°c) over the entire gage length of the specimen, using Chromel-Alumel thermocouples for temperature sensing. Tensile tests were conducted at a cross-head speed of 0.05 inches/minute (0.127 cm/min).

2.1.5. Elevated Temperature Creep Tests

All creep testing was done utilizing leveled creep racks (12,000 lb. capacity) modified to produce constant load or constant stress. The furnaces were of the Satec tube-type, with a maximum temperature of 2200°F (1204°c) and an accuracy in the hot zone of ±2°F (±1°c). Strains were measured with a dial indicator with an accuracy of 0.001 inch (0.0025 mm) or an LVDT (Linearly Variable Differential Transformer) with an accuracy of ±0.00005 inch (0.0013 mm). The test piece designs used in the determination of creep properties were basically the same as those used to determine tensile properties. However, it became necessary to modify the cylindrical specimen geometry slightly, Figure 3.

The quantities of primary interest measured during creep tests

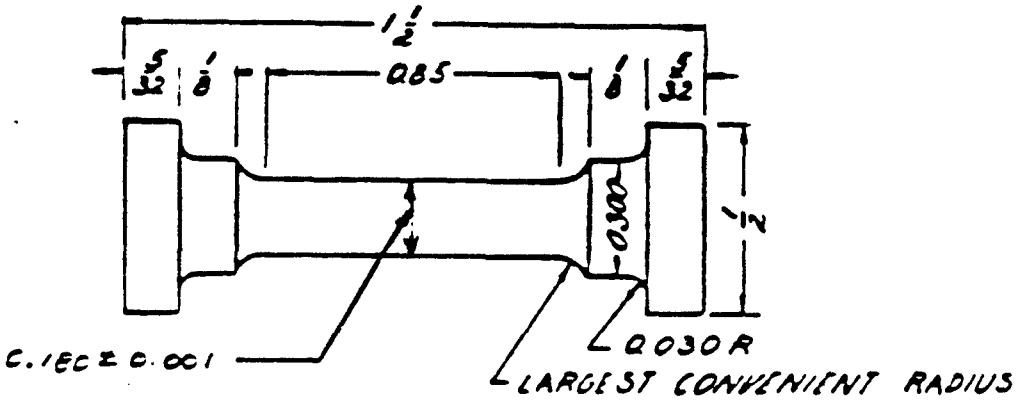

Figure 2-1. **Specimen Design Used in the Determination of the Tensile Properties of the As-Received MA754.**

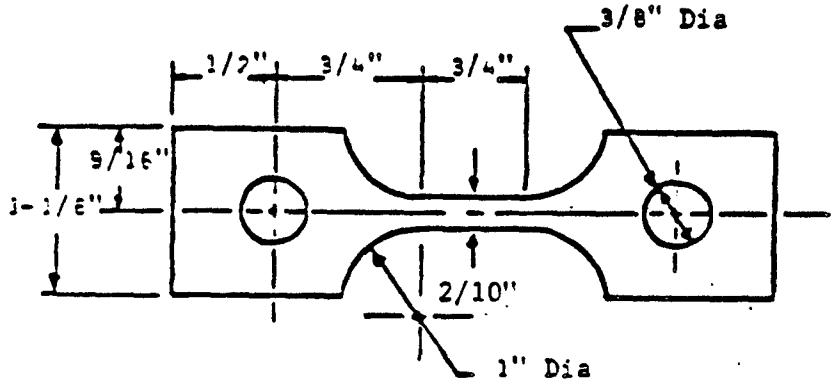

Figure 2-2. Design of Test Piece Used for Tensile and Creep Testing of the Cold Rolled Plus Annealed Materials.

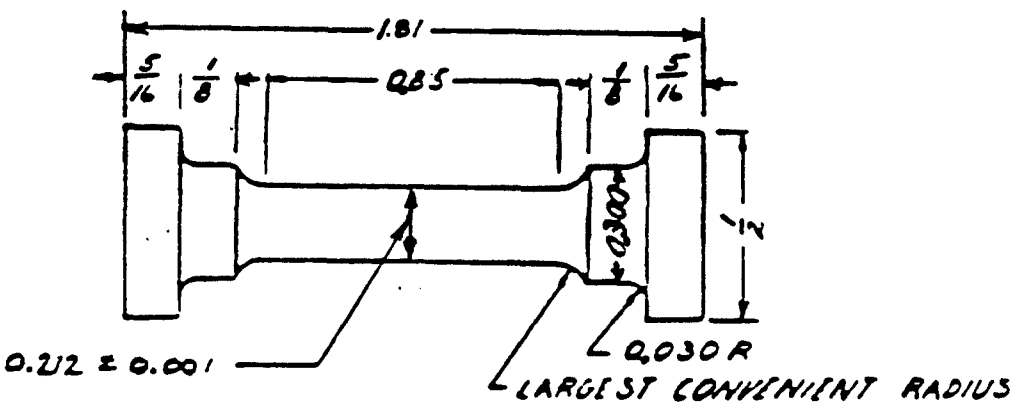

All dimensions in inches.

Figure 2-3. **Specimen Design Used in the Determination of the Tensile and Creep Properties of the As-Received MA754.**

in the present study were 1) steady state creep rate, ϵ_s; 2) time to failure (rupture time) t_r; and 3) the elongation at time of rupture. These values were determined at three different temperatures, 1600°F (871°c), 1800°F (982°c), and 2000°F (1093°c). The various material conditions were evaluated in duplicate for each stress level.

2.1.6. Cold Work and Anneal of MA754

All cold working operations were carried out by cold rolling the as-received material using a Fenn 75 HP cold rolling mill. The cold rolling mode of deformation was chosen because of the control that it permits, and because it is generally representative of the kinds of deformation systems which might be used to make the preforms for the high temperature components.

The rolling tests were performed utilizing blanks of as-received material, with typical dimensions of 4.0 x 1.5 x 0.350 inches (101.6 mm x 38.1 mm x 8.9 mm). In all cases, the cold rolling was performed in a direction parallel to the extrusion direction with no intermediate anneals, unless otherwise indicated.

The anneal treatments of cold rolled specimens were conducted utilizing a standard tube furnace with a dried argon atmosphere (unless otherwise indicated). Temperatures ranged from 1000°F to 2400°F (538°c to 1315°c) and were controlled to ±3°F (±1.7°c). Annealing times ranged from 0.5 to 4.0 hours.

2.2. Results

2.2.1. Characterization of the As-Received Material

2.2.1.1. Optical Microscopy

Optical photomicrographs of typical longitudinal and transverse sections from Bar #1 are provided in Figure 2-4. Quantitative grain dimension measurements reveal an L_{AVE} of 0.17 mm and an L/D ratio of $\sim$7.0. Material from Bars #2 and #3 exhibit a microstructure which appears to vary between that shown in Figure 2-4, and a somewhat compromised microstructure, as shown by the extensive regions of small grains, Figure 2-5. Grain size and shape measurements of this material in Figure 2-5 reveal an 84% decrease in L_{AVE} and a 65% decrease in the aspect ratio, L/D, Taboe 2-2.

2.2.1.2. Elevated Temperature Tensile Properties

The results of the tensile tests in the extrusion direction of material from Bar #1 are shown in Figure 2-6. It is significant to note that the material is very ductile at ambient temperature, and that it retains good strength and ductility at 2000°F (1093°c), indicating high usable load carrying capability and toughness at this temperature.

Figure 2-7 shows the tensile behavior of material from Bars #2 and #3 in the extrusion direction. The region between the smaller grained MA754 (Bars #2 and #3) and the larger grained as-received MA754 is cross-hatched to delineate the range in which the as-received

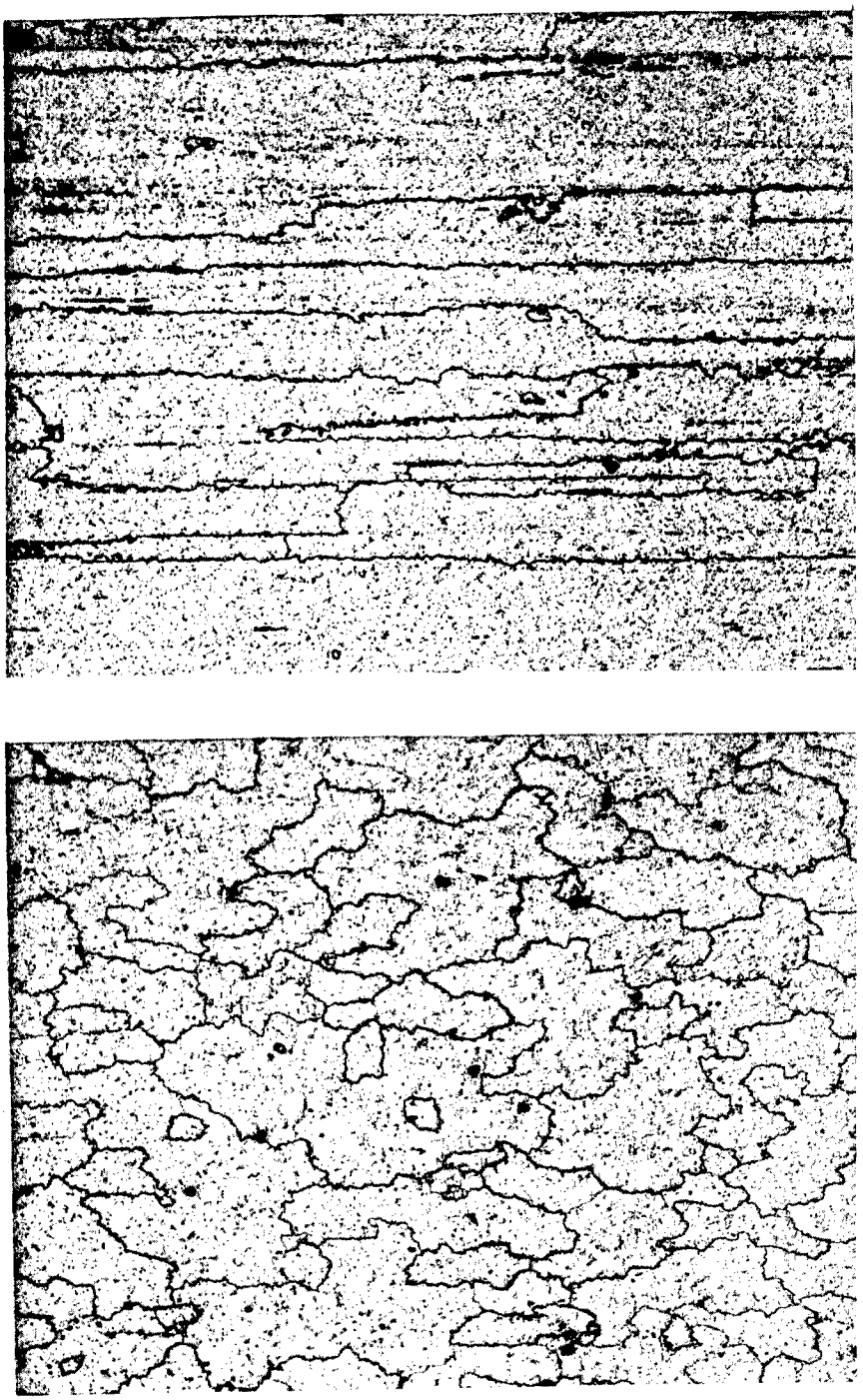

Figure 2-4. Optical Photomicrographs of a Longitudinal (Extrusion Direction) Section (TOP) and a Transverse (Cross-Extrusion Direction) Section (BOTTOM) of the MA754 Alloy Bar #1. 100X Magnification.

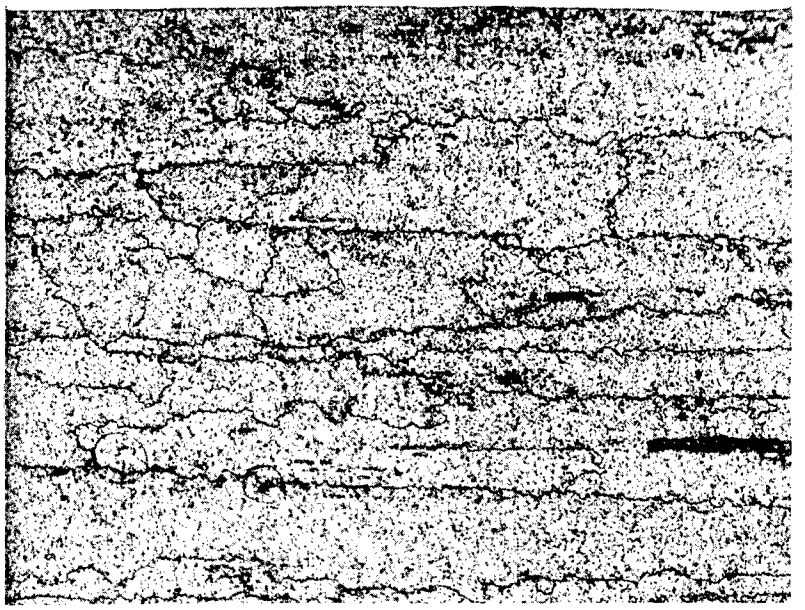

Figure 2-5. **Optical Photomicrograph of Longitudinal Section of As-Received MA754, Bar #2 and #3. Note the prevalence of small grains (etched, 160X).**

Table 2-2.

Grain Size and Shape Measurements of the As-Received MA754

	Grain Size (L_{AVE} mm)	Aspect Ratio (L/D)
Bar #1	0.1727	6.9
Bars #2 & #3	0.027	2.4

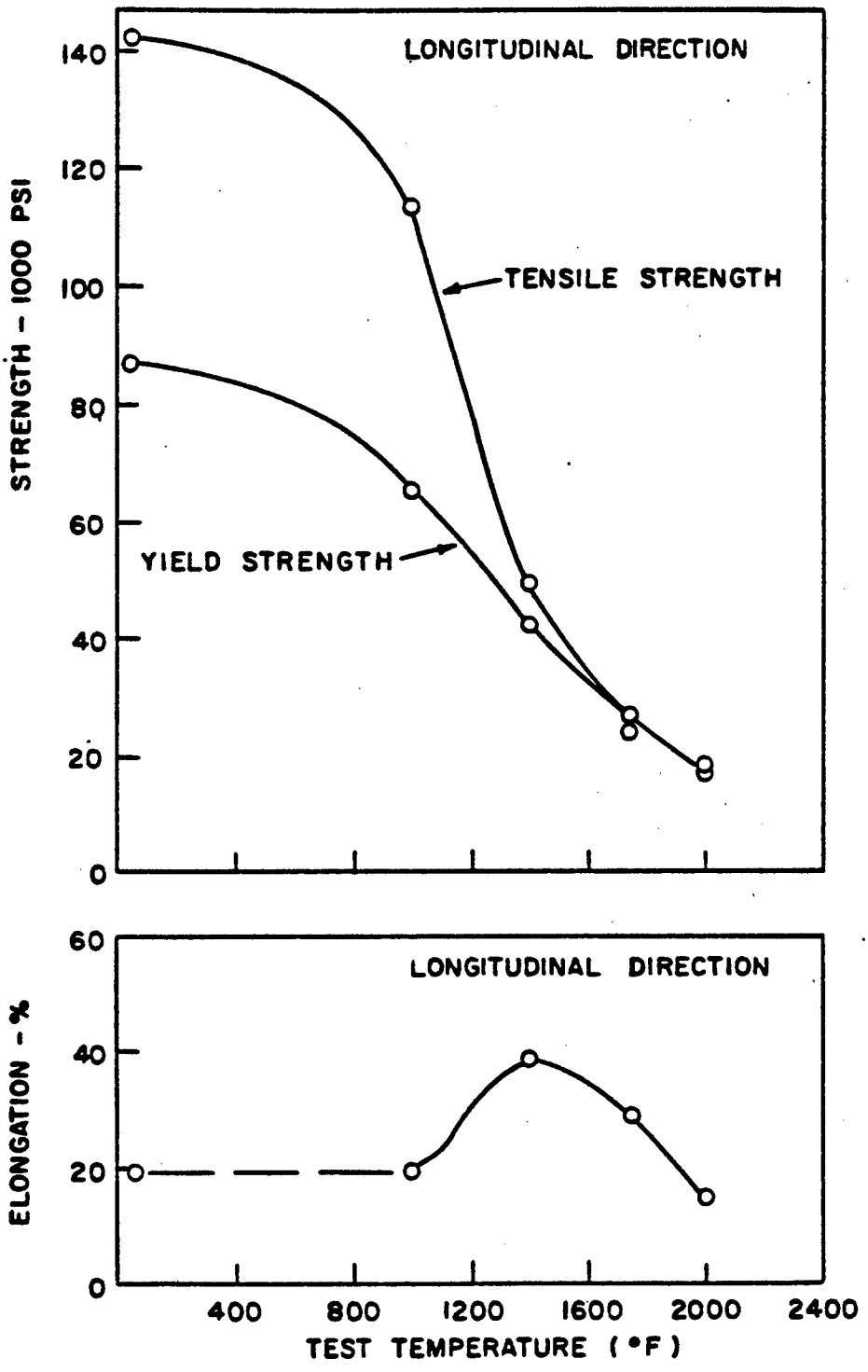

Figure 2-6. The Manner in which the Longitudinal (Extrusion Direction) Tensile Properties vary with Test Temperature for MA754 (Bar #1).

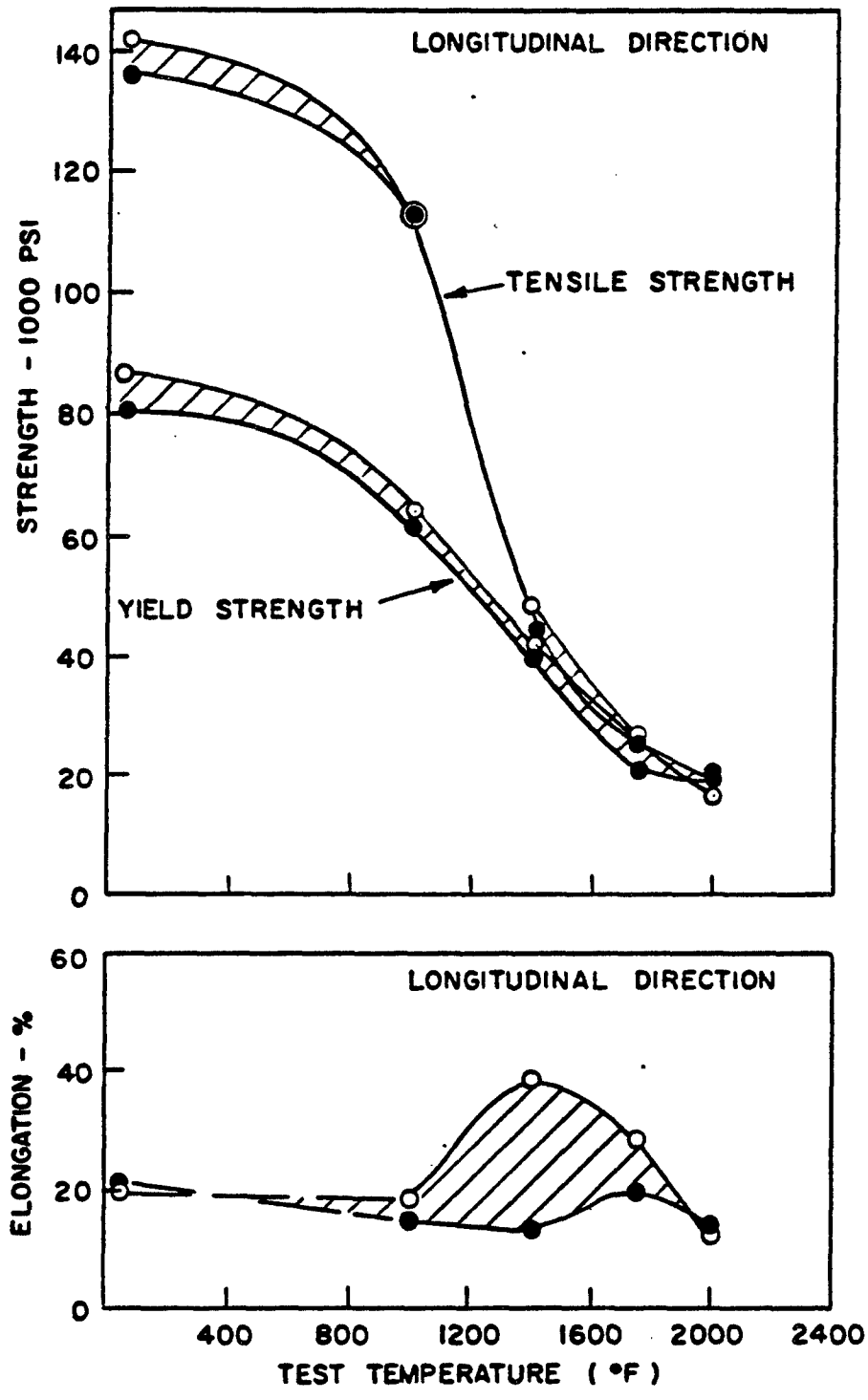

Figure 2-7. The Manner in which the Longitudinal (Extrusion Direction) Tensile Properties Vary with Test Temperature for MA754 (Bars #2 and #3).

properties could be expected to fall. Complete summaries of all longitudinal tensile data are shown in Tables 2-3 and 2-4.

Microscopic examination of longitudinal tensile piece fractures revealed two primary failure modes. At temperatures below 1000°F (538°c), transgranular failure is readily apparent, Figure 2-8. Above 1000°F, intergranular failure, accompanied by extensive cavitation, is observed, Figure 2-9.

An important feature of the intergranular mode is the intrinsic nature of the failure. Figure 2-10 is an optical photomicrograph of a longitudinal test piece section far from the fracture surface. Note that the intergranular cracking characteristic of this failure mode occurs only at transverse grain boundaries. It is apparent that any effort to improve the high temperature performance of MA754 should include a reduction in the number of transverse grain boundaries.

While it is often possible to design components so that the major loading axis is coincident with the strong material direction of the component, in many cases, the "transverse" properties play a significant role. Hence, a limited study has been done to assess the short transverse properties of MA754 from Bar #1. The results are shown in Figure 2-11.

Microstructural examination of fractured transverse tensile test specimens reveals a situation quite similar to that found in fractured longitudinal test specimens. Below 1000°F (538°c), transgranular failure predominates, Figure 2-12, while above 1000°F, intergranular failure is apparent with extensive cracking at transverse grain boundaries (Figure 2-13).

Table 2-3.

Tensile Properties As-Received MA754 Bar #1

°F	Tensile Strength (psi)	0.2% Strength (psi)	% Elongation
Ambient	142,600	87,300	20
1000	113,900	65,100	19
1400	48,800	42,400	39
1750	26,800	25,000	29
2000	18,500	17,700	15

Table 2-4.

Tensile Properties As-Received MA754 Bars #2 & #3

°F	Tensile Strength (psi)	0.2% Strength (psi)	% Elongation
Ambient	136,600	80,600	22
1000	113,600	60,800	17
1400	45,300	39,600	14
1750	25,800	20,400	21
2000	20,100	19,100	17

Figure 2-8. Optical Photomicrograph of the Mid-Section of a Longitudinal Tensile Test Piece, Bar #1, showing the Fracture Edge. Note the trans-granular fracture mode. Test conducted at ROOM TEMPERATURE. Etched Condition. 100X Magnification.

Figure 2-9. **Optical Photomicrograph of the Mid-Section of a Longitudinal Tensile Test Piece, Bar #1, showing the Fracture Edge. Note the intergranular nature of the fracture, and the extensive cavitation. Test conducted at 2000°F (1093°c). Etched Condition. 100X Magnification.**

Figure 2-10. **Optical Photomicrograph of the Midplane of a Longitudinal Tensile Test Piece (Bar #1) taken well away from the Fracture. Test conducted at 1750°F (954°c). Note the intergranular cracks at the transverse grain boundaries. Etched Condition. 100X Magnification.**

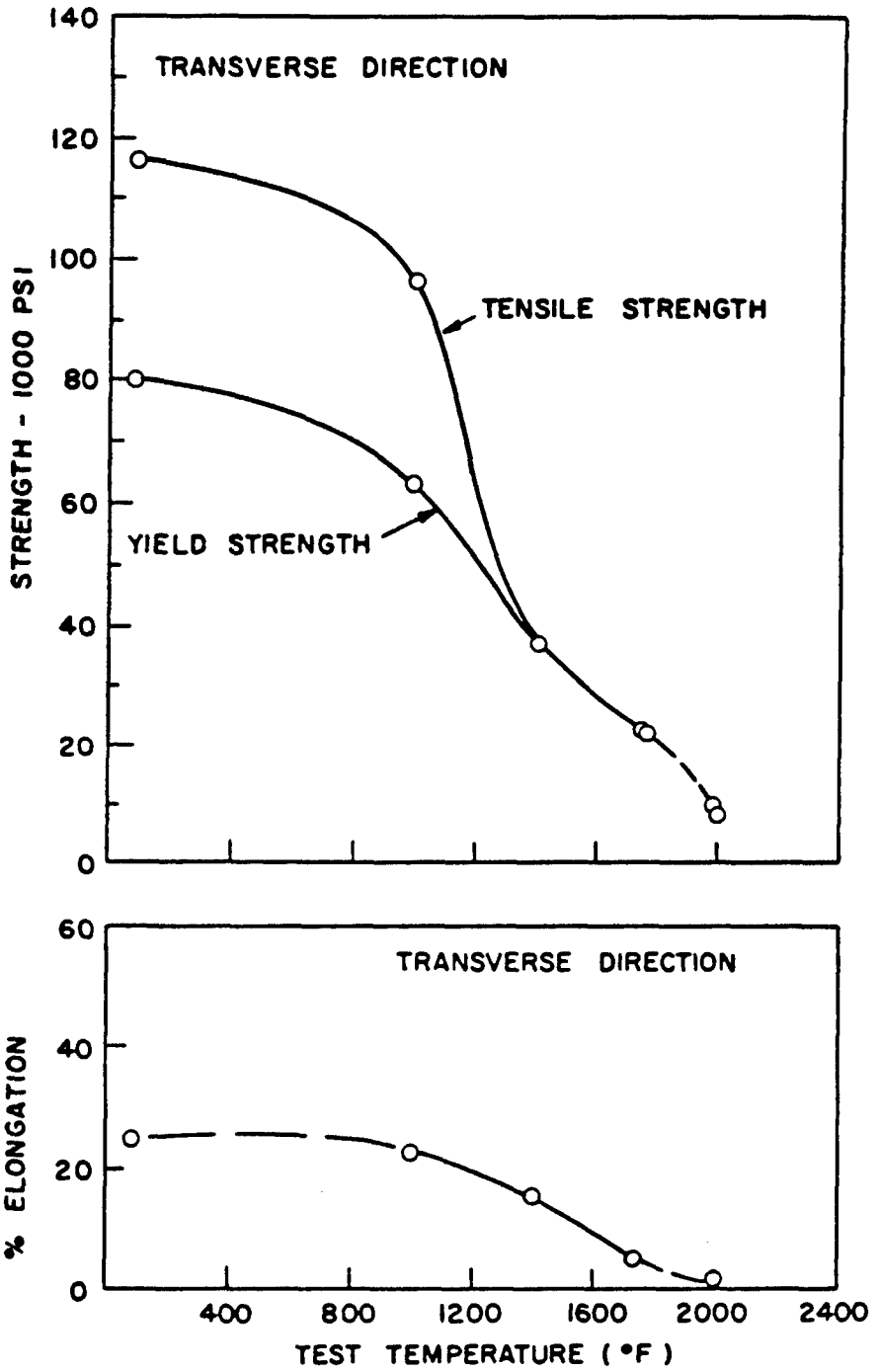

Figure 2-11. The Manner in which the Transverse (Cross-Extrusion Direction) Tensile Properties vary with Test Temperature for MA754 (Bar #1).

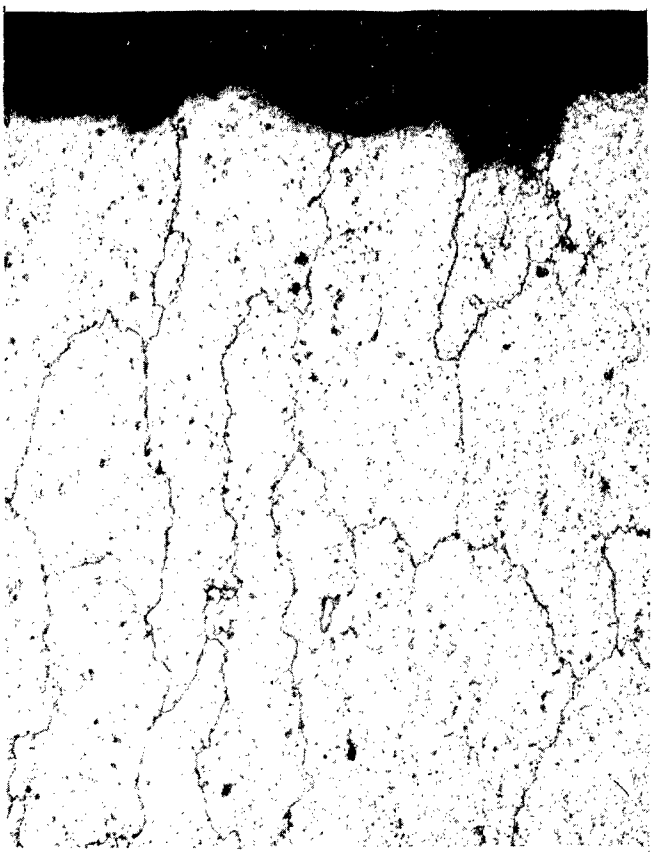

Figure 2-12. Optical Photomicrograph of the Midplane of a Transverse Tensile Test Piece, Bar #1, Tested at 1000°F (537°c), showing the Fracture Edge. Note the transgranular fracture mode. 200X Magnification. Etched Condition.

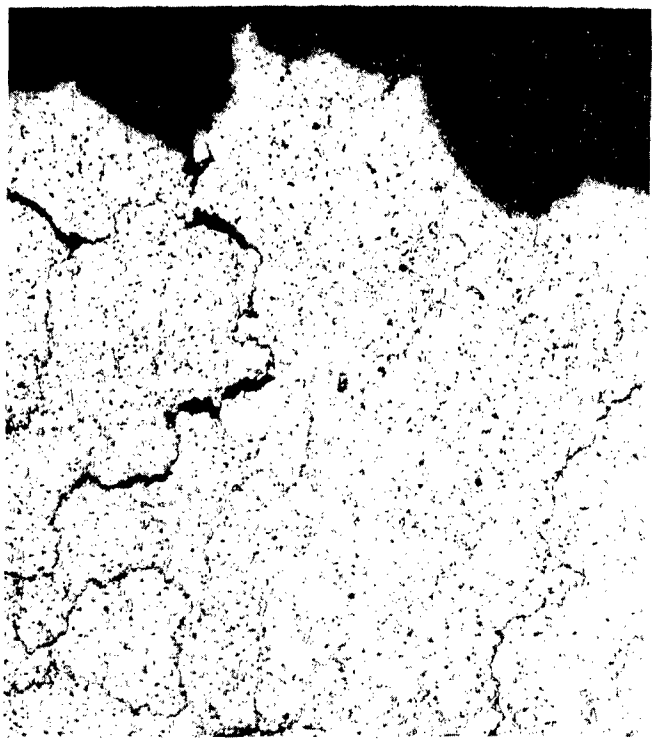

Figure 2-13. Optical Photomicrograph of the Midplane of a Transverse Tensile Test Piece, Bar #1, Tested at 1400°F (760°c), showing the Fracture Edge. Note the intergranular fracture mode, and the extensive cavitation. 200X Magnification. Etched Condition.

2.2.1.3. Elevated Temperature Creep Properties

Creep behavior was evaluated as a function of stress at 1600°F (871°c), 1800°F (982°c) and 2000°F (1093°c) for the as-received material, Tables 2-5 through 2-9. As with the longitudinal tensile data, the creep data of Bars #2 and #3 should be considered to fall within the region defined by the limits of microstructure. In addition, Figures 2-14 and 2-15 reveal typical creep curves for material tested at 1600°F (871°c) and 1800°F (982°c).

Figures 2-16 and 2-17 show the steady state creep rate as a function of applied stress at 1600°F (871°c) and 1800°F (982°c) for the material from Bar #1. The stress dependence of MA754 in creep is quantified by the stress exponent, n, which is related to the steady state creep rate and the applied stress by the following relation: $\dot{\epsilon}_s \propto \sigma^n$

By plotting $\ln \dot{\epsilon}_s$ versus $\ln \sigma a$, the stress exponent, n, can be determined as the slope of the curve.

According to Figures 2-16 and 2-17, the stress exponent of MA754 (Bar #1) at 1600°F (871°c) is 19.6, and at 1800°F (982°c) is 28.2. As a result, it would appear that the stress dependence is not independent of temperature. However, these values are consistent with the high stress dependence of the steady state creep rate observed for ODS materials.

Metallography of failed specimens of MA754 revealed that fracture is intergranular at the temperatures studied. It is important to note that this failure mode is the same as that observed upon microstructural examination of longitudinal tensile specimen frac-

Table 2-5.

Creep-Rupture Properties of the As-Received MA754 Bar #1 at 1600°F (871°c)

Stress Level (Fraction of Tensile Strength at 1600°F)*	Minimum Creep Rate (In. per In. per Sec.)	Rupture Time (Hours)	Rupture Elongation (%)	Total Time (Non-Rupture) (Hours)**
0.57	1.48×10^{-9}	—	—	238.0
0.65	7.94×10^{-9}	—	—	253.0
0.70	4.72×10^{-8}	347.0	11.0	—
0.75	4.38×10^{-7}	41.5	14.0	—

*Longitudinal Tensile Strength at 1600°F is ~ 35,000 psi.
**Tests interrupted prior to fracture.

Table 2-6.

Creep-Rupture Properties of the As-Received MA754 Bar #1 at 1800°F (982°c)

Stress Level (Fraction of Tensile Strength at 1800°F)*	Minimum Creep Rate (In. per In. per Sec.)	Rupture Time (Hours)	Rupture Elongation (%)	Total Time (Non-Rupture) (Hours)**
0.75	5.19×10^{-9}	—	—	338.0
0.80	3.77×10^{-8}	205.5	8.6	—
0.85	1.55×10^{-7}	70.0	10.0	—
0.90	9.83×10^{-7}	19.7	12.6	—

*Longitudinal Tensile Strength at 1800°F is ~ 25,000 psi.
**Tests interrupted prior to fracture.

Table 2-7.

Creep-Rupture Properties of the As-Received MA754 Bar #1 at 2000°F (1093°c)

Stress Level (Fraction of Tensile Strength at 2000°F)*	Minimum Creep Rate (In. per In. per Sec.)	Total Time (Non-Rupture) (Hours)**
0.60	1.6×10^{-8}	117.0
0.50	6.1×10^{-9}	118.5

*Longitudinal Tensile Strength at 2000°F is ~ 20,000 psi.
**Tests interrupted prior to fracture.

Table 2-8.

Creep-Rupture Properties of the As-Received MA754 Bars #2 & #3 at 1600°F (871°c)

Stress Level (Fraction of Tensile Strength at 1600°F)*	Minimum Creep Rate (In. per In. per Sec.)	Rupture Time (Hours)	Rupture Elongation (%)	Total Time (Non-Rupture) (Hours)**
0.50	1.36×10^{-9}	—	—	210.2
0.70	1.22×10^{-7}	103.0	8.0	—
0.75	1.61×10^{-6}	9.7	11.0	—

*Longitudinal Tensile Strength at 1600°F is ~ 35,000 psi.
**Tests interrupted prior to fracture.

Table 2-9.

Creep-Rupture Properties of the As-Received MA754 Bars #2 & #3 at 1800°F (982°c)

Stress Level (Fraction of Tensile Strength at 1800°F)*	Minimum Creep Rate (In. per In. per Sec.)	Rupture Time (Hours)	Rupture Elongation (%)	Total Time (Non-Rupture) (Hours)**
0.40	1.3×10^{-8}	—	—	182.2
0.70	1.24×10^{-6}	6.1	15.0	—
0.85	1.6×10^{-5}	2.2	19.8	—

*Longitudinal Tensile Strength at 1800°F is ~ 25,000 psi.
**Tests interrupted prior to fracture.

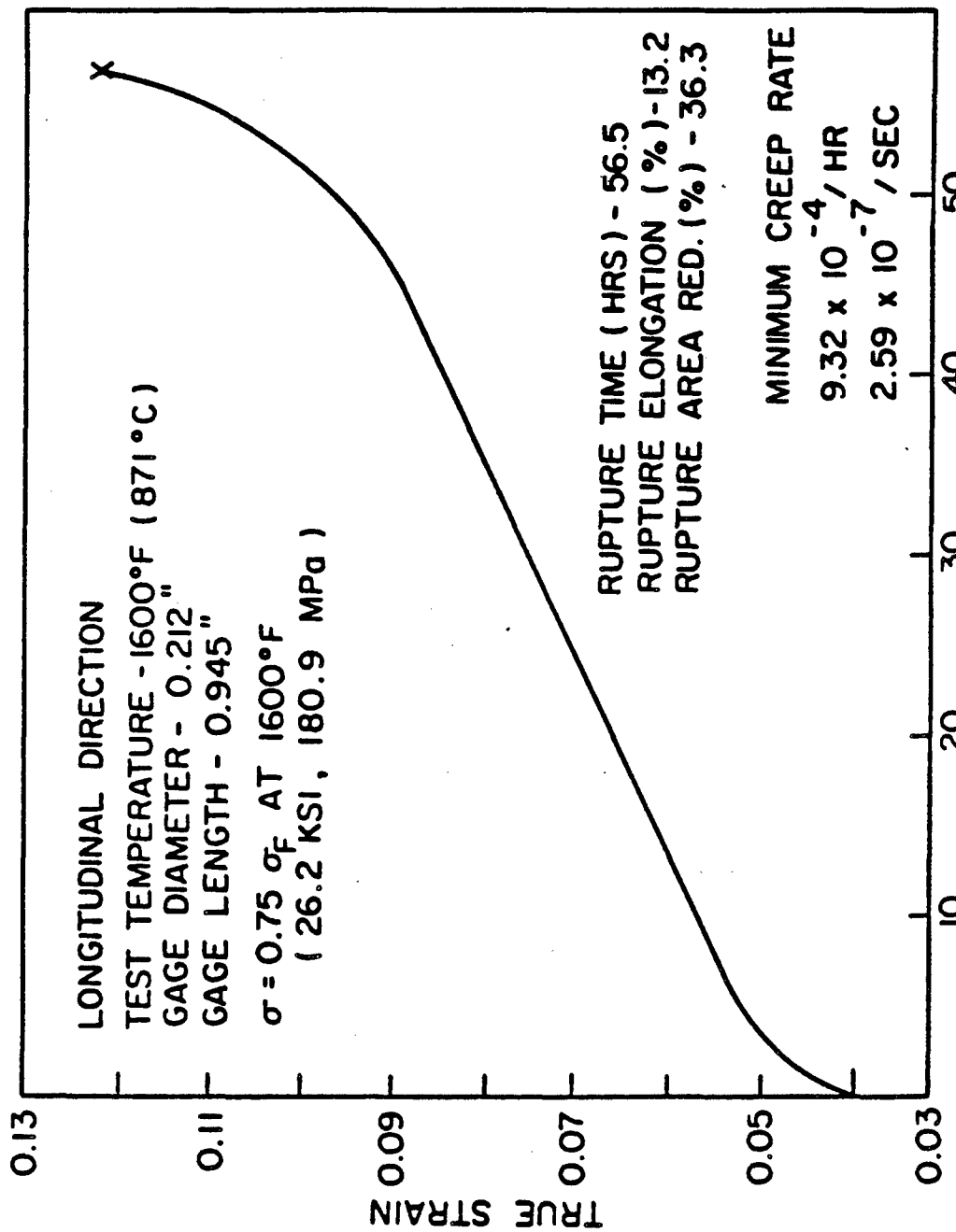

Figure 2-14. Creep Rupture Curve for the MA754 Tested at 1600°F (Bar #1).

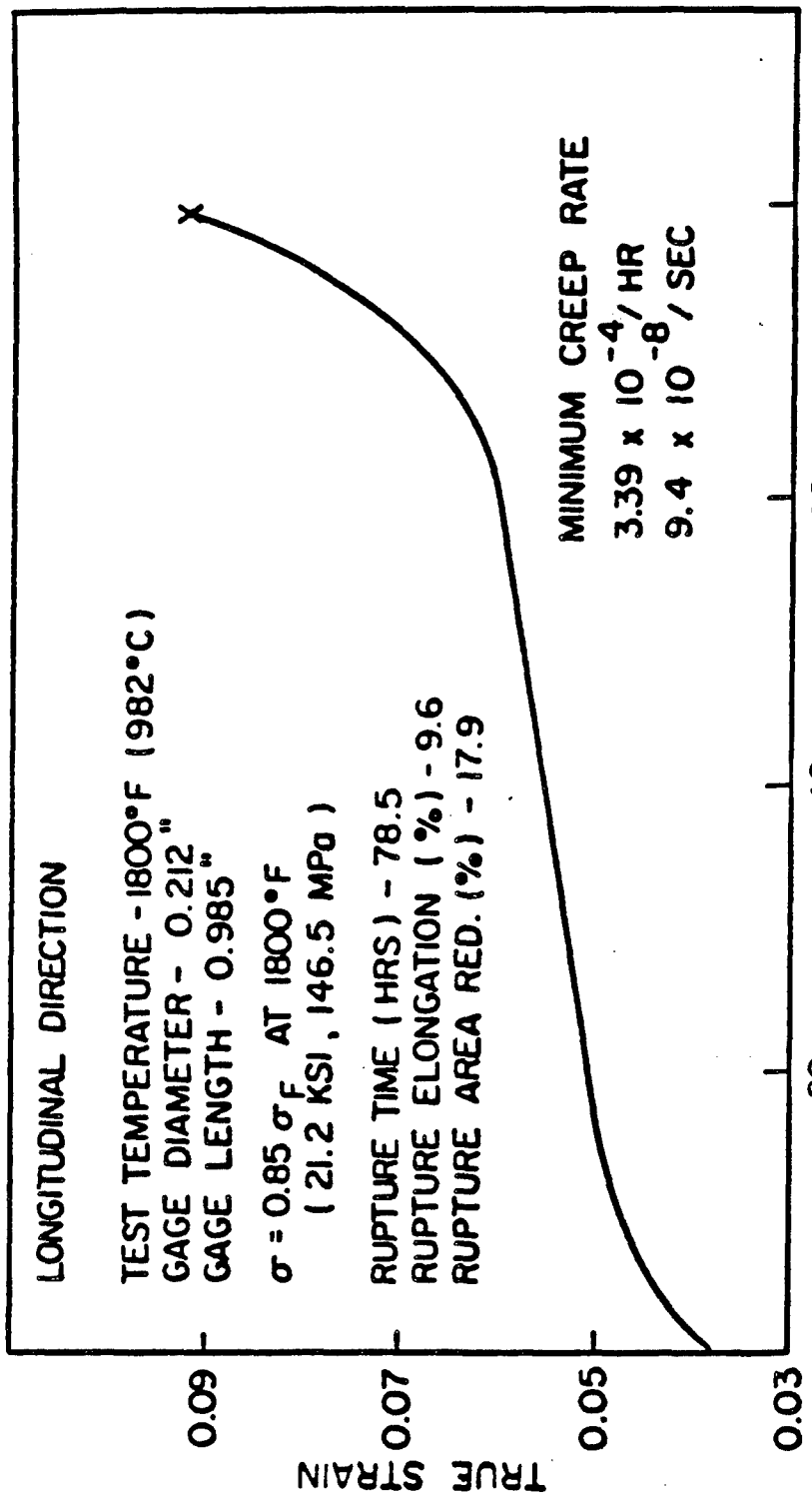

Figure 2-15. Creep Rupture Curve for the MA754 Tested at 1800°F (Bar #1).

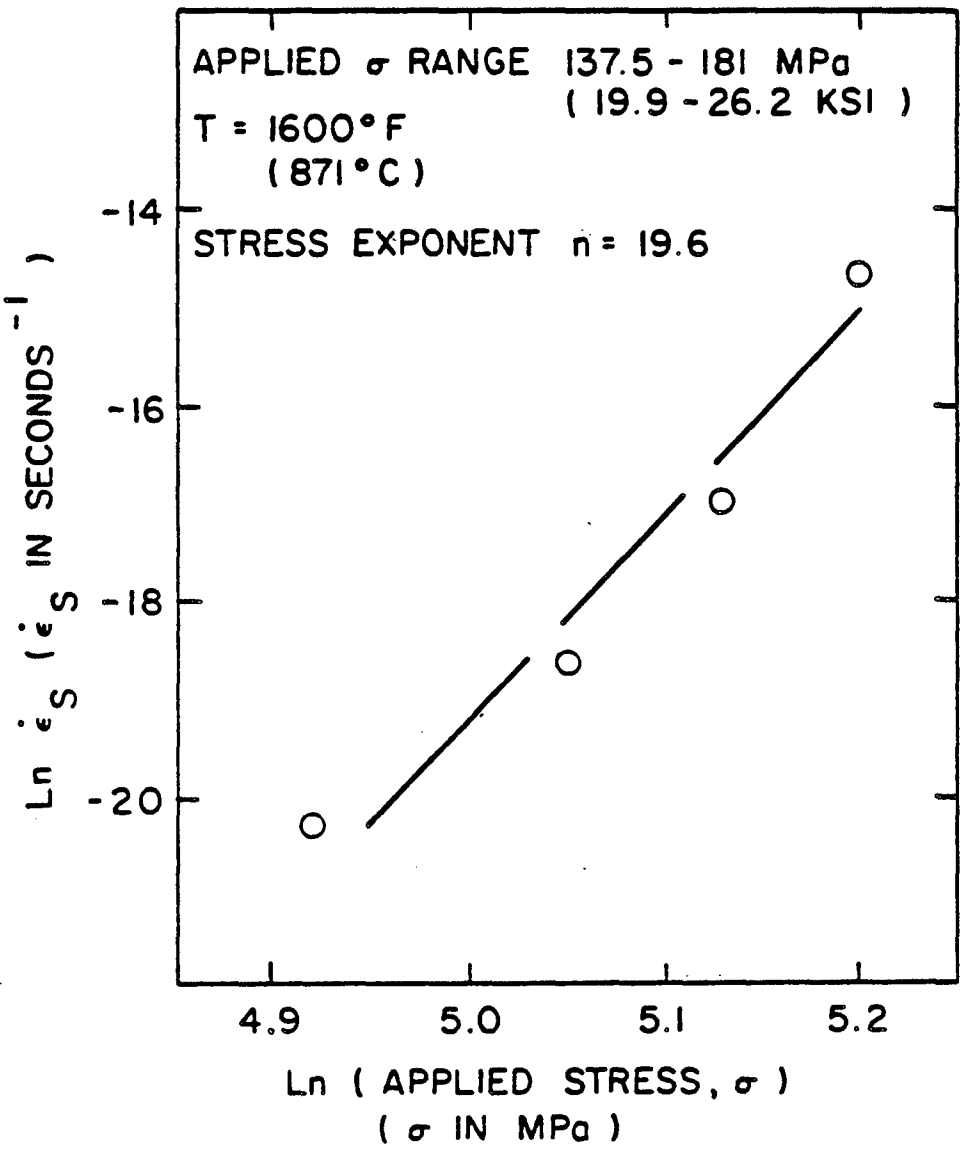

Figure 2-16. Ln (Steady State Creep Rate) vs. Ln (Applied Stress) for the As-Received MA754 Alloy in Creep at 1600°F (871°c), (Bar #1).

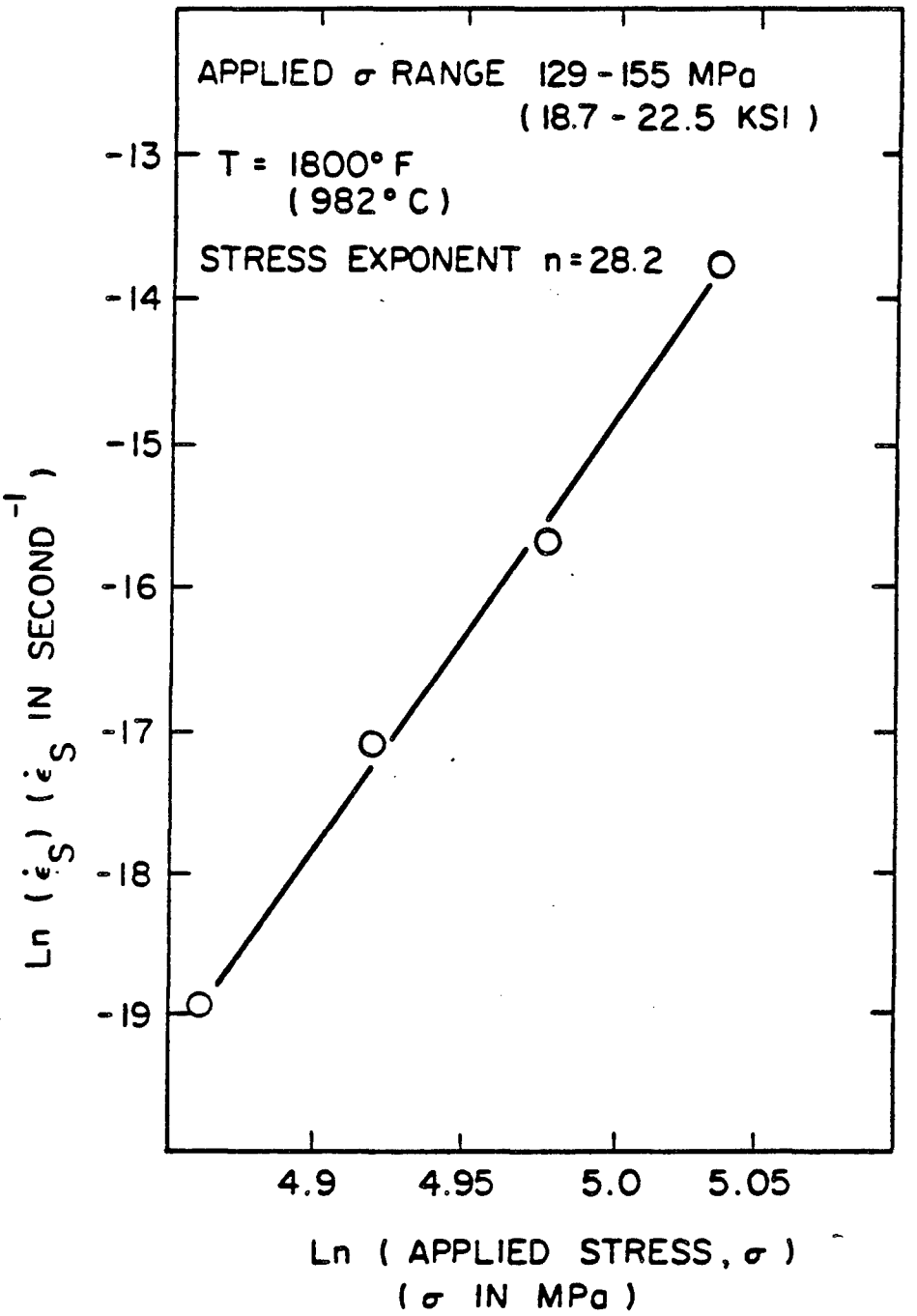

Figure 2-17. Ln (Steady State Creep Rate) vs. Ln (Applied Stress) for the As-Received MA754 Alloy in Creep at 1800°F (982°c), (Bar #1).

tures (Figure 2-10).

2.2.1.4. Creep Characterization of MA754 Under Constant Load

Most creep-rupture testing performed during this investigation utilized leveled creep racks modified to produce constant stress rather than constant load. While constant load tests are convenient and may approximate some types of service conditions, constant stress tests are needed to gain an understanding of the nature of the deformation process. However, for the purposes of comparing the results of this investigation with published data, a limited study was undertaken to generate creep-rupture data for the MA754 alloy under the constant load condition.

Table 2-10. shows the results of these tests along with the results of constant stress creep testing for the same material at the same stress levels. The data indicates that there is no difference in minimum creep rate when the material is tested at the highest stress level. However, when the applied stress is decreased, the material tested under the constant load condition produces a minimum creep rate that is significantly greater than that tested under the constant stress condition.

2.2.1.5. Structure-Property Variations of the As-Received MA754 Material

As stated earlier, the material from Bars #2 and #3 was found to exhibit a grain structure that was quite variable. Due to the complexity of the manufacturing process, the final material state is dependent upon several factors, such as hot working temperature,

Table 2-10.

Creep Properties of the As-Received MA754 (Bars #2 & #3) Tested under Two Conditions at 1800°F (982°c)

CONDITION: CONSTANT LOAD

Stress Level* (Fraction of Tensile Strength at 1800°F)	Minimum Creep Rate ($\dot{\epsilon}$/s)
0.85	7.5×10^{-6}
0.70	3.0×10^{-8}
0.60	1.0×10^{-8}

CONDITION: CONSTANT STRESS

Stress Level* (Fraction of Tensile Strength at 1800°F)	Minimum Creep Rate ($\dot{\epsilon}$/s)
0.85	6.86×10^{-6}
0.70	5.6×10^{-9}
0.60	2.3×10^{-9}

*Longitudinal Tensile Strength at 1800°F is ~ 25,000 psi.

working strain and strain rate, and the influence of thermal gradients during annealing. As a result of these factors, the material structure can be expected to vary from the edge of the bar to the center, and from the front of the bar to the back. However, the grain structure variability found in Bars #2 and #3 was much more than expected.

Creep-rupture properties of the as-received material were most affected by the variability in grain structure. For example, at 1800°F (982°c) and 21.2 KSI, the material from Bars #2 and #3 was found to exhibit a 100-fold increase in minimum creep rate and a 30-fold decrease in rupture life when compared to material from Bar #1. At 1600°F (871°c), the effect is somewhat less, due to the decreased stress sensitivity of the material at that temperature. Manufacturer's specifications allow for a 3- to 7-fold difference in rupture properties.

2.2.2. Ambient Temperature Deformation and Annealing Response of MA754

As stated earlier, the primary purpose of this investigation was one of pursuing the implications of the beneficial effects of stress relaxation treatments through a basic study of the mechanisms governing the deformation and annealing response of MA754. In other words, one of the intents of the study was that of determining whether or not it might be possible to develop a technique whereby the alloy can be cold worked usable amounts, while at the same time maintaining a favorable grain morphology. All cold work (rolling)

experiments were conducted utilizing material from Bar #1.

2.2.2.1. Cold Rolling the MA754 Material

In order to find the degree to which the ODS alloy MA754 was amenable to ambient temperature deformation for pre-form purposes, rolling tests were performed on a blank of the as-received material, Figure 2-18. The blank was found to be amenable to rolling to a thickness reduction of at least 70%, with no intermediate anneals. The cold rolling was halted At 70% reduction so that the rolled piece was thick enough for subsequent annealing processing and property evaluation. It appeared that the material was capable of even more cold rolling reduction, because, at the time the rolling was stopped, there was no evidence of edge or side cracking of the piece.

Cold rolling of the MA754 blank greatly improved the aspect ratio of the long grains, and produced flattening in the short transverse direction. Figure 2-19 shows the longitudinal and transverse microstructures of the rolled material.

In order to determine if a reduction in the amount of stored strain energy would influence the annealing response of cold rolled MA754, a second effort involved cold rolling a blank of MA754 to 35% reduction in thickness, Figure 2-20.

2.2.2.2. Recrystallization Response

After cold rolling the as-received alloy, attempts were made to develop appropriate strain energy relaxation treatments in order to stabilize the improved grain morphologies shown in Figures 2-19 and 2-20. This becomes necessary because, without it, recrystallization

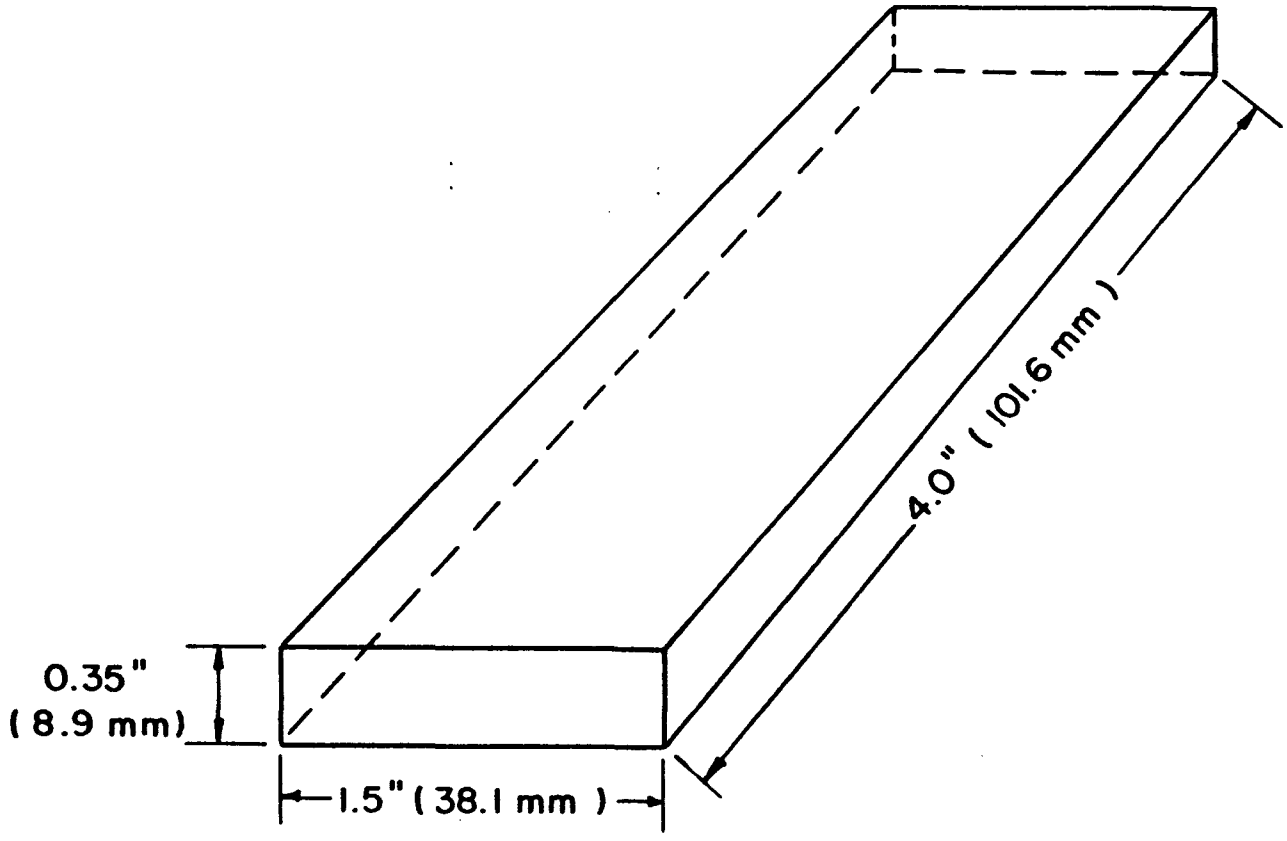

Figure 2-18. Schematic illustration depicting the typical rolling blank specimen design utilized in this investigation.

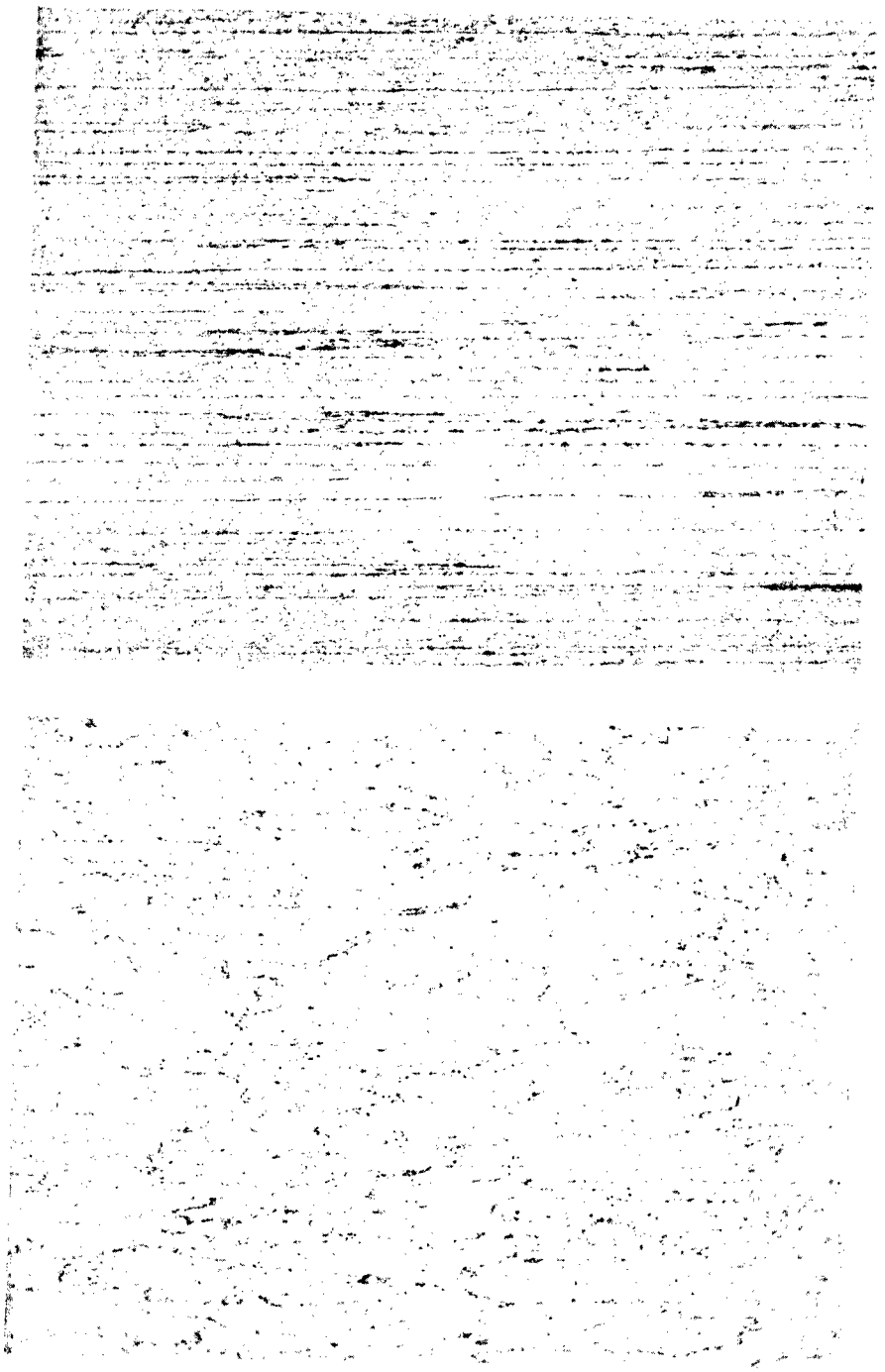

Figure 2-19. Optical Photomicrographs of a Longitudinal (TOP) and a Transverse (BOTTOM) Section of a Cold Rolled Plate of CDS Alloy, MA754. (70% Reduction in Thickness by Rolling; 100X Magnification; Etched Condition).

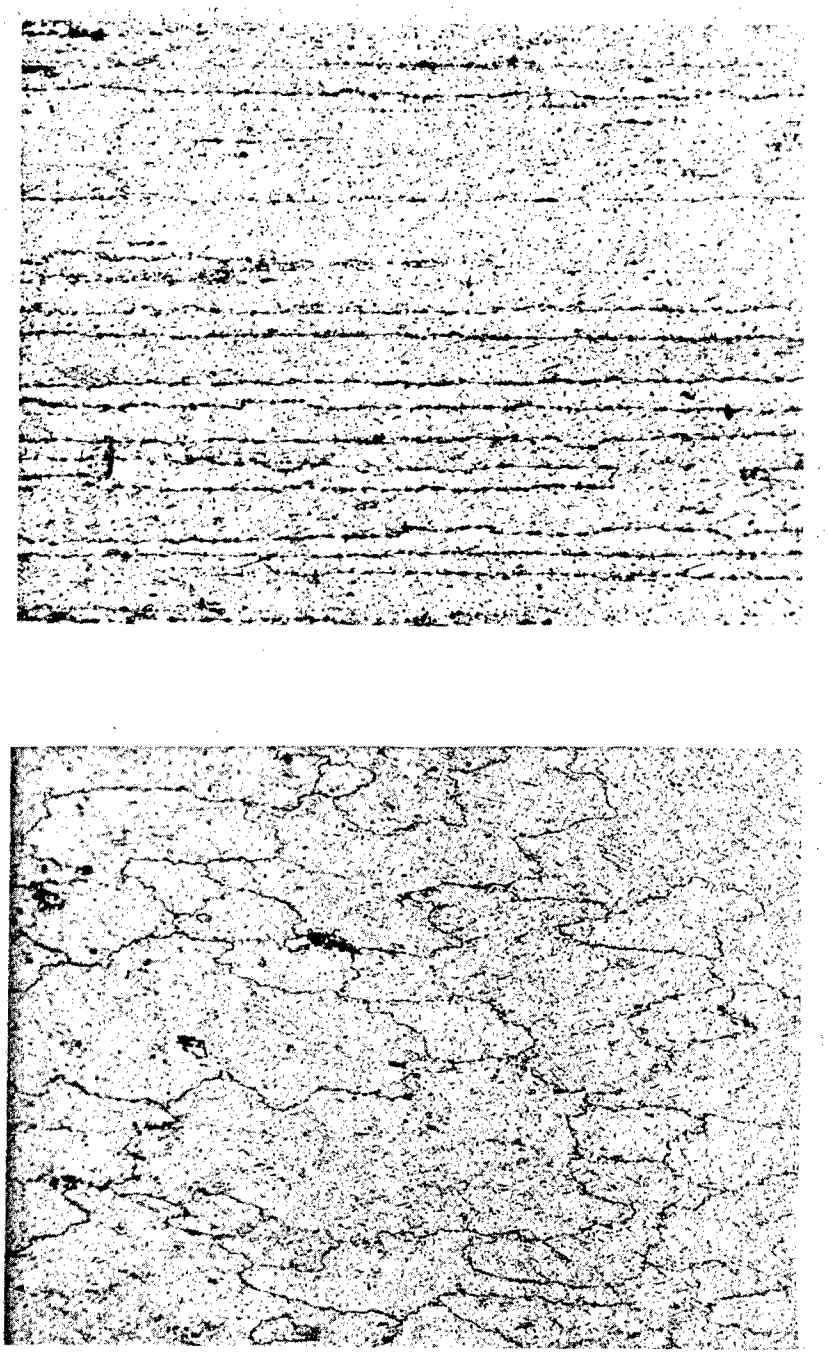

Figure 2-20. Optical Photomicrographs of a Longitudinal (TOP) and a Transverse (BOTTOM) Section of a Cold Rolled Plate of ODS Alloy MA754 (35% Reduction in Thickness by Rolling; 160X Magnification; Etched Condition).

of unfavorable small grain sizes would occur at the high use temperatures.

As a prelude to the development of the treatment, the recrystallization responses of MA754 cold rolled 70% and 35% were determined from separate annealing experiments. Specimens were machined from the as-rolled blanks, and annealed for 4 hours at specified temperatures from 1000°F to 2400°F (538°c to 1315°c). The anneals were conducted utilizing a standard tube furnace with a dried argon atmosphere.

Figures 2-21 and 2-22 are the recrystallization curves for the cold rolled materials. For MA754 cold rolled 70%, the annealing temperature at which fine, equiaxed grains were first noted was 1200°F (649°c) corresponding to an approximate 5% drop in hardness as compared to the as-rolled material. For MA754 cold rolled 35%, the temperature at which recrystallization was first apparent was 1500°F (815°c), this resulted in a 10% drop in hardness as compared to the as-rolled hardness value. These temperatures are important because it is the temperature limit for all the possible actions of strain relaxation mechanisms prior to recrystallization. The hardness values for each of the recrystallization curves are shown in Tables 2-11 and 2-12.

2.2.2.3. Intermediate Anneal Response of Cold Rolled MA754

In order to test the effectiveness of the possible action of strain relaxation mechanisms in preventing the recrystallization of MA754 cold rolled 70% and 35%, the following experiments were performed:

A) As-received MA754 Cold Rolled 70% + Anneal at 1200°F, 4 Hours + Final Anneal at 2400°F, 4 Hours.

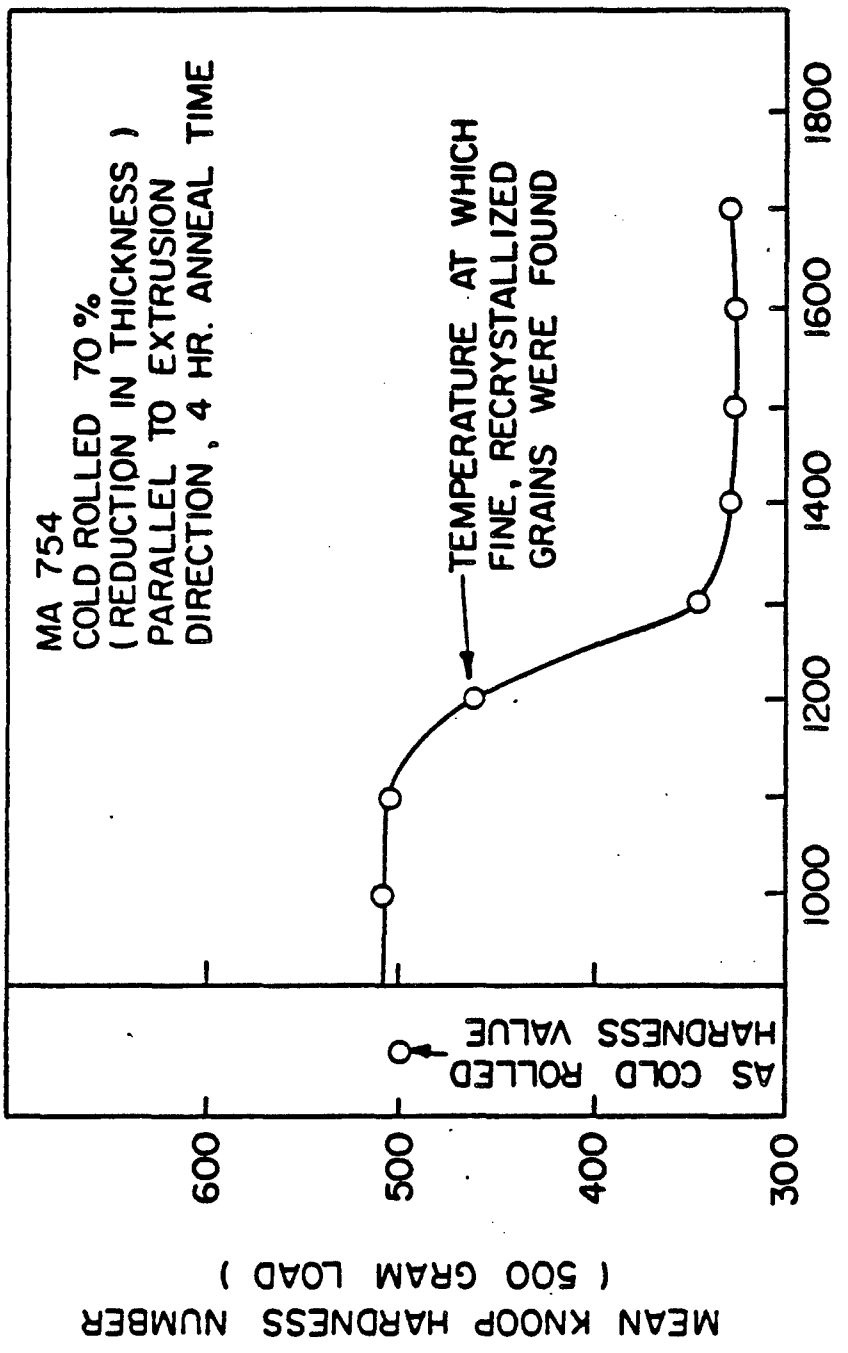

Figure 2-21. Recrystallization Curve for MA754 Cold Rolled 70% (Reduction Thickness) Parallel to the Extrusion Direction.

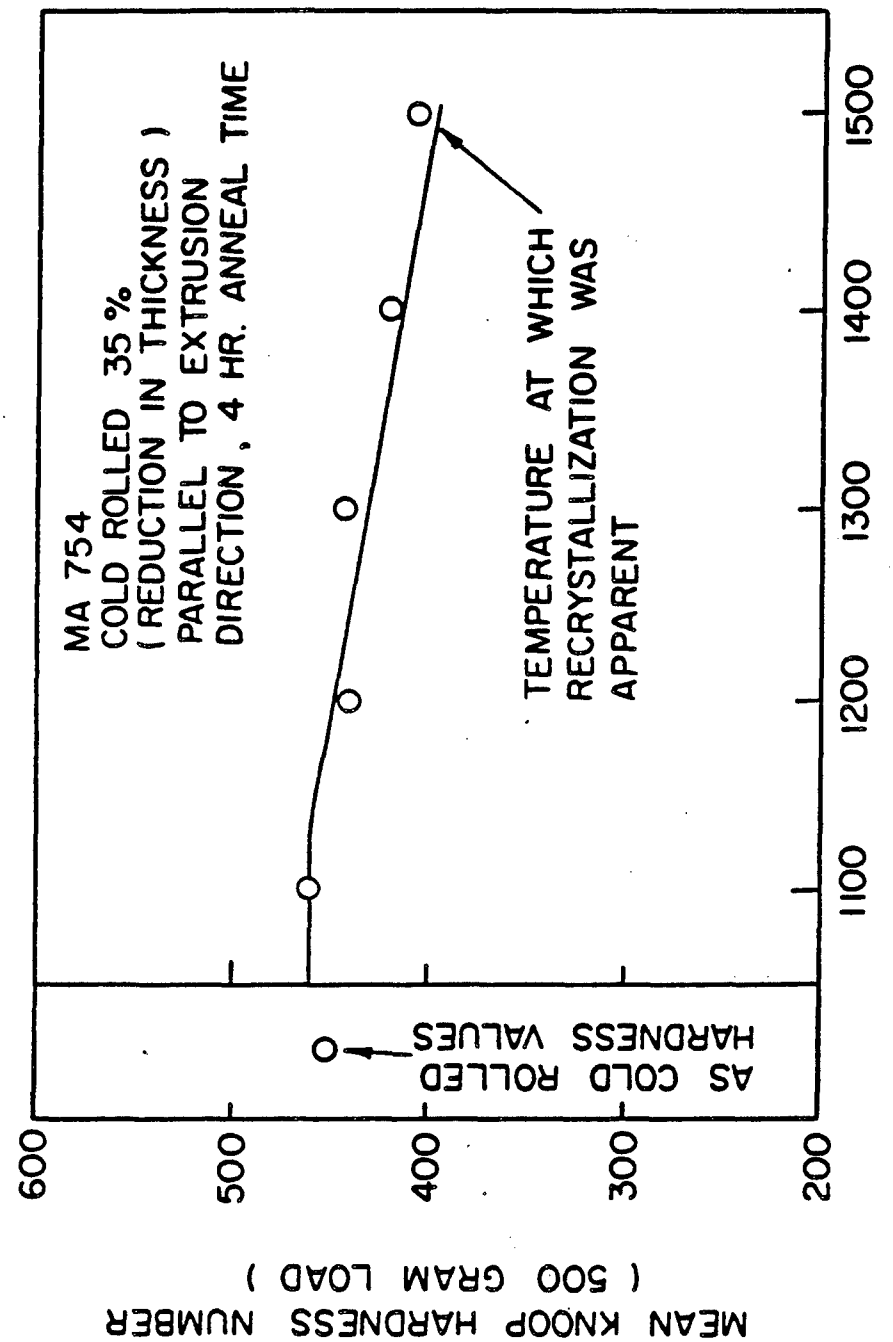

Figure 2-22. Recrystallization Curve for MA754 Cold Rolled 35% (Reduction in Thickness) Parallel to the Extrusion Direction.

Table 2-11.

Hardness Values for MA754 Alloy Cold Rolled 70%* Reduction in Thickness and Annealed at Various Temperatures**

Anneal Temperature (°F)	Mean Knoop Hardness Number (500 Gram Load)
As Rolled	499.6
1000	505.9
1100	503.1
1200	467.4
1300	346.4
1400	334.1
1500	332.5
1600	330.2
1700	333.2

*Rolling was performed in a direction parallel to the hot extrusion direction.
**Annealing time was 4 hours.

Table 2-12.

Hardness Values for MA754 Alloy Cold Rolled 35%* Reduction in Thickness and Annealed at Various Temperatures**

Anneal Temperature (°F)	Mean Knoop Hardness Number (500 Gram Load)
As Rolled	458.9
1100	460.2
1200	441.3
1300	443.6
1400	421.8
1500	407.8

*Rolling was performed in a direction parallel to the hot extrusion direction.
**Annealing time was 4 hours.

B) As-received MA754 Cold Rolled 70% + Anneals at 1100°F, 1200°F, and 1300°F, 4 Hours Each + Final Anneal at 2400°F, 4 Hours.

C) As-received MA754 Cold Rolled 70% + Anneal at 2400°F, 4 Hours.

D) As-received MA754 Cold Rolled 35% + Anneal at 2400°F, 4 Hours.

E) As-received MA754 Cold Rolled 35% + Anneal at 1400°F, 4 Hours + Final Anneal at 2400°F, 4 Hours.

F) As-received MA754 Cold Rolled 35% + Anneal at 1100°F, 1200°F, 1300°F, 1400°F, 4 Hours Each + Final Anneal at 2400°F, 4 Hours.

Figure 2-23 is an optical photomicrograph revealing a microstructure common to samples A through C. Figure 2-24 is an optical photomicrograph revealing a microstructure common to samples D through F. It became apparent that the intermediate anneals have no effect on structure, since all samples of a particular reduction produced a similar microstructure upon annealing at 2400°F (1315°c).

The recrystallization response of MA754 appears to be controlled by primary recrystallization concepts in the following manners.
1) The recrystallized grain size depends upon the amount of deformation given to the specimens before annealing; the grain size increases with decreasing deformation. This is clearly evident in Figures 2-23 and 2-24, and even more so in Figures 2-25 and 2-26, which reveal the microstructure of MA754 cold rolled 20% and annealed at 2400°F for 4 hours in air. Some sections of the sample have a recrystallized

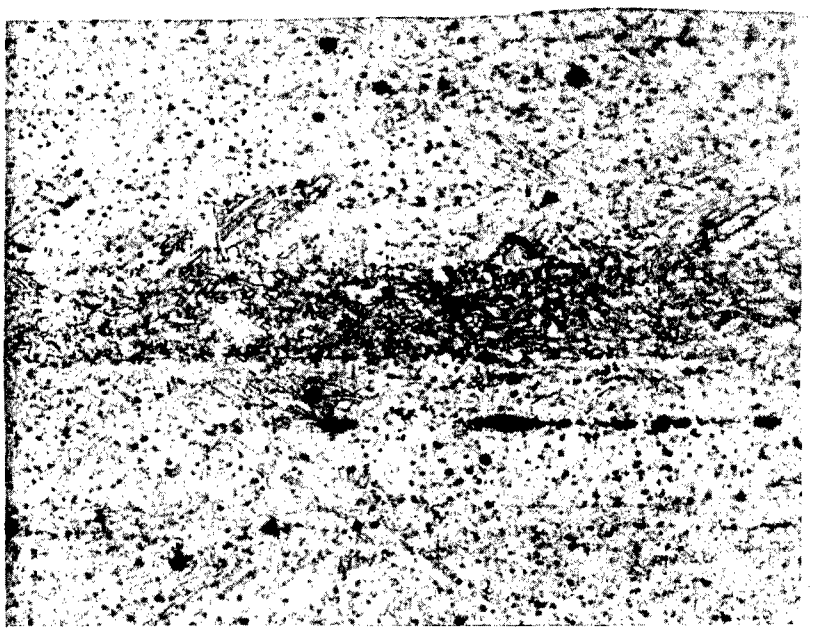

Figure 2-23. Optical Photomicrograph of a Longitudinal Section of MA754 Cold Rolled 70% (Reduction in Thickness) and Annealed 4 hours at 2400°F (1315°c). (Etched Condition; 680X).

Figure 2-24. Optical Photomicrograph of a Longitudinal Section of MA754 Cold Rolled 35% (Reduction in Thickness) and Annealed at 2400°F (1315°c) for 4 Hours. (Etched Condition; 420X)

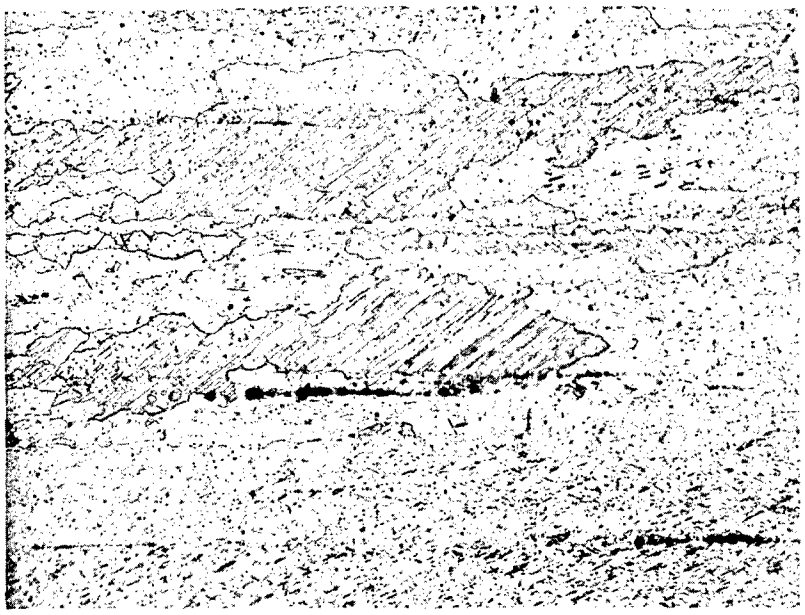

Figure 2-25. Optical Photomicrograph of a Longitudinal Section of MA754 Cold Rolled 20% (Reduction in Thickness) and Annealed 4 hours at 2400°F (1315°c) Revealing a Structure similar to that found in samples Cold Rolled 35% and Annealed at 2400°F (Figure 2). (Etched Condition; 160X).

Figure 2-26. Optical Photomicrograph of a Longitudinal Section of MA754 Cold Rolled 20% (Reduction in Thickness) and Annealed 4 hours at 2400°F (1315°c) Revealing a Stable Cold Worked Structure. (Etched Condition; 160X).

structure similar to that shown in Figure 2-24 (35% reduction plus anneal), while others appear to have a more favorable grain morphology. 2) Recrystallization is promoted by increasing amounts of cold work. The samples with the larger amount of cold work recrystallized much faster than with the lesser reduction, as shown by the recrystallization curves in Figures 2-21 and 2-22.

2.2.2.4. Elevated Temperature Tensile Properties of Cold Worked and Annealed MA754

In order to determine the basic strength and ductility of MA754 cold rolled 35% and annealed at 2400°F (1315°c) for 4 hours in air, tensile tests were performed at temperatures ranging from ambient to 2000°F (1093°c). The specimen design used to examine the tensile properties is shown in Figure 2-2.

Figure 2-27 reveals the tensile behavior of the cold rolled plus annealed material in addition to the tensile properties of the as-received alloy (Bar #1). These results show that strength values of the material were unaffected by the cold work plus anneal treatment. However, the cold rolled plus annealed material had lost a certain amount of ductility, especially at the higher temperatures when compared to the as-received material. On the other hand, it is possible to recover some of the tensile ductility by reducing the amount of cold work as shown by Table 2-14 that reveals the results of tension tests conducted at 2000°F (1093°c) with MA754 cold rolled 20% and annealed at 2400°F for 4 hours in air. The individual tensile property values of MA754 cold rolled 35% + Anneal at 2400°F are contained in Table 2-13.

Microscopic examination of MA754 cold rolled 35% plus annealed

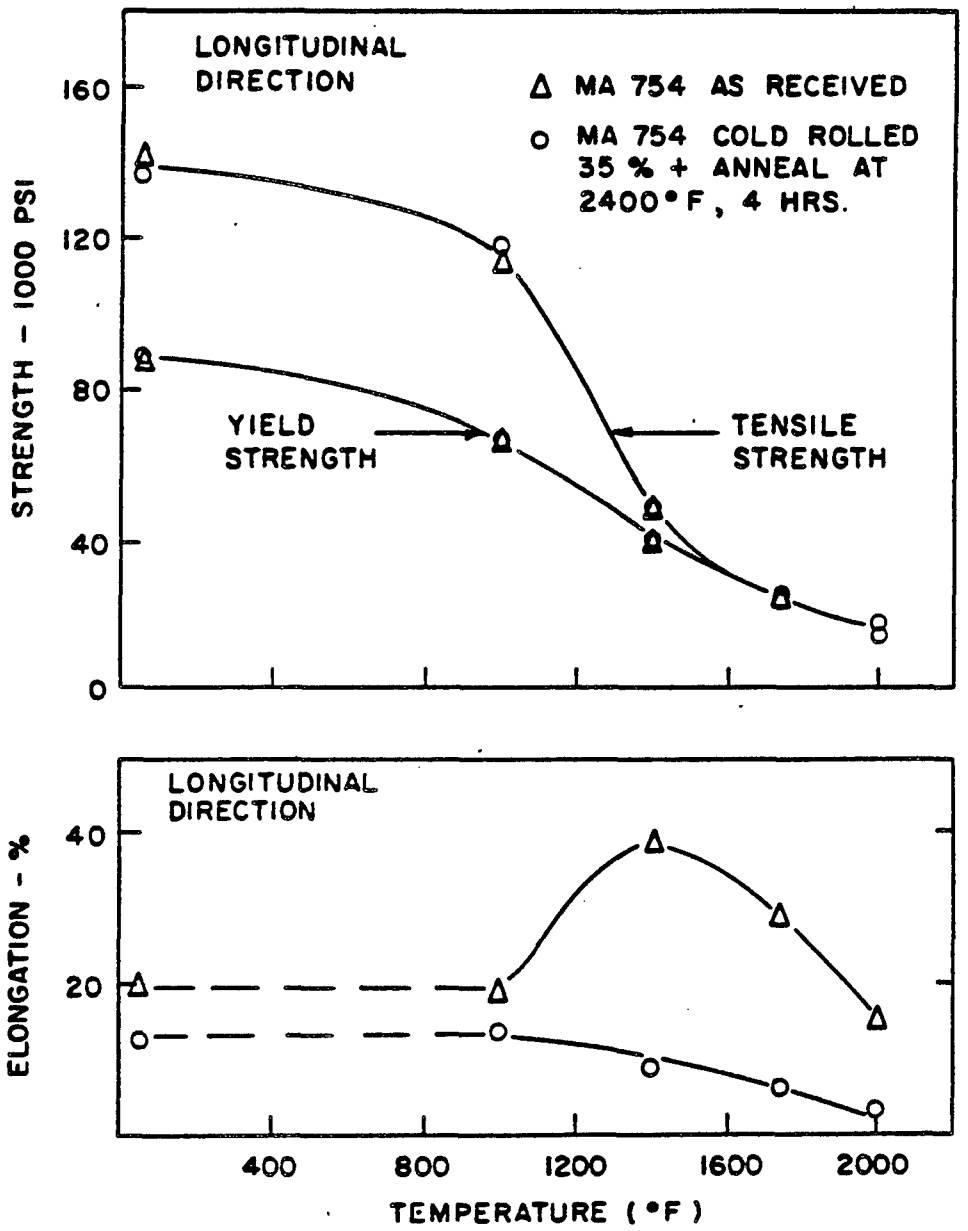

Figure 2-27. Elevated Temperature Tensile Properties of MA754 Alloy As-Received and After Cold Working and Annealing.

Table 2-13.

Elevated Temperature Tensile Properties of MA754 Alloy As-Received and After Cold Working* and Annealing**

CONDITION: AS-RECEIVED

°F	Tensile Strength (psi)	0.2% Yield Strength (psi)	% Elongation
Ambient	142,700	87,300	20
1000	113,900	65,100	19
1400	48,800	42,400	39
1750	26,800	25,000	29
2000	18,500	17,700	15

CONDITION: COLD ROLLED 35% + ANNEAL 2400°F, 4 HOURS

°F	Tensile Strength (psi)	0.2% Yield Strength (psi)	% Elongation
Ambient	138,500	88,300	13
1000	117,700	67,100	14
1400	49,400	40,300	9
1750	26,400	24,800	6
2000	17,500	15,900	3

*Cold Rolled (35% reduction in thickness) was performed in a direction parallel to the hot extrusion direction.
**Annealing time runs 4 hours.

Table 2-14.

Elevated Temperature (2000°F) Tensile Properties of MA754 in Three Different Process Conditions

Condition	Tensile Strength (psi)	0.2% Yield Strength (psi)	% Elongation
As-Received	18,500	17,700	15
Cold Rolled 35% + Anneal at 2400°F, 4 Hrs.	17,500	15,900	3
Cold Rolled 20% + Anneal at 2400°F, 4 Hrs.	20,600	19,200	10

tensile test fractures revealed two primary failure modes. At temperatures below 1000°F (538°c), transgranular failure is readily apparent, Figure 2-28. Above 1000 F, intergranular failure is observed (Figure 2-29). As in the case of the as-received material, the locus of failure in the intergranular mode for the cold rolled plus annealed material is at transverse grain boundaries.

2.2.2.5. Effects of Cyclic Cold Working and Annealing of MA754

On the basis of the data described above, it became apparent that, while cold working might be used to bring the MA754 material to near net-shapes, it could not be given extensive amounts of cold working without undergoing some undesirable recrystallization. Hence, it became necessary to establish the degree to which the material could be cold worked and stabilized microstructurally by thermal relaxation treatments.

In the attempt to utilize the beneficial effects of reducing the amount of cold work while retaining useful reductions, the cold rolling plus anneal schedule was revised into one involving step-wise cold working and annealing:

Step 1: Cold Roll As-Received MA754 X%

Step 2: Anneal Material in (1) at 2400°F, ½ Hours, in Air

Step 3: Cold Roll Annealed Material in (2) X%

Step 4: Anneal Material (3) at 2400°F, ½ Hour, in Air

Subsequent steps, as warranted, according to the above. The annealing time for each cycle was reduced from 4 hours to ½ hour in order to minimize surface oxidation.

An integral part of this schedule involved determining the

Figure 2-28. **Optical Photomicrograph of the Mid-Section of a Longitudinal Tensile Test Piece of MA754 Cold Rolled 35% (Reduction in Thickness) Plus Annealed at 2400°F (1315°c) for 4 hours, showing the fracture edge. Note the Transgranular Fracture Mode. Test conducted at 1000°F (538°c). (Etched Condition; 240X Magnification).**

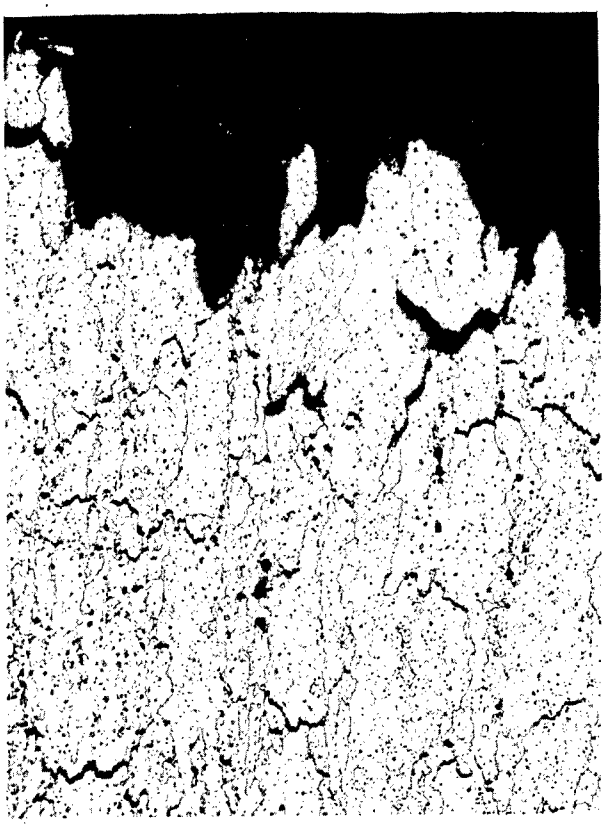

Figure 2-29. Optical Photomicrograph of the Mid-Section of a Longitudinal Tensile Test Piece of MA754 Cold Rolled 35% (Reduction in Thickness) Plus Annealed at 2400°F (1315°c) for 4 hours, showing the fracture edge. Note the intergranular nature of the fracture. Test conducted at 2000°F (1093°c). Etched Condition; 160X Magnification.

maximum deformation ("X"%) that can be applied during each rolling cycle without recrystallization occurring upon subsequent annealing. This was accomplished by cold rolling a wedge-shaped blank 3.7" long (94.0 mm) x 1.3" wide (33.0 mm) x 0.35" thick (8.9 mm) at the large end, with a 5.4° included angle to a uniform thickness, that of the small end of the wedge. The resulting reduction in thickness within the price varied from 0 to 35%. The blank was then annealed at $2400^{\circ}F$, in air, for 4 hours. Because of the cold work gradient, part of the bar (that with higher amounts of cold work) recrystallized while the part with subcritical amounts of cold work did not. From metallographic examination of the annealed wedge, the maximum reduction, "X", was determined for the processing schedule.

The results of this experiment indicate that cold rolling MA754 to 10% reduction in thickness, plus annealing at $2400^{\circ}F$, produces a very small amount of recrystallized structure (Figure 2-30). Therefore, the maximum reduction, "X", was taken to be 5%.

Figures 2-31 through 2-34 are optical photomicrographs of MA754 cold rolled and annealed to three different total reductions according to the revised schedule, along with the as-received MA754 annealed at $2400^{\circ}F$ for ½ hour in air. Utilization of the step-wise cold rolling plus annealing schedule permits total reductions of at least 40% while still maintaining the favorable grain morphology of the as-received material.

Two mechanisms, recovery or recrystallization, may be used to explain the behavior of MA754 cold rolled plus annealed according to the step-wise schedule. Since it appears that primary recrystalliza-

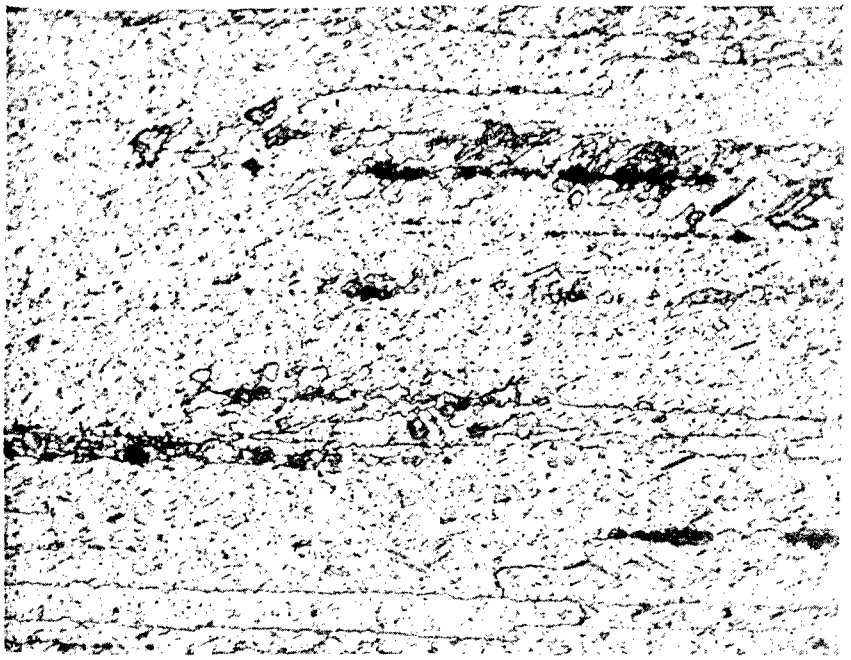

Figure 2-30. Optical Photomicrograph of MA754 Cold Rolled 10% Plus Anneal at 2400°F, 4 hours, Revealing Evidence of Recrystallization. (Etched Condition; 200X Magnification).

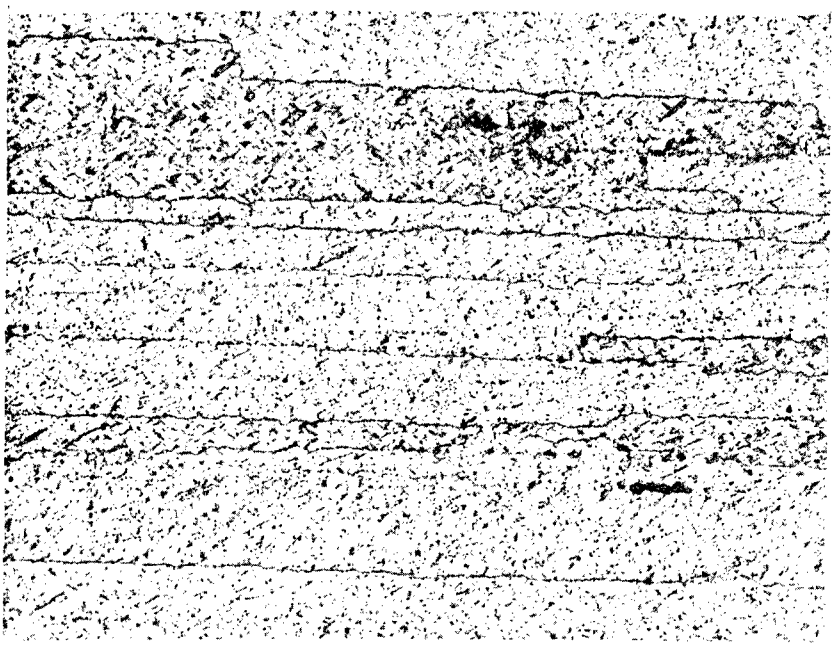

Figure 2-31. Optical Photomicrograph of As-Received MA754 Annealed, 1/2 hour, 2400°F (Longitudinal Section). (Etched Condition; 200X Magnification).

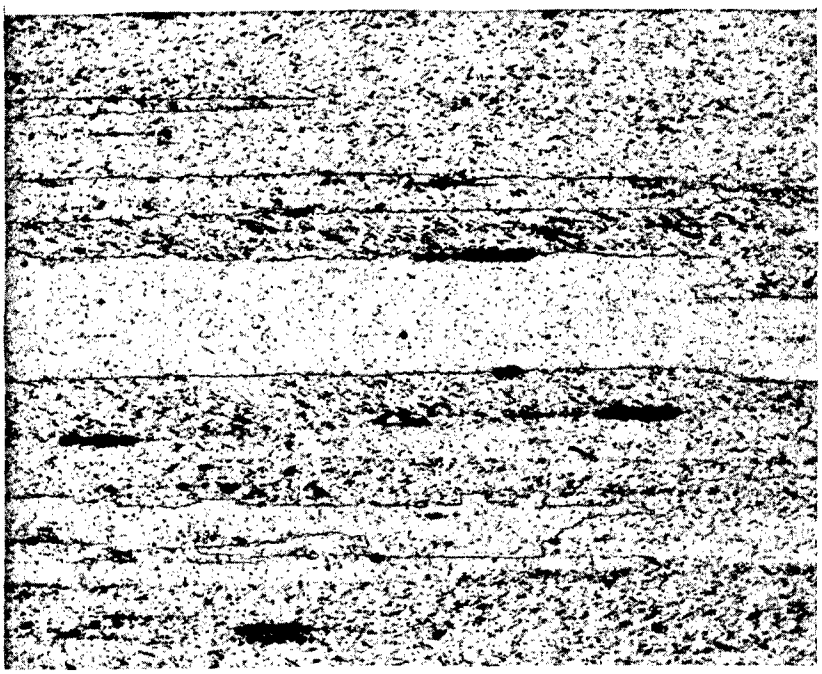

Figure 2-32. Optical Photomicrograph of MA754 Cold Rolled 15% (Reduction in Thickness) Utilizing the Revised Cold Rolling Plus Anneal Schedule (Longitudinal Section). (Etched Condition; 100X Magnification).

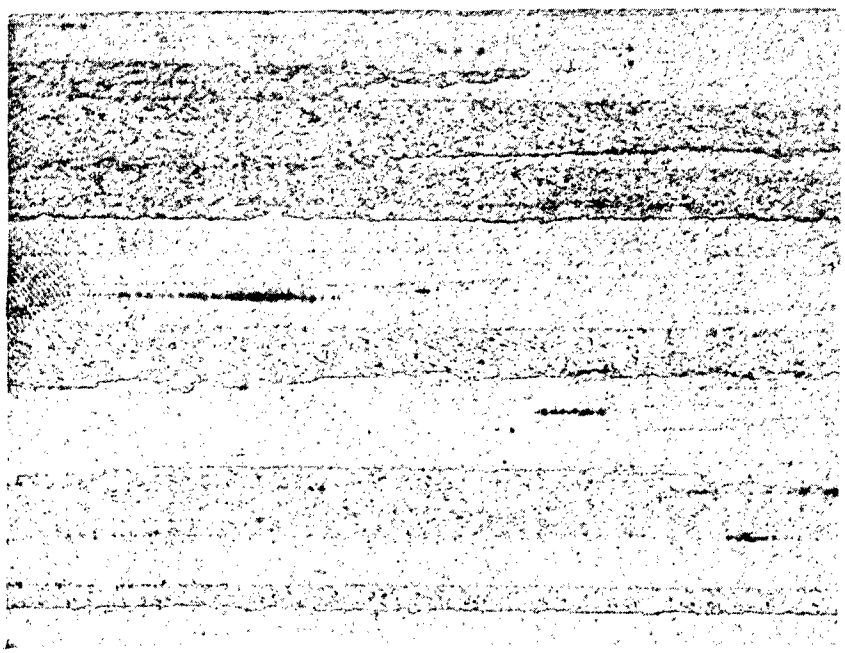

Figure 2-33. Optical Photomicrograph of MA754 Cold Rolled 22% (Reduction in Thickness) Utilizing the Revised Cold Rolling Plus Anneal Schedule (Longitudinal Section). (Etched Condition; 100X Magnification).

Figure 2-34. Optical Photomicrograph of MA754 Cold Rolled 40% (Reduction in Thickness) Utilizing the Revised Cold Rolling Plus Anneal Schedule (Longitudinal Section). (Etched Condition; 100X Magnification).

tion controls the deformation and annealing response of MA754, the choice of mechanism would depend upon whether or not the amount of deformation given in each rolling step (5%) was enough to allow the specimen to recrystallize following the anneal at 2400°F.

If a recovery mechanism is operable, the grain structure of the material following the anneal should not be different than that of the as-rolled material with no anneal. In addition, there should be only a very slight drop in hardness in the material following the anneal.[31] Table 2-15 lists the grain size measurements of MA754 cold rolled 22% in one step with no anneals, and of MA754 cold rolled 22% plus annealed according to the step-wise schedule. The results indicate that the material cold rolled and annealed according to the step-wise schedule does not have the same grain size and shape as the as-rolled material.

Figure 2-35 reveals the Rockwell hardness measurements of samples cold rolled and annealed according to the step-wise schedule with total reductions ranging from 0 to 40%. For comparison purposes, the Rockwell hardness measurements of MA754 cold rolled 20% and 35% in one step with no anneals are plotted on the graph. The results of these experiments serve to warrant two observations:

1) MA754 cold rolled and annealed according to the step-wise schedule has recrystallized. However, it appears that it has retained the favorable grain morphology of the as-received material.
2. The hardness of MA754 cold rolled and annealed according to the step-wise schedule does not appear to vary signifi-

Table 2-15.

Grain Size and Shape Measurements of MA754 Processed in Two Conditions

Condition	Direction	L (mm)	L_{AVE} (mm)	L/D
MA754 Cold Rolled 22% in One Step with No Anneals	Longitudinal	1.04	0.1680	9.5
	Long Transverse	0.1730		
	Short Transverse	0.0437		
MA754 Cold Rolled 22% Plus Anneal According to the Revised Schedule	Longitudinal	0.948	0.195	7.9
	Long Transverse	0.1529		
	Short Transverse	0.0846		

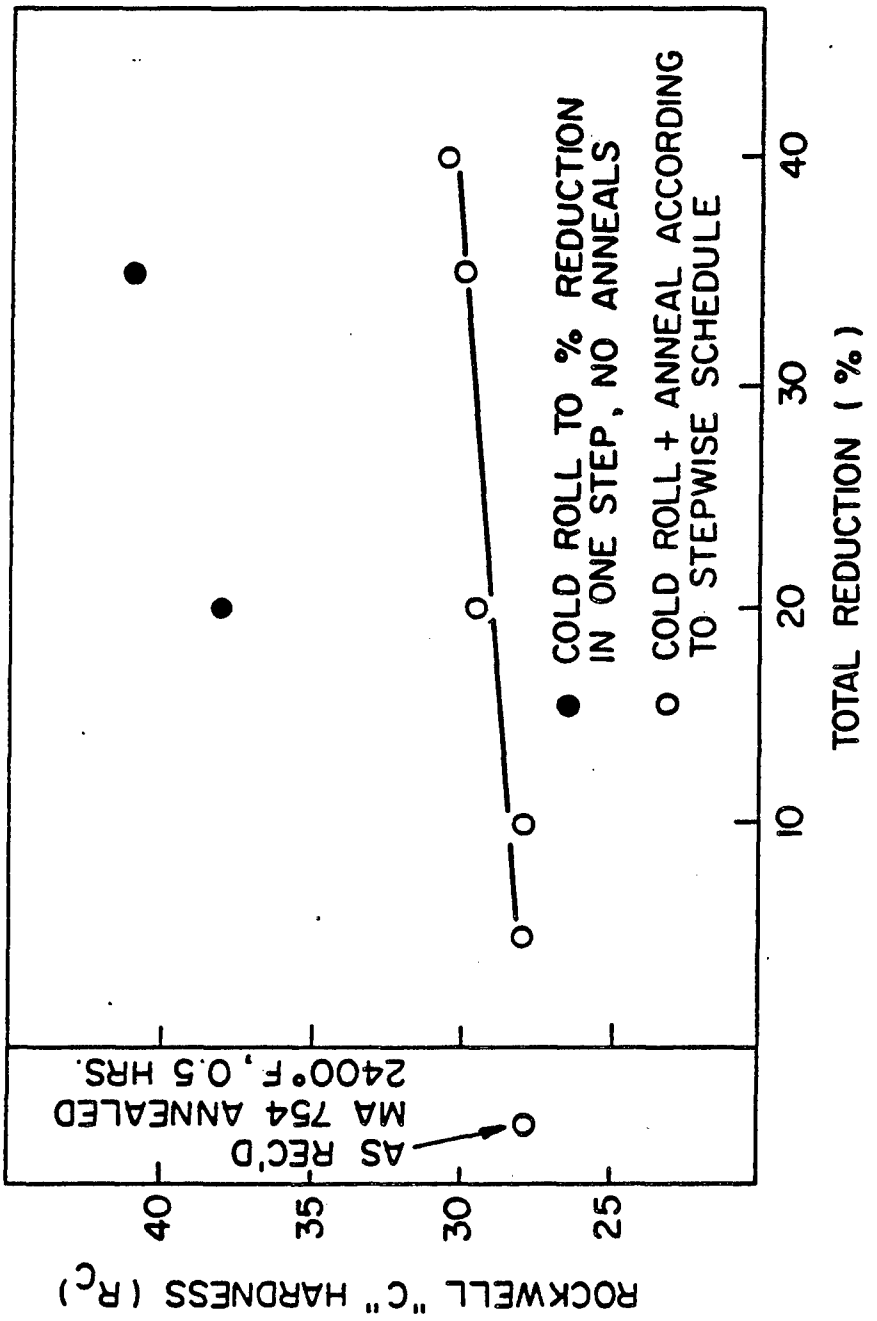

Figure 2-35. Rockwell "C" Hardness Versus % Total Reduction by Cold Rolling under two different conditions.

cantly with increasing reduction. This observation is consistent with the structures observed in Figures 2-31 through 2-34.

2.2.2.6. Elevated Temperature Tensile Properties of MA754 Cold Rolled 22% Plus Anneal According to the Step-wise Schedule

Figures 2-36 through 2-38 show the elevated temperature tensile properties of MA754 cold rolled 22% plus anneal according to the step-wise schedule, along with the tensile properties of MA754 cold rolled 22% plus anneal in one step and the as-received MA754 Bar #1. These results give evidence of the cold work effects, as shown by the large increase in yield strength of the rolled materials at ambient and 1000°F when compared to the as-received material. In addition, the material cold rolled and annealed according to the step-wise schedule exhibits somewhat greater ductility at the higher temperatures. The individual elevated temperature tensile property values of these three materials are given in Tables 2-8 and 2-16.

2.2.2.7. Elevated Temperature Creep Properties of Ma754 Cold Rolled 22% Plus Anneal According to the Step-wise Schedule

Creep rupture behavior was evaluated as a function of stress at 1600°F (871°c) and 1800°F (982°c) for MA754 cold rolled 22% plus anneal according to the step-wise schedule, Figures 2-39 through 2-44. For comparison purposes, the creep properties of MA754 cold rolled 22% plus anneal in one step and the as-received material (Bar #1) are also given. Individual values of the creep-rupture properties of these materials are given in Tables 2-5, 2-6, and 2-17 though 2-20.

The results of the tests conducted at 1600°F and 1800°F show

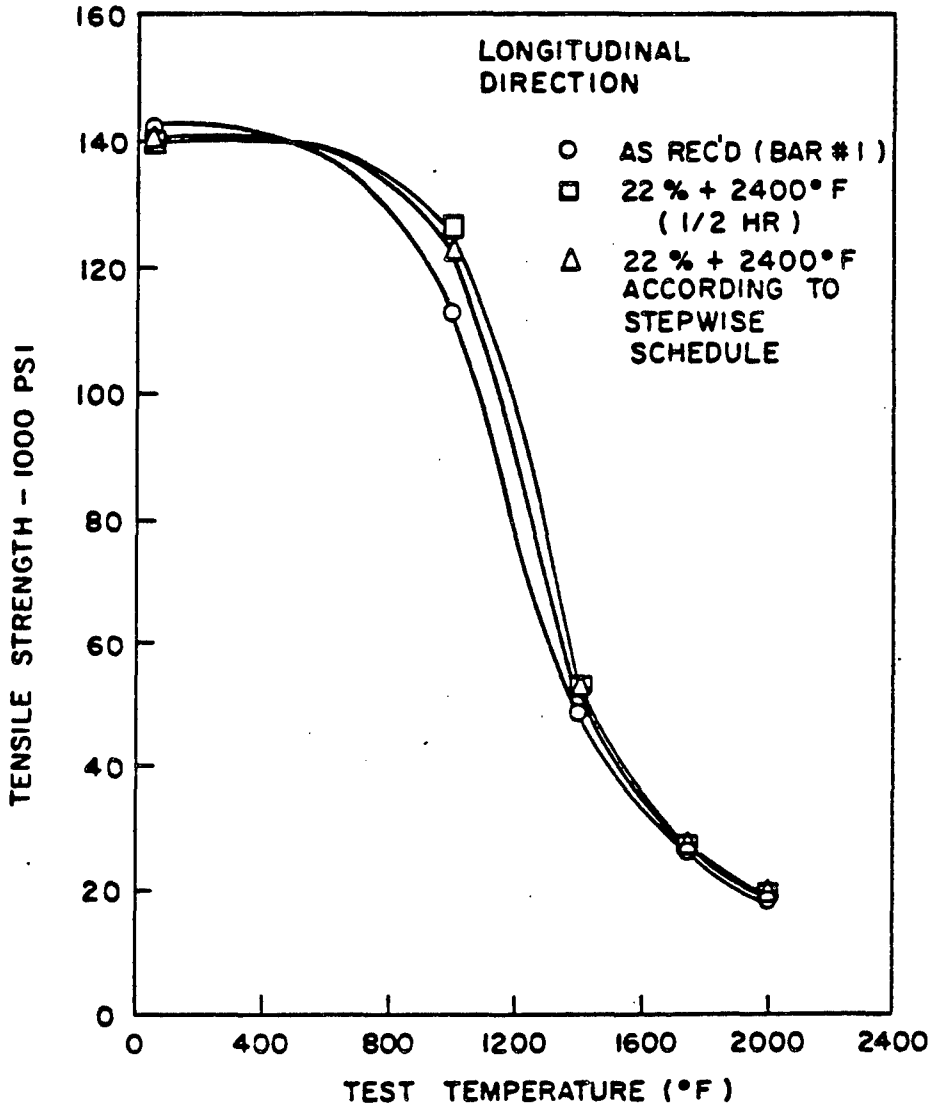

Figure 2-36. The manner in which the longitudinal tensile strength varies with temperature for MA754 in three conditions.

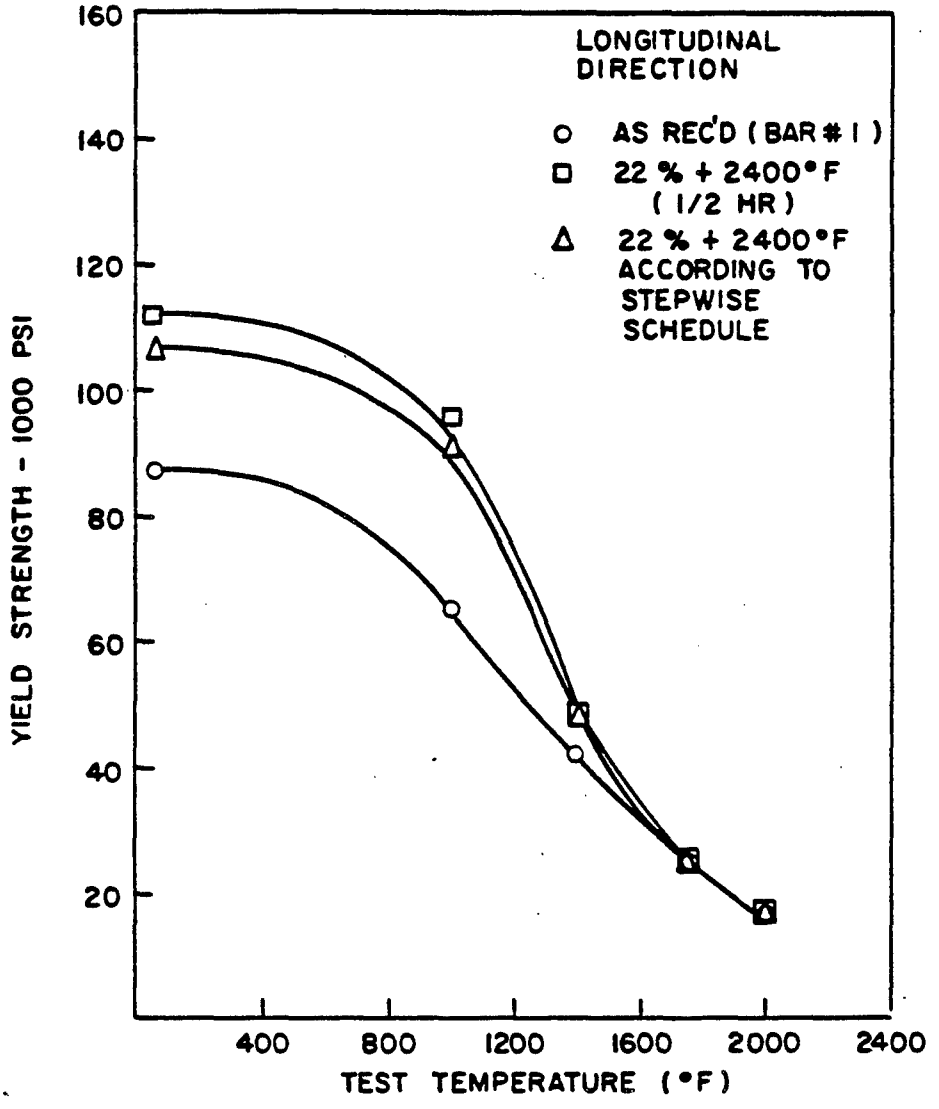

Figure 2-37. The manner in which the longitudinal yield strength varies with temperature for MA754 in three conditions.

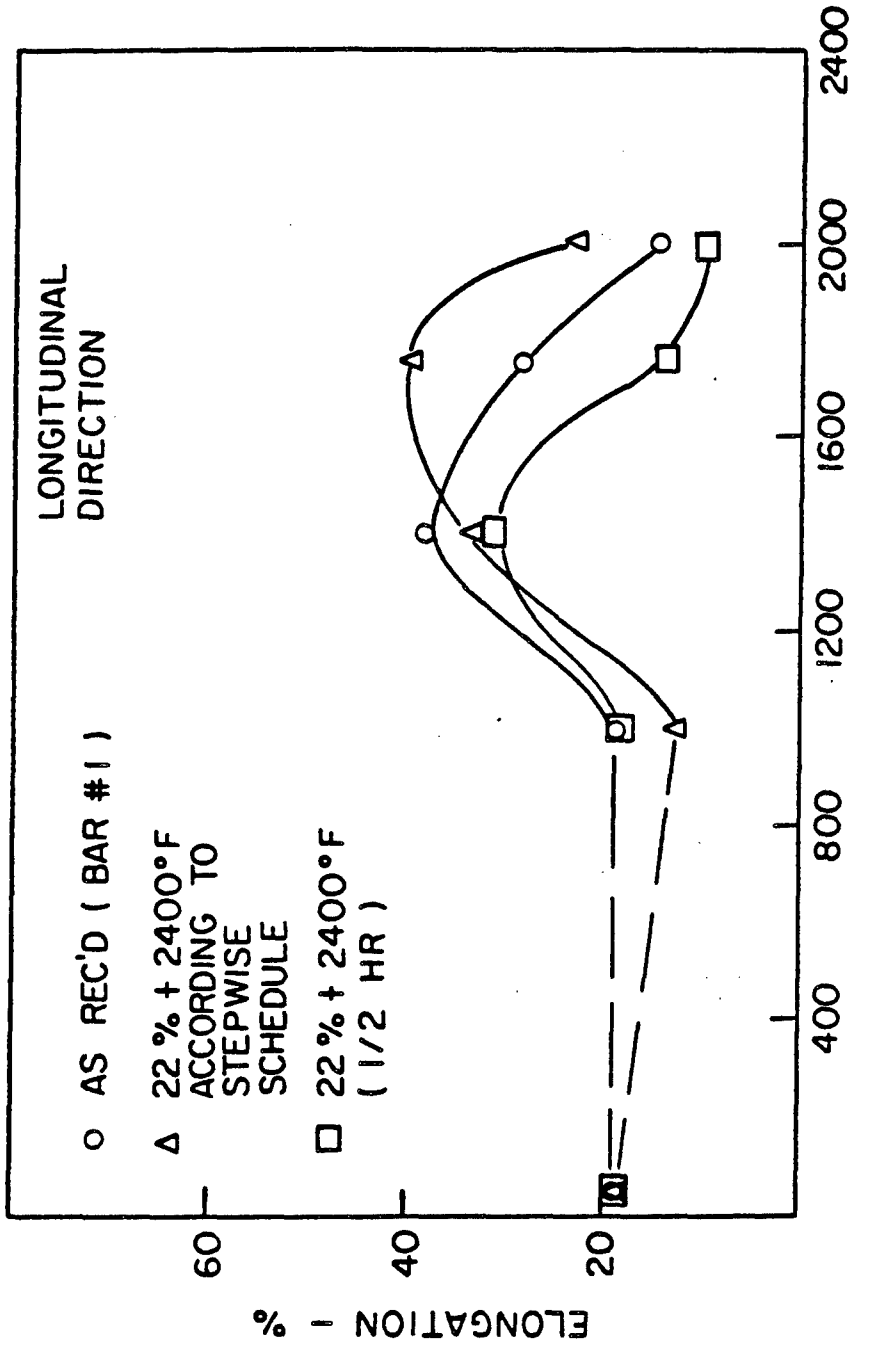

Figure 2-38. The manner in which the longitudinal ductility varies with temperature for MA754 in three conditions.

Table 2-16

Elevated Temperature Tensile Properties of MA754
with Single-Step and Multiple-Step Cold Work and Anneal Processing

CONDITION: MA754 COLD ROLLED 22% + ANNEAL 2400°F, ½ HOUR

°F	Tensile Strength (psi)	0.2% Yield Strength (psi)	% Elongation
Ambient	142,500	112,700	19
1000	126,400	96,600	19
1400	52,600	48,300	32
1800	28,100	26,100	14
2000	20,600	19,200	10

CONDITION: MA754 COLD ROLLED 22% PLUS ANNEAL
ACCORDING TO THE STEPWISE SCHEDULE

°F	Tensile Strength (psi)	0.2% Yield Strength (psi)	% Elongation
Ambient	141,400	107,200	19
1000	123,600	91,400	13
1400	52,600	48,600	34
1800	27,600	24,700	40
2000	20,700	18,800	24

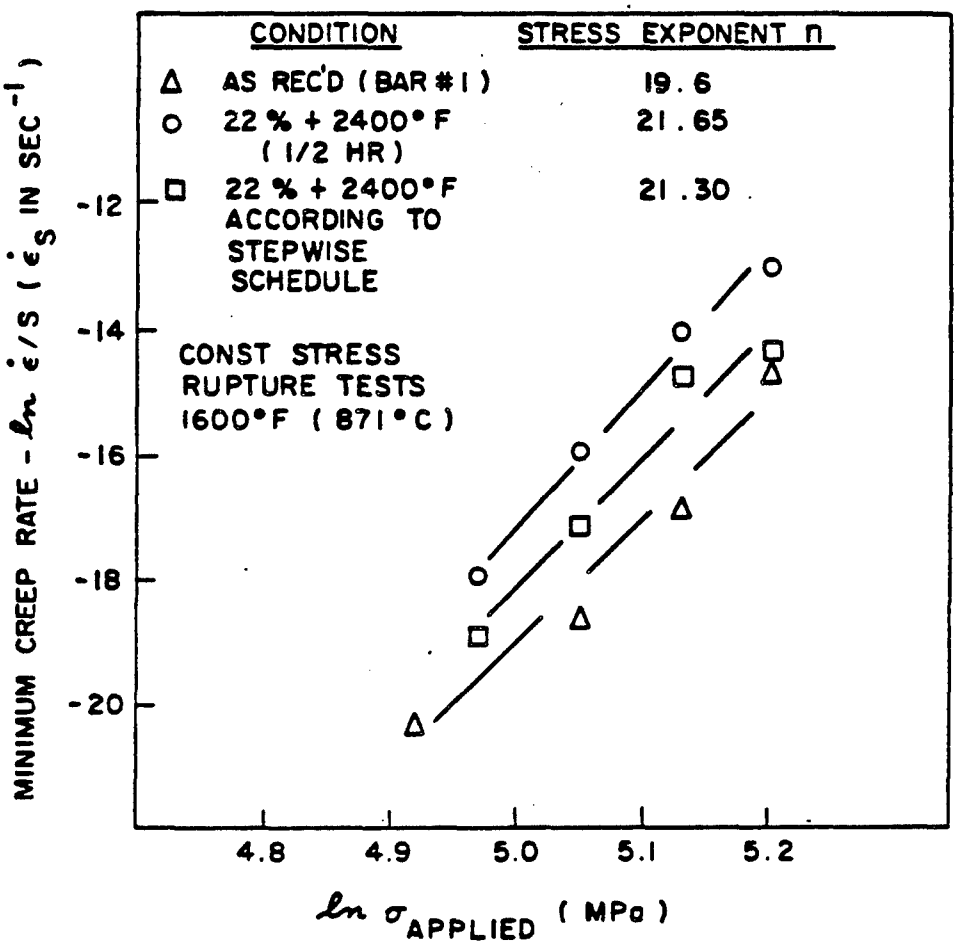

Figure 2-39. Ln (Minimum Creep Rate sec^{-1}) as a function of applied stress (Ln σ APPLIED) at 1600°F (871°c) for MA754 in three conditions.

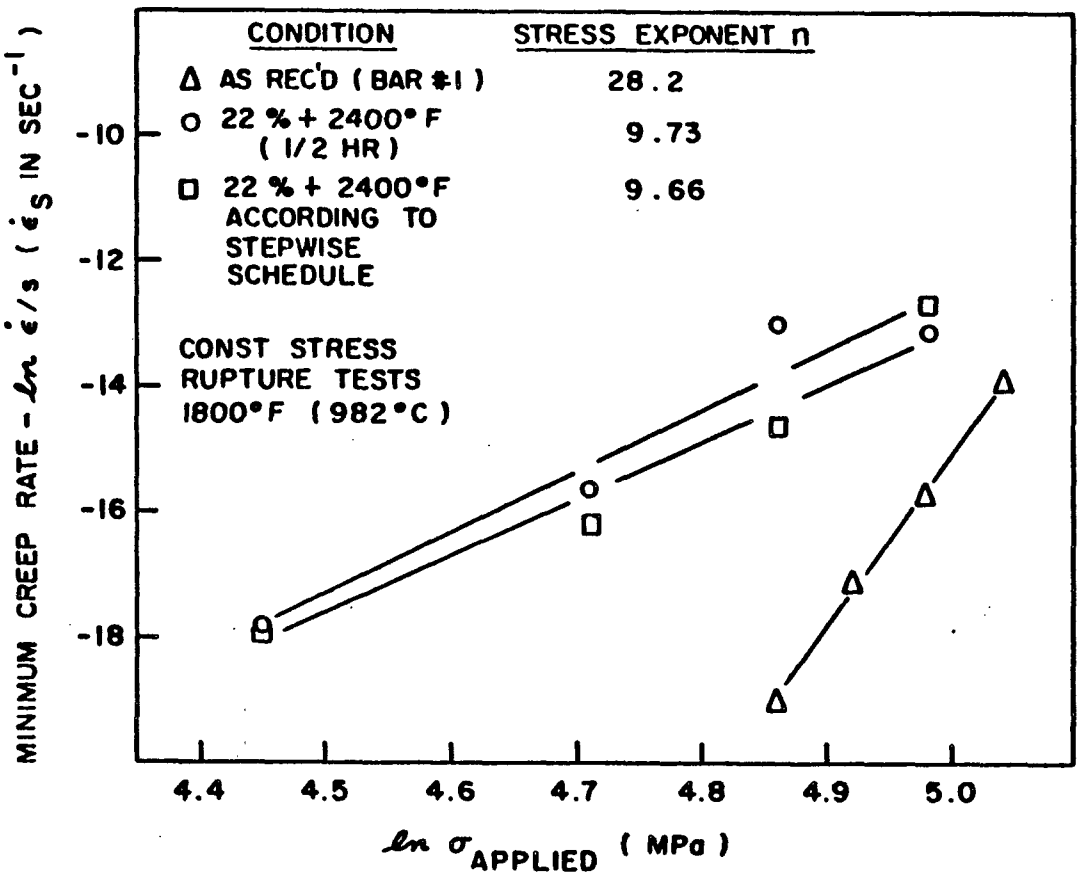

Figure 2-40. Ln (Minimum Creep Rate sec^{-1}) as a function of applied stress ($Ln\ \sigma_{APPLIED}$) at 1800°F (982°c) for MA754 in three conditions.

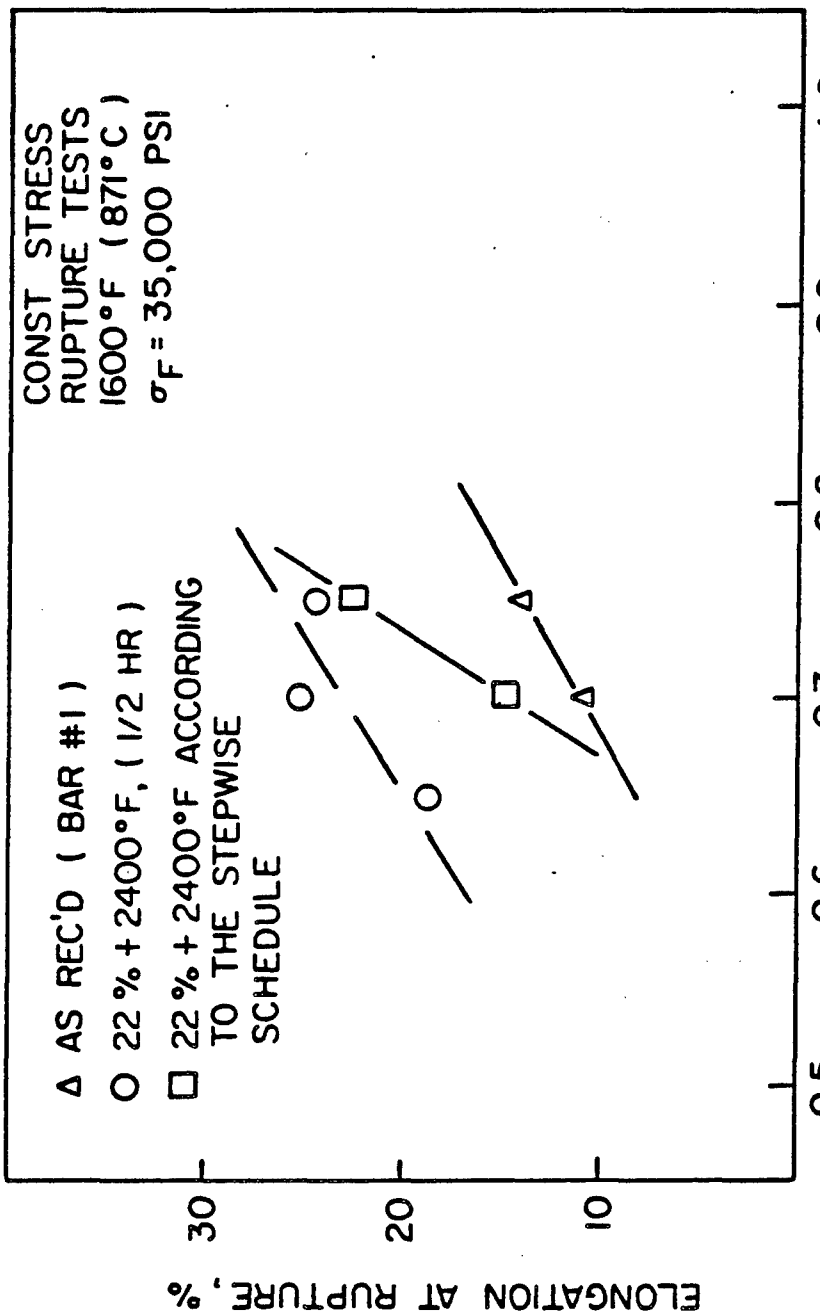

Figure 2-41. Rupture Elongation as a function of applied stress for MA754 at 1600°F (871°c) in three conditions.

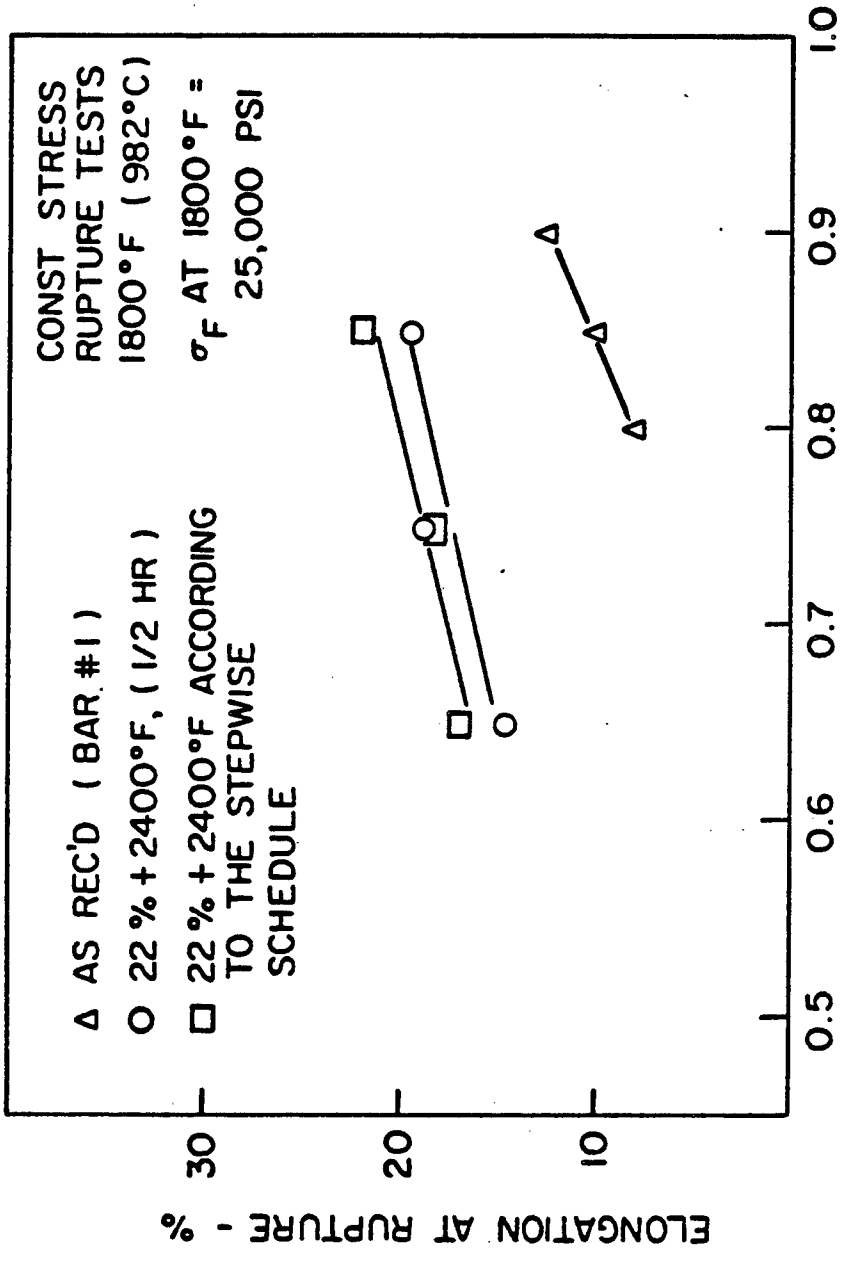

Figure 2-42 Rupture Elongation as a function of applied stress for MA754 at 1800°F (982°c) in three conditions.

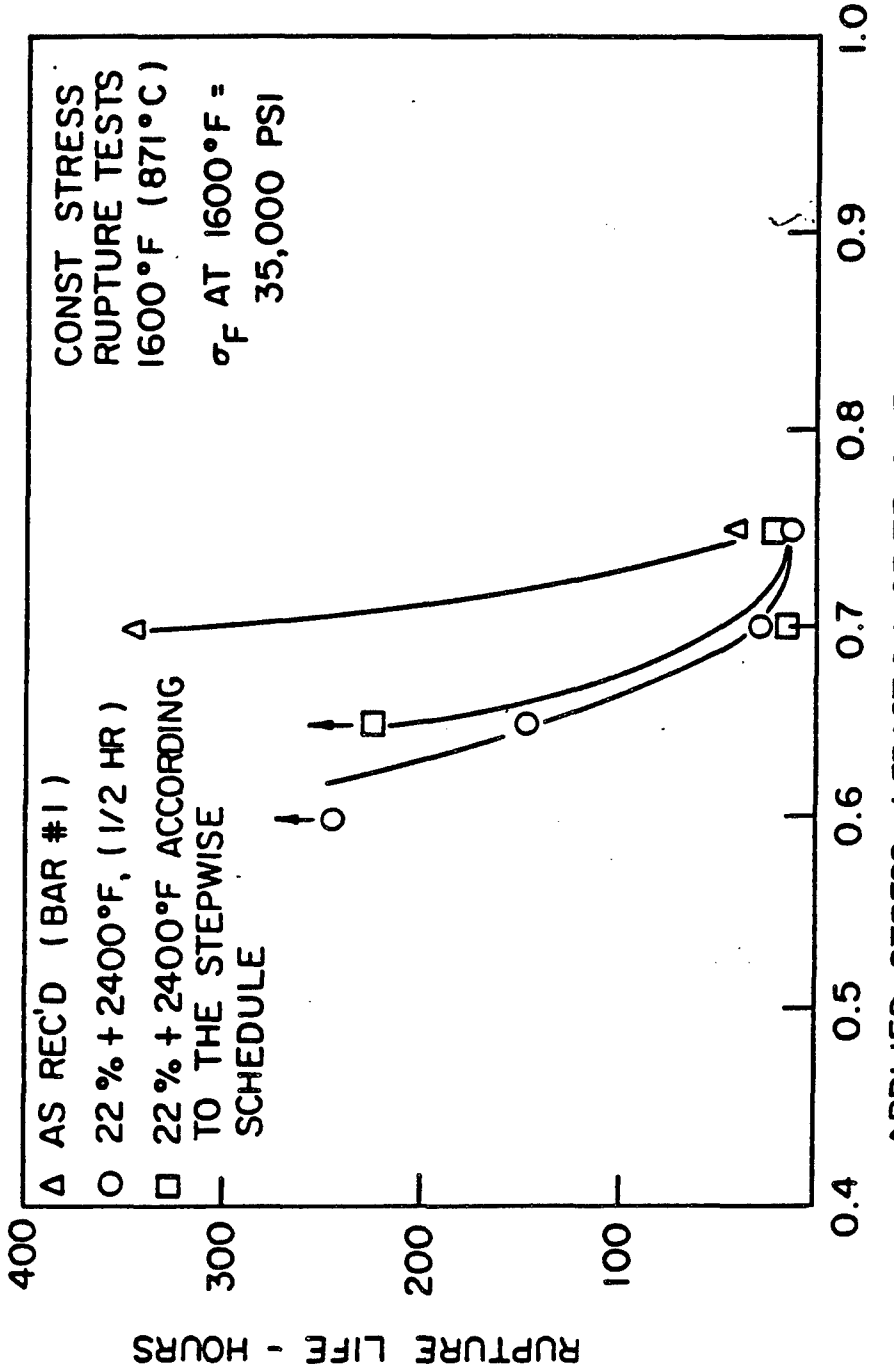

Figure 2-43. Rupture Life as a function of applied stress for MA754 at 1600°F (871°c) in three conditions.

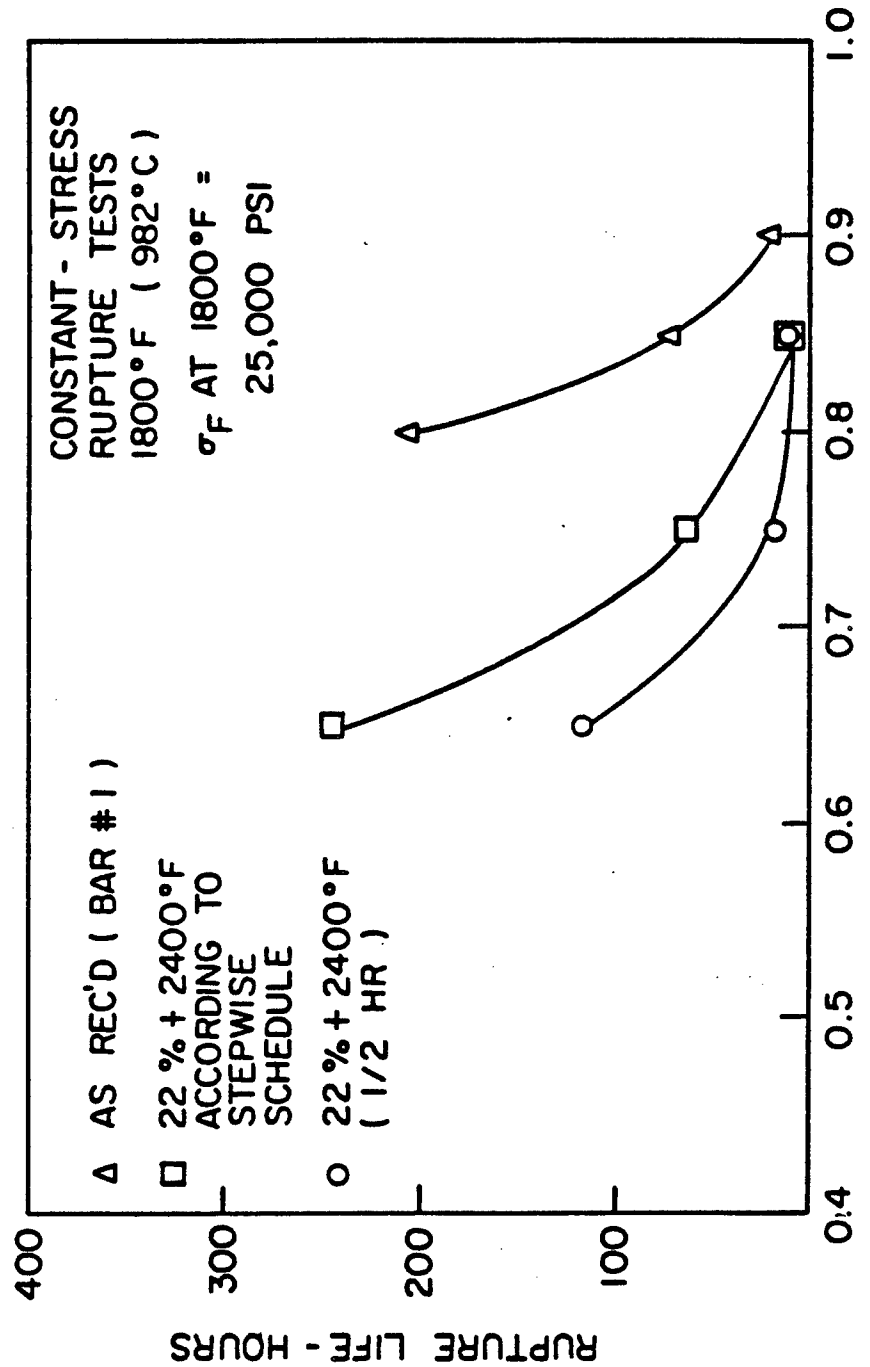

Figure 2-44 Rupture Life as a function of applied stress for MA754 at 1800°F (982°c) in three conditions.

Table 2-17

Creep-Rupture Properties of MA754 Cold Rolled 22% Plus Anneal According to the Stepwise Schedule at 1600°F (871°c)

Stress Level (Fraction of Tensile Strength at 1600°F)*	Minimum Creep Rate (In.per In. per Sec.)	Rupture Time (Hours)	Rupture Elongation (%)	Total Time (Non-Rupture) (Hours)**
0.60	5.92×10^{-9}	—	—	275.0
0.65	3.8×10^{-8}	—	—	225.0
0.70	4.3×10^{-7}	16.1	14.7	—
0.75	6.1×10^{-7}	21.9	22.6	—

*Longitudinal Tensile Strength at 1600°F taken as ~ 35,000 psi.
**Tests interrupted prior to failure.

Table 2-18

Creep-Rupture Properties of MA754 Cold Rolled 22% Plus Anneal According to the Stepwise Schedule at 1800°F (982°c)

Stress Level (Fraction of Tensile Strength at 1800°F)*	Minimum Creep Rate (In per In. per Sec.)	Rupture Time (Hours)	Rupture Elongation (%)	Total Time (Non-Rupture) (Hours)**
0.50	1.54×10^{-8}	—	—	194.9
0.65	9.14×10^{-8}	242.6	17.0	—
0.75	4.44×10^{-7}	63.9	18.17	—
0.85	3.0×10^{-6}	9.2	22.3	—

*Longitudinal Tensile Strength at 1800°F taken as ~ 25,000 psi.
**Tests interrupted prior to failure.

Table 2-19

Creep-Rupture Properties of MA754 Cold Rolled 22% Plus Anneal 2400°F, ½ Hour at 1600°F (871°c)

Stress Level (Fraction of Tensile Strength at 1600°F)*	Minimum Creep Rate (In. per In. per Sec.)	Rupture Time (Hours)	Rupture Elongation (%)	Total Time (Non-Rupture) (Hours)**
0.60	1.66×10^{-8}	—	—	248.4
0.65	1.25×10^{-7}	149.0	18.8	—
0.70	8.11×10^{-7}	28.5	25.2	—
0.75	2.2×10^{-6}	11.7	24.4	—

*Longitudinal Tensile Strength at 1600°F taken as ~ 35,000 psi.
**Tests interrupted prior to failure.

Table 2-20

Creep-Rupture Properties of MA754 Cold Rolled 22% Plus Anneal 2400°F, ½ Hour at 1800°F (982°c)

Stress Level (Fraction of Tensile Strength at 1800°F)*	Minimum Creep Rate (In. per In. per Sec.)	Rupture Time (Hours)	Rupture Elongation (%)	Total Time (Non-Rupture) (Hours)
0.50	1.92×10^{-8}	—	—	216.6
0.65	1.73×10^{-7}	118.5	14.7	—
0.75	2.3×10^{-6}	17.0	18.9	—
0.85	1.92×10^{-6}	14.2	19.5	—

*Longitudinal Tensile Strength at 1800°F taken as ~ 25,000 psi.
**Tests interrupted prior to failure.

that the creep-rupture characteristics of MA754 processed according to the stepwise schedule are superior to those of the material processed according to the schedule which introduces all of the cold work without intermediate anneals. The difference becomes more pronounced when the amount of reduction is increased to approximately 40%, as shown in Table 2-21. However, the creep-rupture properties of both thermomechanically processed materials are poorer than those of the as-received material (Bar #1). For example, the rupture life at 1600°F and 24.5 KSI for the as-received material is almost 20 times greater, Figure 2-43; and the minimum creep rates at both temperatures are significantly reduced, Figures 2-39 and 2-40.

2.2.2.8. Microscopic Examination of Elevated Temperature Creep Test Piece Fracture of MA754 in Three Conditions

Elevated temperature creep test piece fractures were examined with optical and scanning electron microscopy for the as-received material, MA754 cold rolled 22% and annealed according to the stepwise schedule, and MA754 cold rolled 22% and annealed in one step. The results appear to indicate possible explanations for the decreased creep-rupture resistance of the processed materials.

In the case of MA754 cold rolled 22% plus anneal in one step, the primary reason for its decreased creep resistance is the decrease in grain size of the material compared to the as-received MA754. Extensive cracking has taken place as a result of the compromised microstructure, Figure 2-45. For comparison purposes, Figure 2-46 is an optical photomicrograph of a creep-rupture fracture from the as-received material. The high stress rupture ductility observed in this material is a reflection of the difficulty of crack propagation.

Table 2-21

Creep-Rupture Properties of MA754 at 1800°F (982°c) and 21.2 KSI in Two Processing Conditions

Condition	Minimum Creep Rate (In. per In. per Sec.)	Rupture Time (Hours)	Rupture Elongation (%)
Cold Rolled 35% Plus Anneal 2400°F, 4 Hours	1.16×10^{-4}	0.06	9.3
Cold Rolled 40% Plus Anneal According to the Revised Schedule	2.6×10^{-6}	10.1	21.2

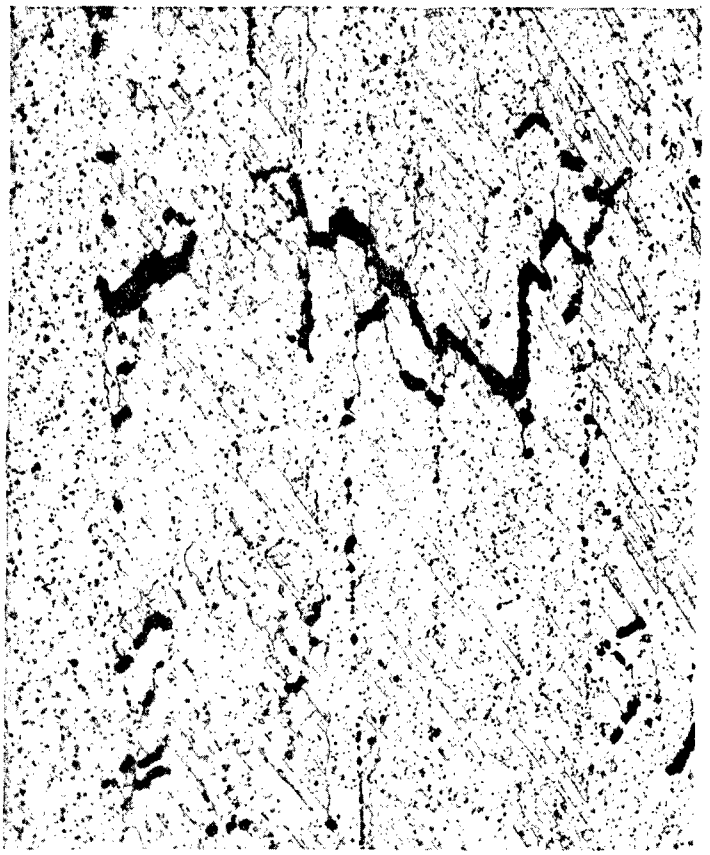

Figure 2-45. Optical Photomicrograph of the Mid-Section of a Fractured Longitudinal Creep Test Piece from MA754 22% (Reduction Thickness) and Anneal at 2400°F (1316°c) in One Step, showing Recrystallization of Grains and Void Formation on Grain Boundaries. (200X Magnification; Etched Condition).

Test Temperature: 1800°F (982°c)

Applied Stress: 0.65 σ_F

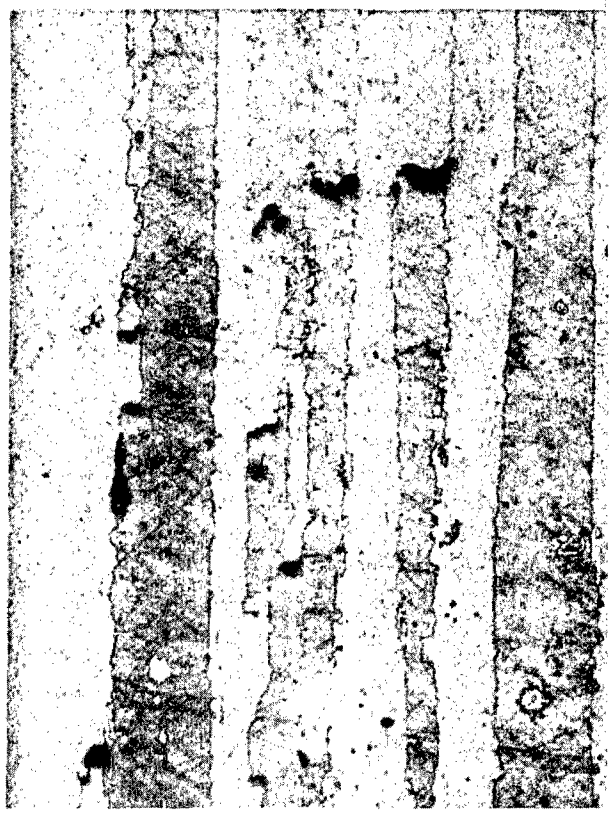

Figure 2-46. Optical Photomicrograph of the Mid-Section of a Fractured Longitudinal Creep Test Piece from As-Received Material showing Void Formation at Transverse Grain Boundaries. (Thermal Etch, 0.5 hour at 1100°F, 100X).

Test Temperature: 1800°F (982°c)

Applied Stress: 22.5 KSI (155 MPa)

In the as-received MA754, cracks were observed to propagate along transverse grain boundary paths offering a relatively easy propagation path.[32] However, in MA754 cold rolled 22% plus annealed in one step, cracks were observed at included grains, many of which did not propagate to include the larger grain.

The loss in creep resistance found in MA754 cold rolled 22% plus annealed according to the stepwise schedule is not due to a decrease in grain size, but to the influence of coarsened particles situated primarily at grain boundaries, Figure 2-47. The degree of coarsening is quite extensive, as shown by Figure 2-48, occurs prior to testing, Figure 2-49, and is not affected by the air atmosphere in which the annealing takes place.

Figure 2-50 contains scanning electron micrographs taken from a creep-rupture failure of the processed material which showed longitudinal grain boundary particles. For comparison purposes, typical longitudinal grain boundary particles from an untested specimen are shown in Figure 2-51. At no time were cracks observed to be nucleating from these coarsened particles. However, it does appear that the crack nucleation process in this material can be influenced by coarsened particles situated at transverse grain boundaries, as shown in Figure 2-52. In addition, the "holes" containing the grain boundary particles from the tested specimens are larger and their shape is somewhat elongated when compared to their counterparts in the untested specimens. It does not appear that this size and shape change is due to a particle coarsening mechanism operative during testing, since as-received specimens do not undergo a similar change

Figure 2-47. Optical Photomicrograph of the Mid-Section of a Fractured Longitudinal Creep Test Piece from Material Cold Rolled 22% and Annealed according to the Stepwise Schedule showing Void Formation at Transverse Grain Boundaries. (Thermal Etch, 0.5 hour at 1100°F, 40X). (Mechanical polish prior to etching.)

Test Temperature: 1800°F (982°c)

Applied Stress: 21.2 KSI (146.5 MPa)

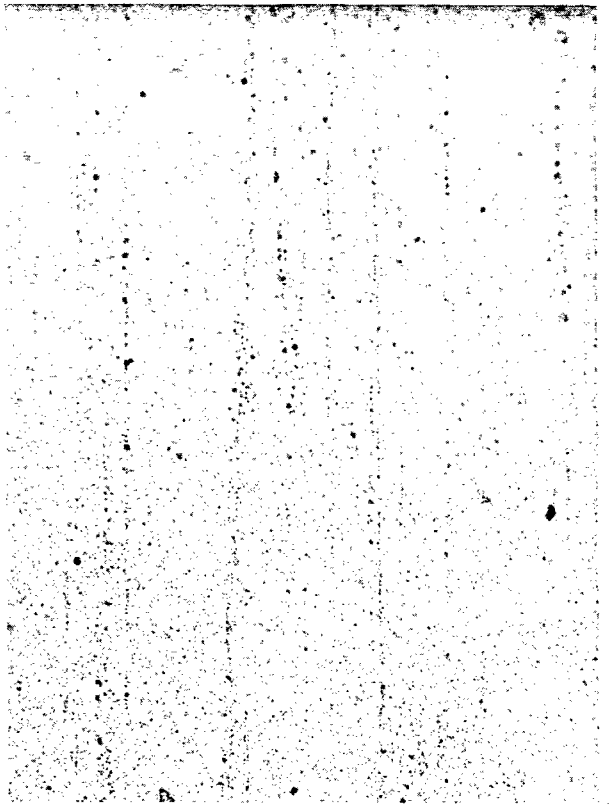

As-Received MA754 Bar #1; Longitudinal Section; 100X Magnification; Electropolished.

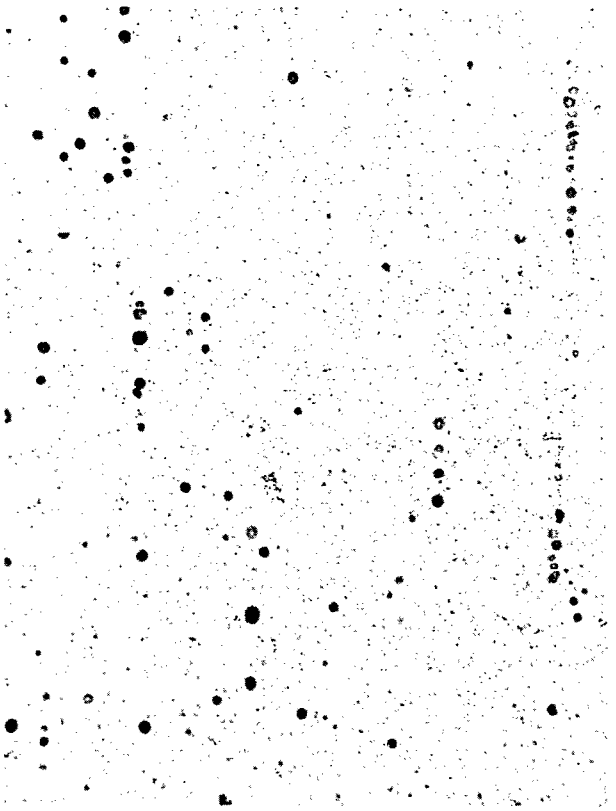

MA754 Cold Rolled 22% Plus Anneal according to the Stepwise Schedule (Bar #1); Longitudinal Section; 100X Magnification; Electropolished.

Figure 2-48. Optical Photomicrographs of MA754 Before and After Thermomechanical Processing.

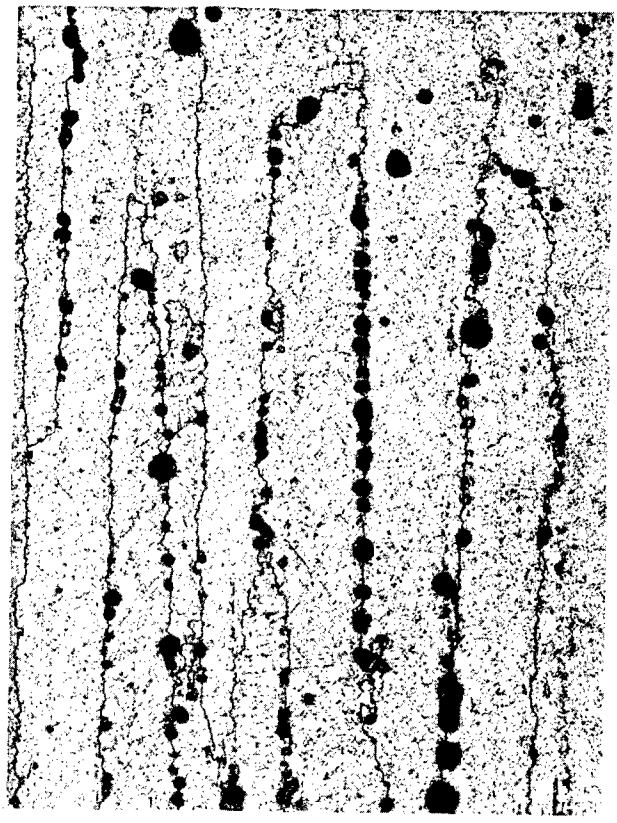

Figure 2-49. Optical Photomicrograph of MA754 Cold Rolled 22% Plus Anneal according to the Stepwise Schedule; Longitudinal Section; 160X Magnification; Etched Condition. (Electropolished Prior to Etching.)

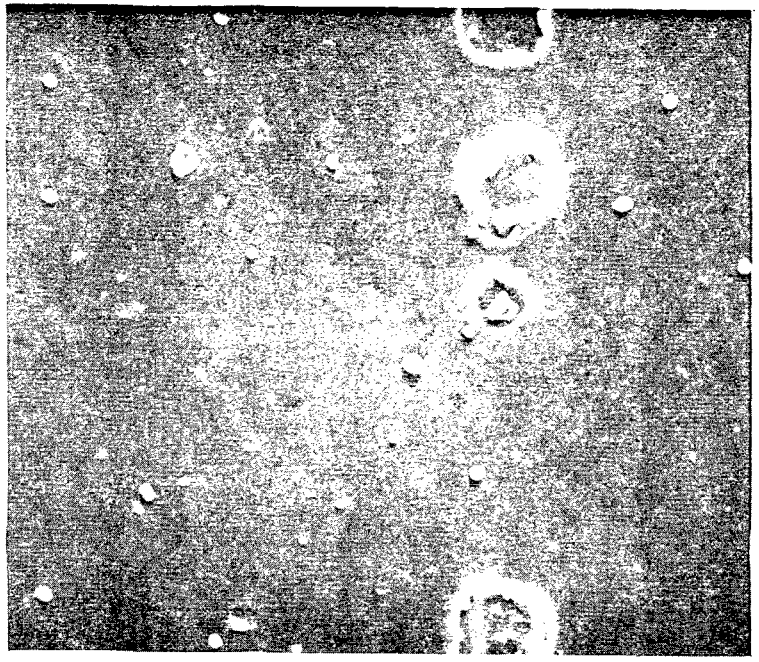

2000X

5000X

Figure 2-50. Scanning Electron Photomicrographs of the Mid-Section of a Fractured Longitudinal Creep Test Piece from MA754 Cold Rolled 22% Plus Annealed according to the Stepwise Schedule Revealing Grain Boundary Particles at Longitudinal Grain Boundaries. Test Temperature 1800°F (982°c); Applied Stress 21.2 KSI; Electropolished Condition.

Figure 2-51. Scanning Electron Photomicrograph of MA754 Cold Rolled 22% Plus Anneal according to the Stepwise Schedule Revealing Coarsened Grain Boundary Particles. 5000X Magnification; Longitudinal Section; Electropolished.

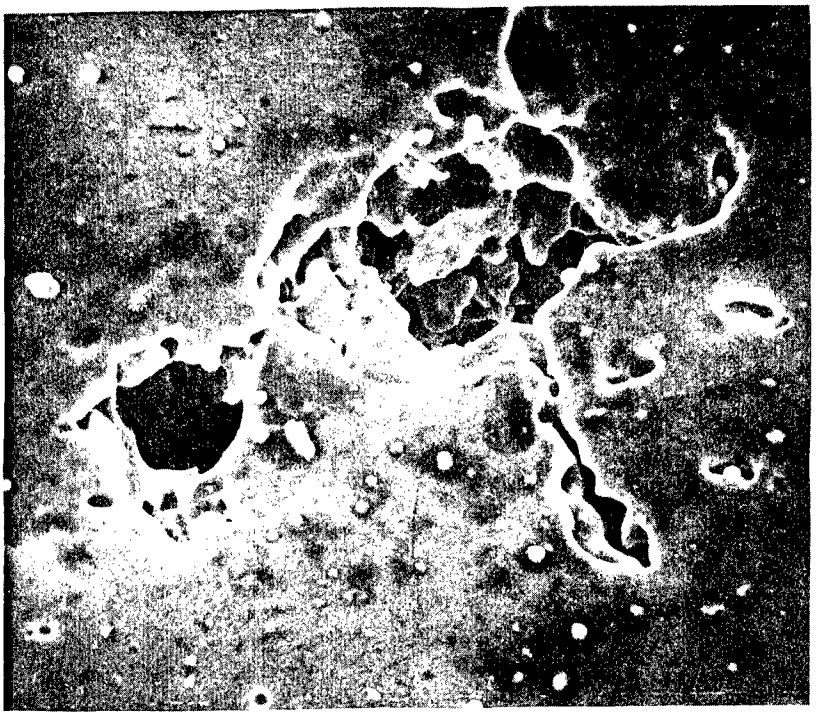

Figure 2-52. **Scanning Electron Photomicrograph of the Mid-Section of a Fractured Longitudinal Creep Test Piece from MA754 Cold Rolled 22% Plus Annealed according to the Stepwise Schedule Revealing a Fracture at an Apparent Grain Boundary Triple Point. Test Temperature 1800°F (982°c); Applied Stress 21.2 KSI; Electropolished Condition.**

after being tested at the same temperature and stress level (Figures 2-53 and 2-54).

It is well known[18,19,33] that modification of the dispersion in ODS materials can affect the creep rupture properties of ODS materials. It appears that, in the case of MA754 cold rolled 22% plus annealed according to the stepwise schedule, a coarsening process has modified the distribution of the dispersion in the area of the coarsened particles. This can produce localized areas of low particle volume fraction which, in turn, leads to a large increase in the minimum creep rate. In addition, it is suggested[16] that regions of high local ductility, produced by these areas of low volume dispersoid fraction, can influence crack propagation rates and thus the observed tertiary strain. This could explain the high rupture ductilities observed in this material.

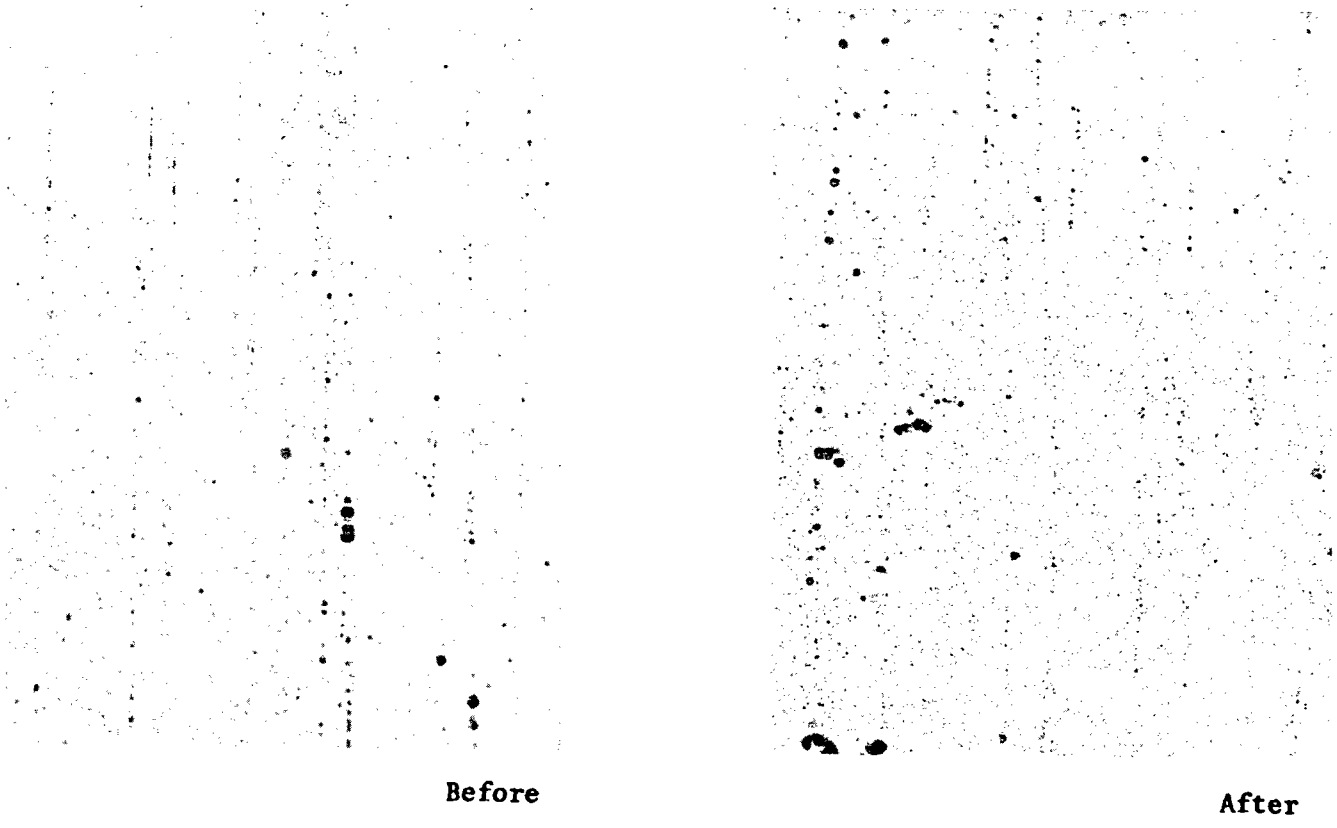

Figure 2-53. Optical Photomicrographs of As-Received MA754 (Bar #1) Before and After Creep Testing at 1800°F and 21.2 KSI. 160X Magnification; Electropolished Condition.

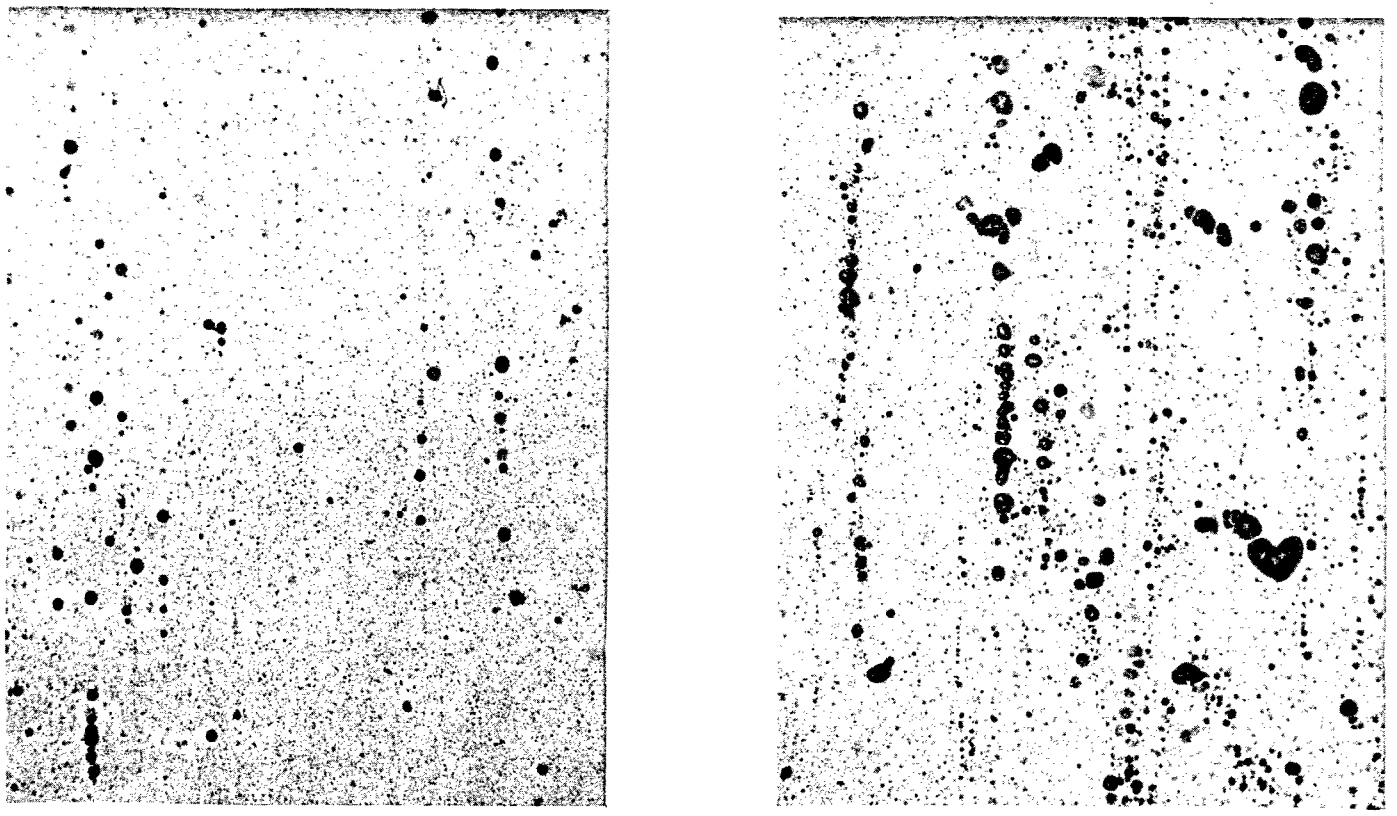

Figure 2-54. Optical Photomicrographs of MA754 Cold Rolled 22% Plus Anneal according to the Stepwise Schedule Before and After Creep Testing at 1800°F (982°c) and 21.2 KSI. 160X Magnification; Electropolished Condition.

2.3. Discussion

It is apparent from the results given in the preceding section that the major factor that controls the creep-rupture performance of MA754 cold rolled 22% plus annealed according to the stepwise sehcdule is a modification of the dispersion through a coarsening process. It is the purpose of this section to propose a mechanism which could explain this behavior, and to investigate the various factors involved in the process.

2.3.1. Statement of the Mechanism

The particle coarsening observed in MA754 may be explained by the theory originally developed by Lifshitz, Slyozov[34] and Wagner,[35] commonly known as Ostwald Ripening. The process is diffusion controlled, and has been applied to explain the coarsening behavior of various nickel-base superalloys.[36,37,38]

According to the theory, the driving force for this ripening is the reduction in total surface energy. This can be expressed by a variation of the Gibbs Thomson equation involving concentrations:

$$C_r = C_\infty + \frac{2\gamma C \Omega}{RT\, r}$$

where C_r is the concentration of the particle, C_∞ is the equilibrium solute concentration in the matrix, r is the particle radius, Ω is the molar volume and γ is the surface energy. As a result, there

is a concentration gradient between the particle and the matrix. For a distribution of particles, there will be a distribution of concentrations, resulting in an average concentration $\bar{C}$, which also defines a critical radius $\bar{r}$:

$$\bar{r} = \frac{2\gamma C_\infty \Omega}{RT} \frac{1}{\bar{C} - C}$$

Particles with radii larger than $\bar{r}$ will grow, and particles smaller than $\bar{r}$ will dissolve.

The equations listed above form the basis of the well known "$t^{1/3}$ law," given by the equation:

$$\bar{r}^3 - \bar{r}_o = KT \quad \text{or} \quad \bar{r} \propto t^{1/3}$$

where $\bar{r}$ is the average particle radius at time t, and $\bar{r}_o$ is the average particle radius at the onset of coarsening. The rate constant K is given by:

$$K = \frac{8C_\infty \gamma D\Omega^2}{9RT}$$

In addition, the theory predicts that the particle number per unit volume, N, decreases as t^{-1} during coarsening.

2.3.1.1. Coarsening Behavior of MA754

In the attempt to quantify the observed coarsening behavior of MA754, particle sizes were measured as a function of annealing time at 2400°F through the use of an Optomax Image Analyser, owned by SCM Metal Products, Cleveland, Ohio. Sample preparation involved electrolytic polishing utilizing the method described earlier. For a particular material condition, the average particle radius was

calculated utilizing 3 different samples and 1000 particles per sample. Since the coarsening behavior of the material is not uniform (that is, more coarsening at the grain boundaries than within the grain), separate measurements were taken for particles at the grain boundary and those within the grain. All measurements were taken at 500X magnification.

Figures 2-55 and 2-56 reveal the variation of the average particle radius as a function of annealing time at 2400°F (1315°c) for as-received MA754 annealed according to the step-wise schedule. From these results, it appears that the coarsening found in the processed material occurs at the grain boundaries. This result is not entirely surprising, since the coarsening mechanism is diffusion controlled and diffusion is more rapid along grain boundaries than in the interiors of grains. In addition, it appears that the coarsening observed in the processed material obeys the "$t^{1/3}$" law stipulated by the theory of Ostwald Ripening. The individual values contained in Figures 2-55 and 2-56 are given in Table 2-22.

2.3.1.2. Effect of Applied Stress on Coarsening Behavior

It has been determined[39,40] that applied stress can have an effect upon coarsening behavior. In order to investigate this possibility, the particle sizes of specimens that were cold rolled and annealed according to the step-wise schedule were measured. Figure 2-57 reveals the variation of particle size as a function of annealing time for these samples. For comparison purposes, the data contained in Table 2-22 is plotted on the same graph. The results indicate that the cold working procedure has no effect upon the

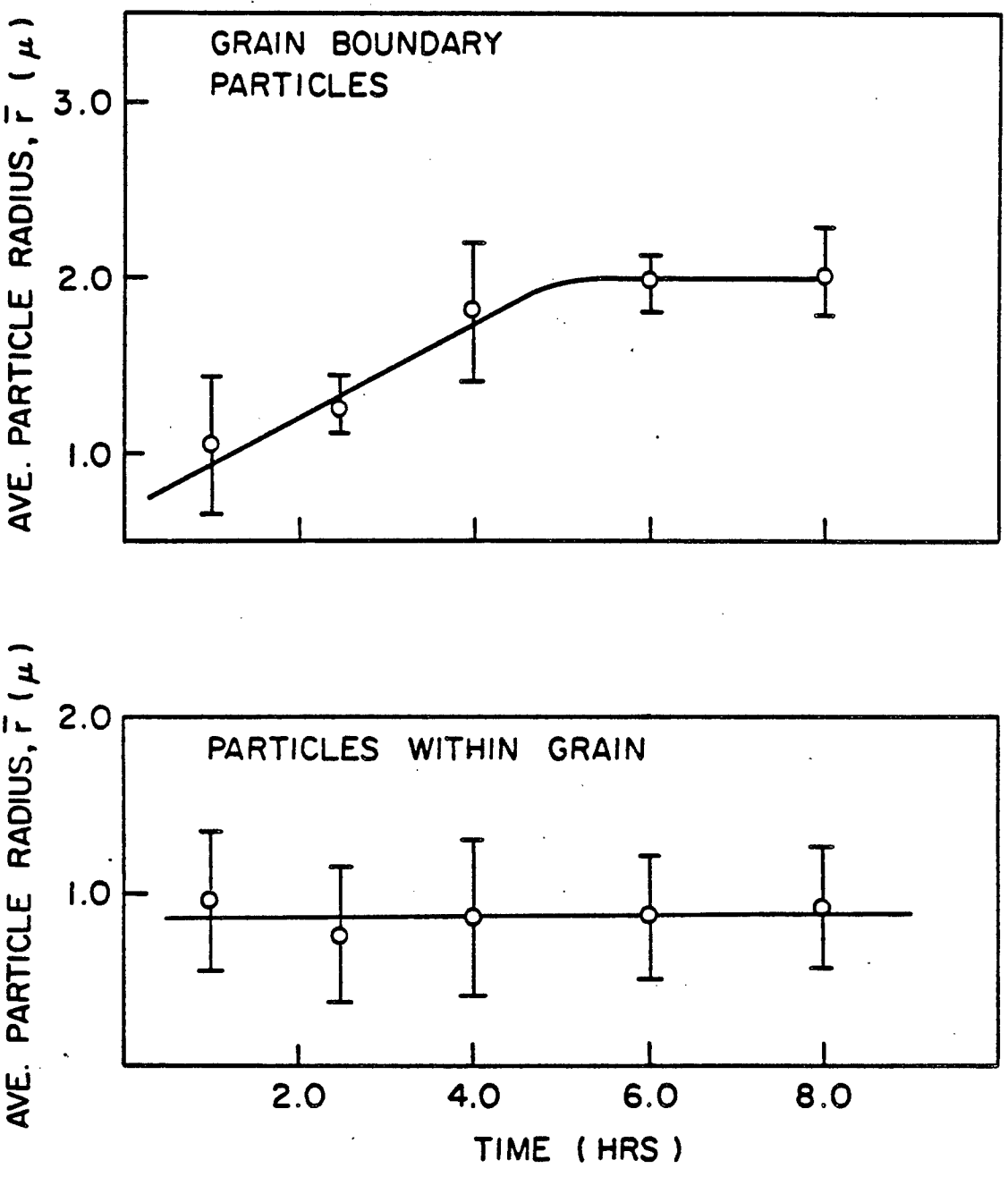

Figure 2-55. Variation of Average Particle Radius as a function of Time for As-Received MA754 Annealed at 2400°F (1315°c).

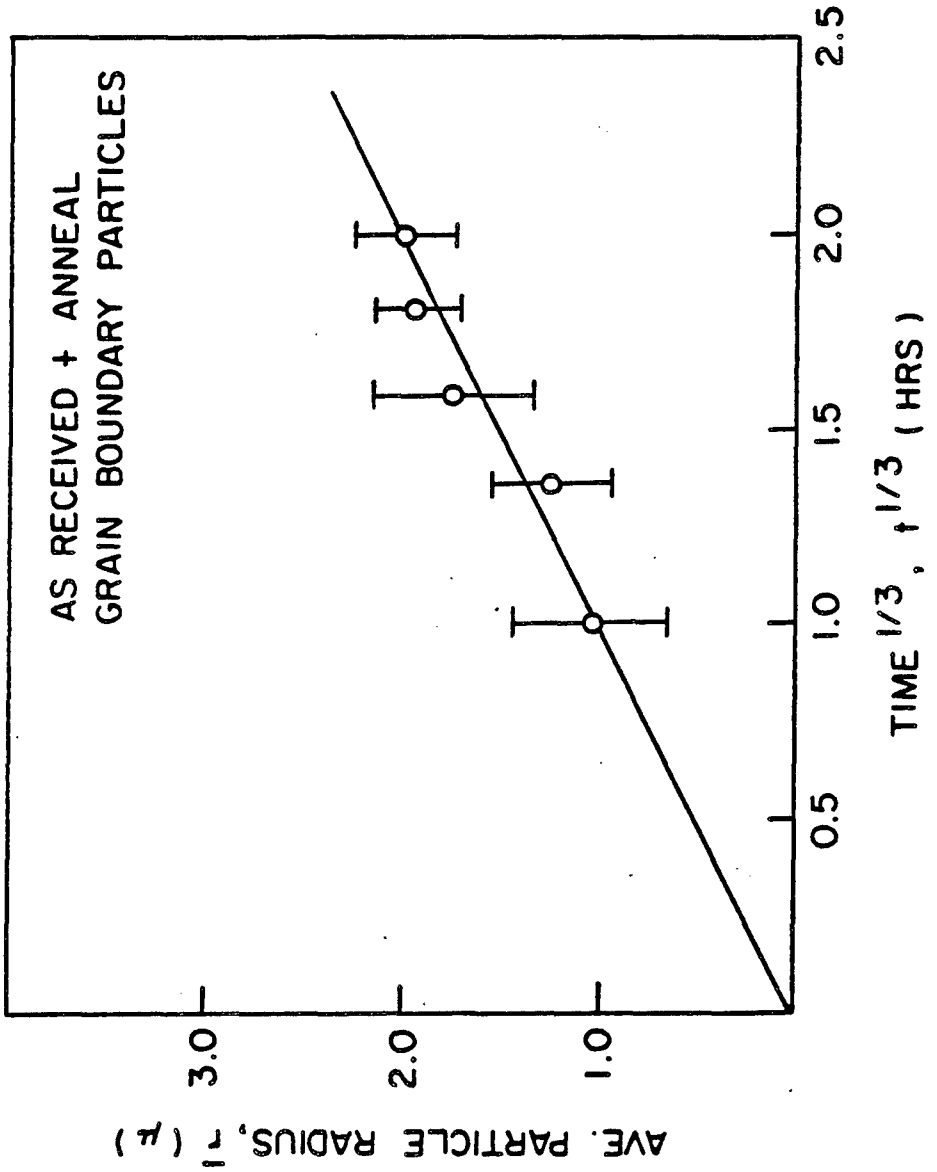

Figure 2-56. Variation of Average Particle Radius as a function of (Time)$^{1/3}$ for As-Received MA754 Annealed at 2400°F (1315°c).

Table 2-22

Average Particle Sizes for As-Received MA754 Annealed at 2400°F (1315°c)

GRAIN BOUNDARY PARTICLES

Condition	$\bar{r}$ ± 95% Confidence Internal
As-Received	1.06 ± .399
As-Received + 1.5 Hour	1.24 ± .306
As-Received + 3.0 Hour	1.78 ± .385
As-Received + 5.0 Hour	1.96 ± .206
As-Received + 7.0 Hour	2.01 ± .265

PARTICLES WITHIN GRAIN

Condition	$\bar{r}$ ± 95% Confidence Internal
As-Received	0.972 ± .384
As-Received + 1.5 Hour	0.741 ± .385
As-Received + 3.0 Hour	0.857 ± .445
As-Received + 5.0 Hour	0.861 ± .337
As-Received + 7.0 Hour	0.899 ± .313

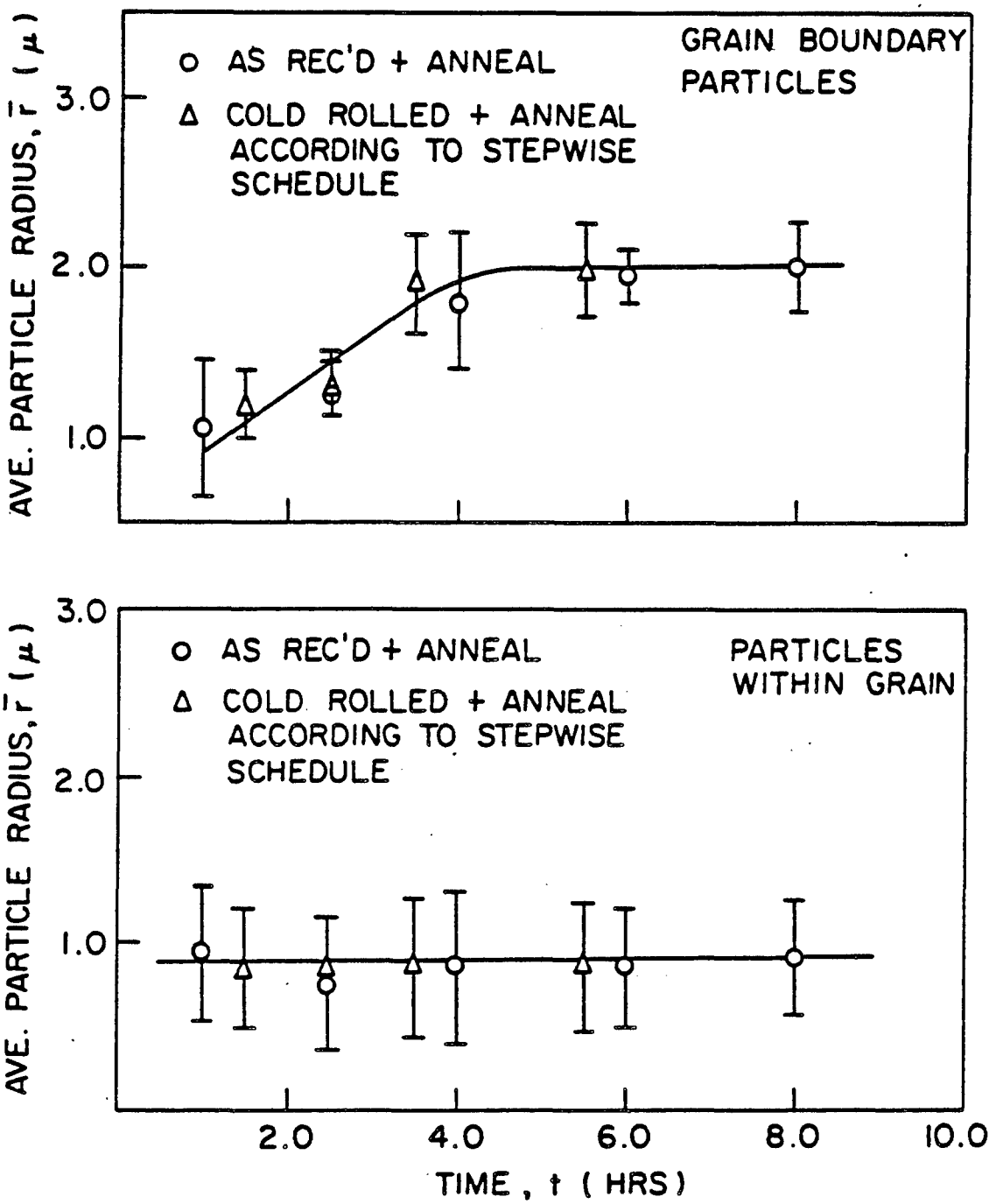

Figure 2-57. Variation of the average particle radius ($\bar{r}$) as a function of annealing time at 2400°F for MA754 in two conditions.

degree of coarsening observed. This conclusion appears to be a valid one, as evidenced by the microstructures of the various material states shown in Figures 2-58 and 2-59. However, when the annealing temperature is lowered to 1800°F (982°c), it appears that the cold work can have an effect, Figure 2-60, although no quantitative measurements were made. The individual values contained in Figure 2-57 for the cold rolled plus annealed material are given in Table 2-23.

As stated above, the theory of Ostwald Ripening predicts that the particle number per unit volume, N, decreases as t^{-1} during coarsening. Figure 2-61 reveals the change in the number of particles as a function of $time^{-1}$ for as-received MA754 annealed at 2400°F. It appears that the material does agree with the prediction after 2.5 hours. The particle number values for as-received MA754 plus anneals are given in Table 2-24.

2.3.1.3. Composition of the Coarsened Particles

In order to determine the chemical elements which make up the composition of the coarsened particles, an EDAX chemical analysis was performed on the grain boundary particles of MA754 cold rolled 22% plus annealed according to the stepwise schedule, as-received MA754 given a 3-hour anneal at 2400°F, and as-received MA754 with no anneals. The results contained in Table 2-25 indicate that the coarsened particles are composed of Ti, Y, and Al. In addition, it is important to note that these elements are present in the grain boundaries particles of the as-received material, and that they compromise the major components of the dispersion.

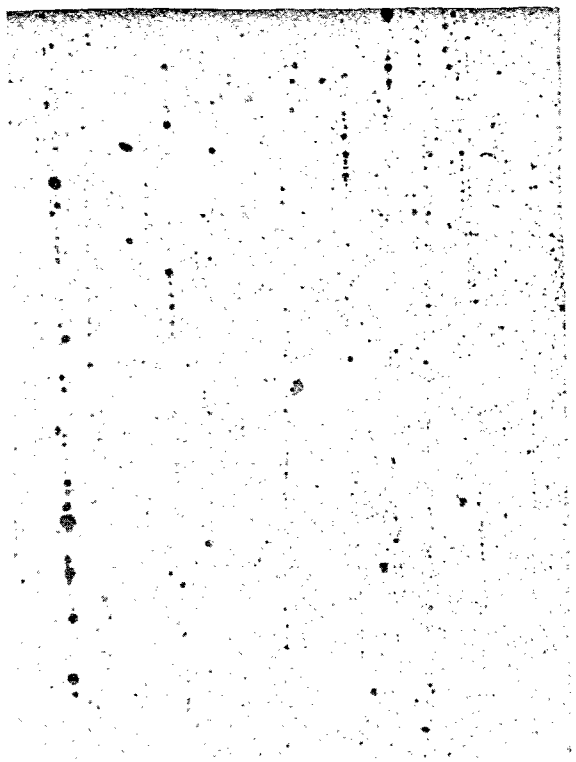

As-Received MA754 Plus Anneal at 2400°F, 1.5 hours.

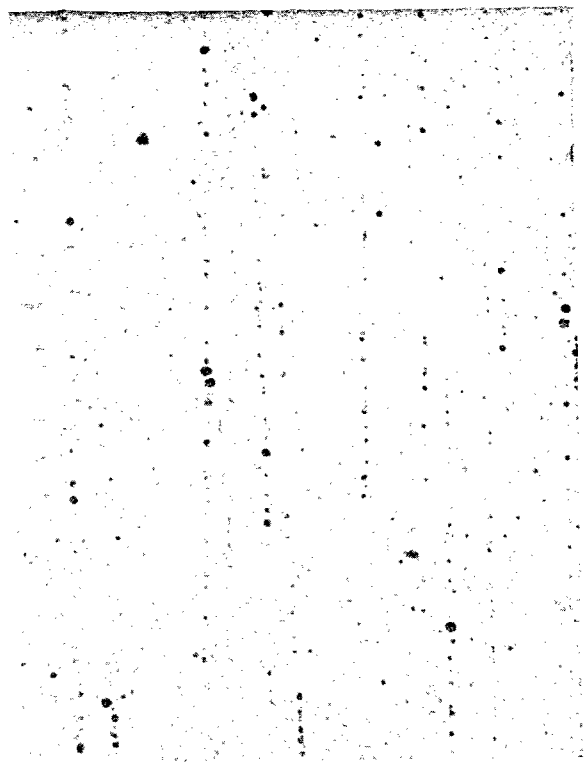

MA754 Cold Rolled 15% Plus Anneal according to the Stepwise Schedule.

Figure 2-58. Optical Photomicrographs of MA754 processed according to two different schedules. 160X Magnification; Electropolished Condition.

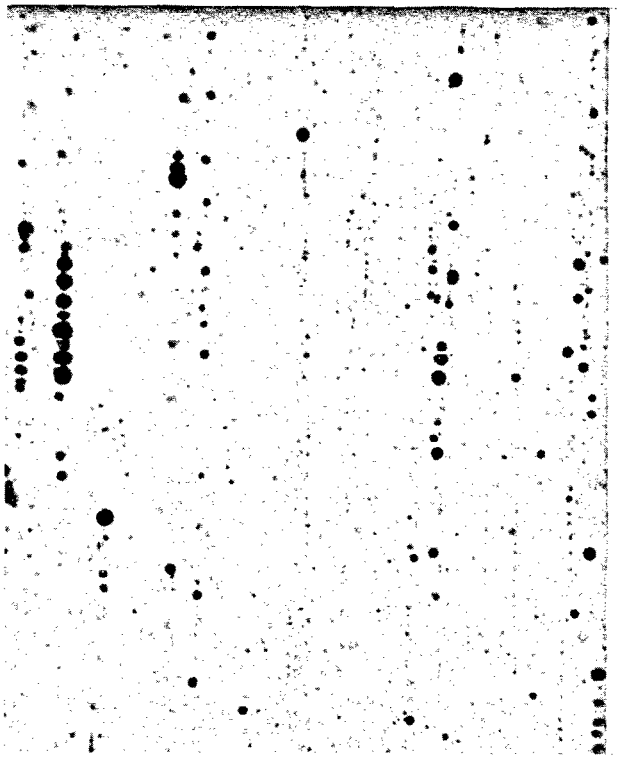

As-Received MA754 Plus Anneal at 2400°F; 2.5 hours.

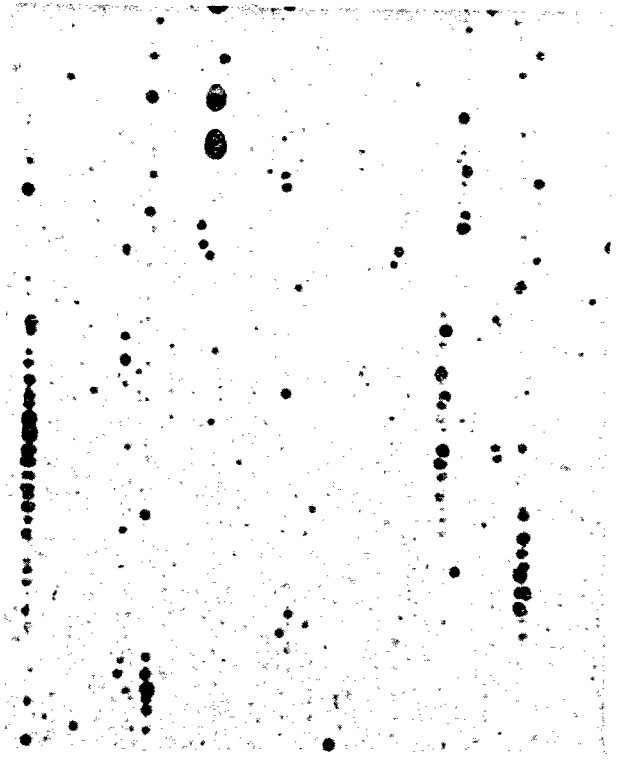

As-Received MA754 Cold Rolled Plus Anneal according to the Stepwise Schedule.

Figure 2-59. Optical Photomicrographs of MA754 Processed according to two different schedules; 160X Magnification; Electropolished Condition.

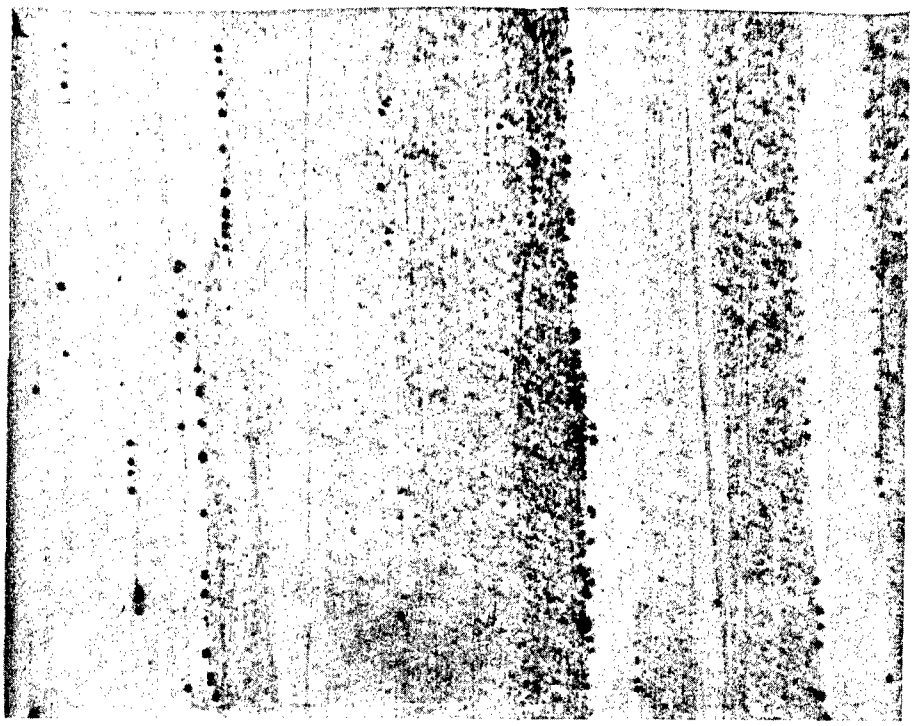

Figure 2-60. Optical Photomicrograph of a Longitudinal Section of MA754 Cold Rolled 22% Stepwise with Intermediate and Final Annealing Temperature of 1800°F (982°c). 100X Magnification; Thermal Etch; Electropolished prior to Etching.

Table 2-23

Average Particle Sizes for MA754 Cold Rolled Plus Annealed to Various Reductions According to the Stepwise Schedule

GRAIN BOUNDARY PARTICLES

Condition	$\bar{r}$ ± 95% Confidence Internal
5% Reduction	1.19 ± .193
15% Reduction	1.27 ± .165
22% Reduction	1.905 ± .298
32% Reduction	1.99 ± .260

PARTICLES WITHIN GRAIN

Condition	$\bar{r}$ ± 95% Confidence Internal
5% Reduction	0.822 ± .336
15% Reduction	0.844 ± .281
22% Reduction	0.882 ± .416
32% Reduction	0.870 ± .383

Table 2-24

Particle Numbers for As-Received MA754 Annealed at 2400°F (1315°c)

Condition	Particle Number X $10^4/mm^2$
As-Received	1.33
As-Received + 1.5 Hour	1.30
As-Received + 3.0 Hour	1.18
As-Received + 7.0 Hour	1.04

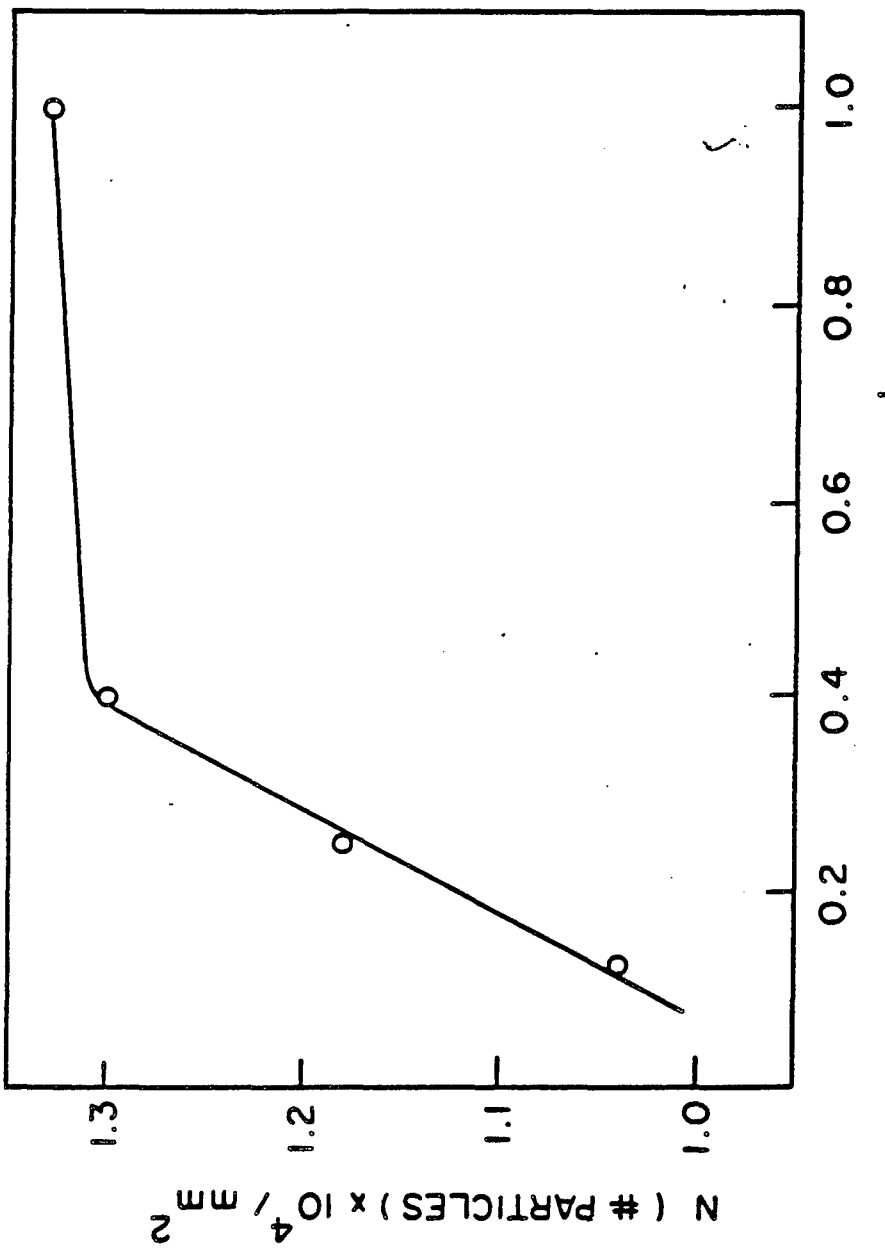

Figure 2-61. Particle Number, N, as a function of $(Time)^{-1}$ for As-Received MA754 Annealed at 2400°F (1315°C).

Table 2-25

EDAX Chemical Analysis of Grain Boundary Particles in As-Received, Annealed, and Rolled and Annealed MA754

BULK ANALYSIS

Element	Weight %
Fe	1.061
S	0.208
Ni	75.26
Cr	21.24
Al	0.586
Ti	0.175
Y	1.585

GRAIN BOUNDARY PARTICLES

	As-Received (wt. %)	Annealed 3 Hours, 2400°F (wt. %)	Rolled 22% Annealed 2400°F According to Stepwise Schedule (wt. %)
Ni	41.20 - 52.22	45.40 - 59.24	48.53 - 51.79
Cr	12.61 - 15.53	13.90 - 19.32	12.95 - 13.10
Al	7.60 - 16.22	17.98 - 30.81	7.74 - 20.70
Ti	0.65 - 3.07	1.47 - 4.40	1.66 - 10.94
Y	11.67 - 36.60	4.40 - 17.41	6.73 - 25.86

3.0. CONCLUSIONS

Based upon the results and analysis of the present investigation, the following conclusions seem warranted:

1. Rupture during high temperature tensile and creep deformation in MA754 is intergranular and occurs as a result of cracking at transverse grain boundaries.
2. It appears that MA754 is very amenable to cold rolling. Reductions of at least 70% were obtained with no evidence of edge or side cracking of the rolling blanks.
3. Results of various cold rolling plus anneal experiments appear to indicate that the excellent grain morphology obtained by cold rolling cannot be stabilized through the use of intermediate anneals. However, it was noted that the recrystallization response of MA754 appears to be controlled by primary recrystallization concepts.
4. Through application of a revised cold rolling plus anneal schedule, total reductions of at least 40% were obtained while at the same time maintaining a favorable grain morphology. In addition, MA754 cold rolled and annealed according to this schedule has recrystallized.
5. The loss in creep resistance found in MA754 cold rolled 22% plus annealed according to the stepwise schedule is due to the influence of coarsened particles situated primarily at grain

boundaries.

6. The coarsening observed in the processed material occurs only at the grain boundaries, and is the result of Ostwald Ripening.
7. Cold work appears to have no effect upon the coarsening process when the annealing temperature is 2400°F (1315°c). However, it may have an effect at lower annealing temperatures.
8. The coarsened particles are composed of Ti, Y, and Al. These elements are present in grain boundary particles of the as-received material, and make up the major components of the dispersion.

4.0. REFERENCES

1. Ansell, G. (Ed.) Oxide Dispersion Strengthening, Gordon & Breach, N.Y., 1966, Pg. 5
2. Anders, F. et al Metal Progress, Vol. 82, #12, 1962
3. Kane, R. Ph.D. Thesis, CWRU 1974
4. Benjamin, J. Met Trans #5, 1974
5. McIntyre, R. Met Eng #2, 1982
6. Petrovic, J. and Ebert, L.J. Met Trans, Vol. 4, May 1973
7. Wilcox, B.A. and Claver, A.H. Acta Met, Vol. 20, 1972
8. Kane, R. and Ebert, L. J. Met Trans, Vol. 7A, 1976, Pg. 133
9. Trela, D. M.S. Thesis, CWRU 1978
10. Whittenberger, J. Met Trans A, July 1977
11. Fraser, W. and Evans, D. Oxide Dispersion Strengthening, Bordon & Breach, N.Y., 1966, Pg. 375-401
12. Doble, G. Ph.D. Thesis, CWRU 1968
13. Anglin, A. NASA Technical Memorandum, 1979
14. Perry, A. Journal of Materials Science 9, 1974
15. Dieter, G. Mechanical Metallurgy, McGraw-Hill, N.Y., 1976
16. McAlarney, M. et al Met Trans, Vol. 13A, 1982
17. Ansell, G. and Weertman, J. Trans Aime 1959, Vol. 215, Pg. 838
18. Wilcox, B.A. and Claver, A.H. Met Sci Journal 1967, Vol. 1, Pg. 86
19. Benjamin, J. and Bomford, M. Met Trans, Vol. 5, 1974
20. Petrovic, J. and Ebert, L. J. Met Trans, Vol. 4, 1973
21. Ashby, M. Scripta Met, Vol. 3, 1969

22. Burton, B. Met Sci Journal, Vol. 5, 1971

23. Petrovic, J. and Ebert, L. J. Met Trans, Vol. 3, 1972

24. Wilcox, B.A. and Claver, A. H. and Hutchinson, W. NASA Contract NAS3-11167, Final Report 1971

25. Nelson, R. and Widmer, R. NASA Contract NAS3-7265, Final Report 1967

26. Sellars, C. and Petkovic-Luton, R. Met Sci & Eng, Vol. 46, 1980

27. Bailey, P. and Kutchera, R. AFML-TR-73 Technical Report 1973

28. Benjamin, J. et al Met Trans A, Vol. 6, 1975

29. Hotzler, R. and Glasgow, T. Met Trans, Vol. 13A, 1982

30. Trela, D. et al Met Trans 7A, 10, 1976

31. Reed-Hill, R. Physical Metallurgy Principles, Litton Publishing, Inc., 1973

32. Howson, T.E. et al Met Trans A, 1980, Vol. 11A, Pg. 1599

33. Nix, W. and Lund, R. Acta Met, Vol. 24, 1975

34. Lifshitz, M. and Slyozov, V. J. Physics Chem. Solids, 1961, Vol. 19

35. Wagner, C. Z. Elektrochem, 1961, Vol. 65

36. Ardell, A. J. and Nicholson, R.B. J. Phys. Chem. Solids, 1966, Vol. 27

37. Davies, C. K. et al Journal of Materials Science, Vol. 15, 1980

38. VanDerMolen, E. and Oblak, J.M. Met Trans, Vol. 2, 1971

39. Tien, J.R. and Copley, S. M. Met Trans, Vol. 2, 1971

40. Burt, H. et al Metal Science, May 1979